Progress of metal organic frameworks-based composites in electromagnetic wave absorption

Shixuan Feng[1], Futian Zhai[1], Huahua Su[1], Deepak Sridhar[2], Hassan Algadi[4,5], Ben Bin Xu[6], Rami Adel Pashameah[7], Eman Alzahrani[8], Hala M. Abo-Dief[9], Yong Ma[1,*], Tingxi Li[1,*], Zhanhu Guo[6*]

[1] School of Material Science and Engineering, Shandong University of Science and Technology, Qingdao 266590, China

[2] Zentek Ltd. 24 Corporate Crt, Guelph, Ontario, N1G 5G5 Canada

[3] Mechanical and Construction Engineering, Faculty of Engineering and Environment, Northumbria University, Newcastle Upon Tyne, NE1 8ST, UK

[4] Department of Electrical Engineering, Faculty of Engineering, Najran University, Najran, 11001, Saudi Arabia

[5] College of Materials Science and Engineering, Taiyuan University of Science and Technology, Taiyuan, 030024, China

[6] Department of Chemical and Biomolecular Engineering, University of Tennessee, Knoxville, TN, 37996, USA

[7] Department of Chemistry, Faculty of Applied Science, Umm Al-Qura University, Makkah 24230, Saudi Arabia

[8] Department of Chemistry, College of Science, Taif University, P.O. Box 11099, Taif 21944, Saudi Arabia

[9] Department of Science and Technology, University College-Ranyah, Taif University, P.O. Box 11099, Taif 21944, Saudi Arabia

[*]Correspondence author: mayong@sdust.edu.cn (Y. Ma), litx@sdust.edu.cn (T. Li), nanomaterials2000@gmail.com or zhanhu.guo@northumbria.ac.uk (Z. Guo)

Abstract

Eelectromagnetic pollution has become an increasingly prominent problem and electromagnetic wave absorbing materials have received widespread attention. Metal organic frameworks (MOFs) derived materials work as wave absorbing materials having the advantages of simple synthesis process, low production cost, high specific surface area and porosity, good thermal stability, and also have excellent impedance matching and various attenuation mechanisms, which have been widely studied in the field of electromagnetic wave absorption. In here, the classification and preparation methods of MOFs are summarized, their wave absorption mechanisms are analyzed. It also details the current research progress and analyses their advantages and disadvantages from the perspectives of monometallic MOF, multi-metallic MOF and wave absorbing materials derived from MOF compounded with other materials (including carbon materials, MXene and conductive polymers). This article aims to illustrate the application of MOFs and their derived composites in the research of electromagnetic wave absorption, and hopes to offer a reference for the further research based on these promising materials.

Keywords: Progress; Metal organic frameworks; Composite materials; Microwave absorption.

1. Introduction

In recent years, technologies such as invisible technology, information technology and electronic equipment have achieved unprecedented development. And with the advent of the 5G era, it will result in a new technological revolution. However, while these technologies bring infinite convenience to human life, they will also be accompanied by a series of hazards. The widespread use of electronic equipment and communication equipment inevitably leads to the deterioration of the electromagnetic environment. The electromagnetic waves can cause serious electromagnetic pollution[1-5]. On the one hand, electromagnetic waves will cause interference to some precision equipment, which gives rise to the failure of the instrument and the interruption of the signal not only interrupting the normal work, but may also causing immeasurable harm[6-10], on the other hand, the leaked electromagnetic waves cause certain harm to human health such as cancer[11-14]. Human beings urgently need to solve electromagnetic waves pollution. In addition, in the military field, the electromagnetic waves stealth technology on the basis of microwave absorbing materials[15-18]. Hence, the research on microwave absorbing materials has become a hot topic in the current society[19-22].

Microwave absorbing materials are able to dissipate electromagnetic waves into different forms of energy[23, 24]. However, the current research on them faces many challenges, such as insufficient absorption capacity of each waveband, and insufficient research on each waveband. More importantly, there are disadvantages for the currently prepared various absorbers, including inappropriate thickness, narrow effective absorption bandwidth (EAB) and inferior practical application value. Therefore, the research on microwave absorbing materials puts forward the requirements of thin thickness, light weight, strong absorption and wide EAB characteristics with multiple losses[25-27].

Microwave absorbing materials can be divided into three categories according to the attenuation mechanism of electromagnetic waves, each of which has its own advantages and disadvantages[28]. The first is conductive materials based on carbon, typically including graphene[29-32], carbon nanotubes (CNTs)[33, 34] and carbon nanofibers[35-37]. The advantages of them are low density, high stability and conductivity. However, their impedance mismatch hinders their further development and application[38, 39]. The second is dielectric materials represented by inorganic ceramics and semiconductors. High thermal stability is a significant advantage, but these materials are accompanied by low attenuation capacity, which limits the absorption of electromagnetic waves[40-42]. The last is magnetic materials, and ferrites and other magnetic metals are typical magnetic absorbers. Such materials inevitably have the disadvantages of high density and inherent impedance mismatch [43-47]. It can be seen from the above results that microwave absorbing materials with a single attenuation mechanism are far from meeting the needs of the current society for electromagnetic wave absorption[48]. In order to overcome the shortcoming of a single attenuation mechanism, the research and design of composite microwave absorbing materials with multiple components realizing multiple absorption mechanisms has become an important task[49-52].

The porous and periodic network-like metal-organic frameworks (MOFs) consist of inorganic metal ions or clusters as centers and organic ligands[53-56]. The former almost covers various metal ions such as main group, transition, lanthanide and rare earth metals, etc. In terms of the latter, they are polyamines, carboxyl, pyridine, porphyrin, cyano, crown ethers and phosphoric acid. So far, more than 20000 MOFs have been prepared since the first one is proposed by Yaghi in 1951, and common MOFs[57] include isoreticular metal-organic frameworks (IRMOFs), coordination pillared-layer (CPL), imidazole zeolite frameworks (ZIFs)[58], materials of institute lavoisier (MIL)[59], university of Oslo (UIO), porous coordination network (PCN)[60], etc.

In recent years, MOFs have attracted a lot of interest because of regular porosity, ultra-high specific surface area, diverse topological structures, and tunable structural units[61, 62]. Moreover, the MOFs fabrication is environmentally friendly[63]. These materials can be used in various fields, such as adsorption[64], medicine, catalysis[65, 66], etc. Especially in the aspect of electromagnetic waves absorption, MOFs with the coexistence of metal and organic components and the highly tunable microstructure, create favorable conditions to be used as absorbing materials. It can not only obtain MOFs-based absorbing materials through further processing such as carbonization, but also combine with other materials to form MOFs-based composite absorbing materials with multiple absorption mechanisms. Compared with other absorbing materials[67], magnetic and dielectric losses as well as impedance matching for MOFs are able to be tuned by in-situ generated metal/metal oxide nanoparticles or clusters, facilitating electromagnetic wave absorption. Meanwhile, their uniform dispersion enhances the reflection ability.

Until now, Zhang et al[68] summarizes in detail the various types of monometallic MOF-derived absorbing materials. Zhang et al[69] focuses on magnetic metal MOF-derived absorbing materials. Zhu et al[70] takes the structure of MOFs as an entry point and introduces different structural wave absorbing materials derived from MOFs. However, there are few papers for a comprehensive introduction of the classification and preparation of MOFs and MOFs-based composites, as well as their wave absorption performances. This paper discusses in detail the classification and preparation methods of MOF-based functional materials, and explains the electromagnetic wave absorption mechanism. It introduces the research progress in recent years of wave absorbing materials derived from monometallic MOFs prepared from magnetic metals such as Fe, Co, Ni and non-magnetic metals such as Cu and Mn as metal sources, and multi-metallic MOFs prepared from bimetallic and trimetallic sources. In addition, a summary of the recent literature on absorbers derived from MOFs compounded with other materials, such as carbon and MXene, is also presented. Finally, the problems faced in the research and the future development trend of MOFs-derived absorbers have been elucidated.

2. Classification and preparation of MOFs

2.1 Classification of MOFs

2.1.1 UIO series materials

UIO series materials have 3D porous structures coordinated by Zr^{4+} and dicarboxylic acid organic ligands. UIO-MOFs series materials prepared from Zr^{4+} and carboxylic acid as raw materials possess the advantages of regular size, high porosity, large specific surface area and good stability, and have been widely studied and applied. Fig.1 shows the atomic structures of UIO-66, UIO-67 as well as UIO-68[71], and these materials with different sizes and morphologies can be prepared by changing ligands and reaction conditions. The face-centered cubic crystal structure of UIO-66 formed by the linking of Zr_6 with 12 terephthalic acid ligands, which is widely used in photocatalysis[72-74], heavy metal adsorption[75] and photovoltaic cells[76]. UIO-67 is composed of Zr ions coordinated with 4,4-biphenyldicarboxylic acid, which can be widely used in plasma catalytic reforming[77] and targeted drug delivery[78]. Moreover, the MOFs of this series possessing large specific surface area and excellent stability due to special linking units, can be widely used in supercapacitors[79-81] and gas storage[82].

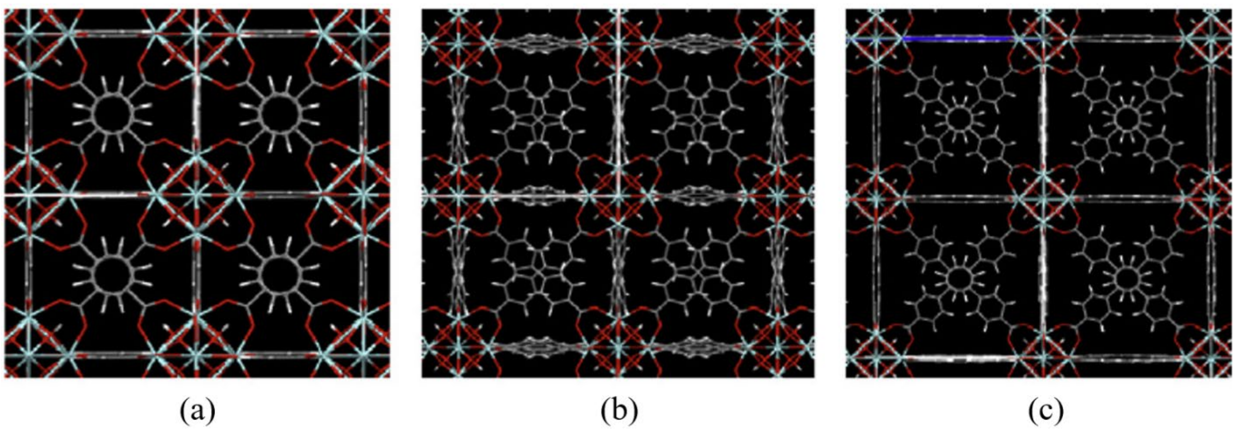

Fig. 1 Atomic structure diagrams of (a) UIO-66, (b) UIO-67 and (c) UIO-68[71].Copyright 2015, Elsevier B.V.

2.1.2 ZIF series materials

ZIF series materials are prepared by the coordination reaction of Co^{2+} or Zn^{2+} with imidazole ligands based on aluminosilicate zeolite meshes, where bridged Si(Al) units and tetrahedral Si(Al) units consist of imidazole-based ligands and transitional Si(Al) units, respectively. Substituted by metal ions, the framework endows ZIFs with excellent stability. Fig. 2 shows the structural topology of ZIF-7 and ZIF-8[83]. Among them, ZIF-8 is synthesized by a hydrothermal method from zinc ions and imidazole-like ligands, which has unique composition and stability, and can be widely used in adsorption[84, 85] and lithium-sulfur batteries[86-88]. Fig. 3 displays the atomic structures of common ZIF samples[89]. Thereinto, ZIF-67 is synthesized by stirring cobalt ions and imidazole ligands in an organic solvent. It has good structural stability and multiple active sites, and is also able to be prepared by high temperature carbonization. Carbon-wrapped cobalt element and cobalt oxide exhibit shows great potential in wave absorption[90].

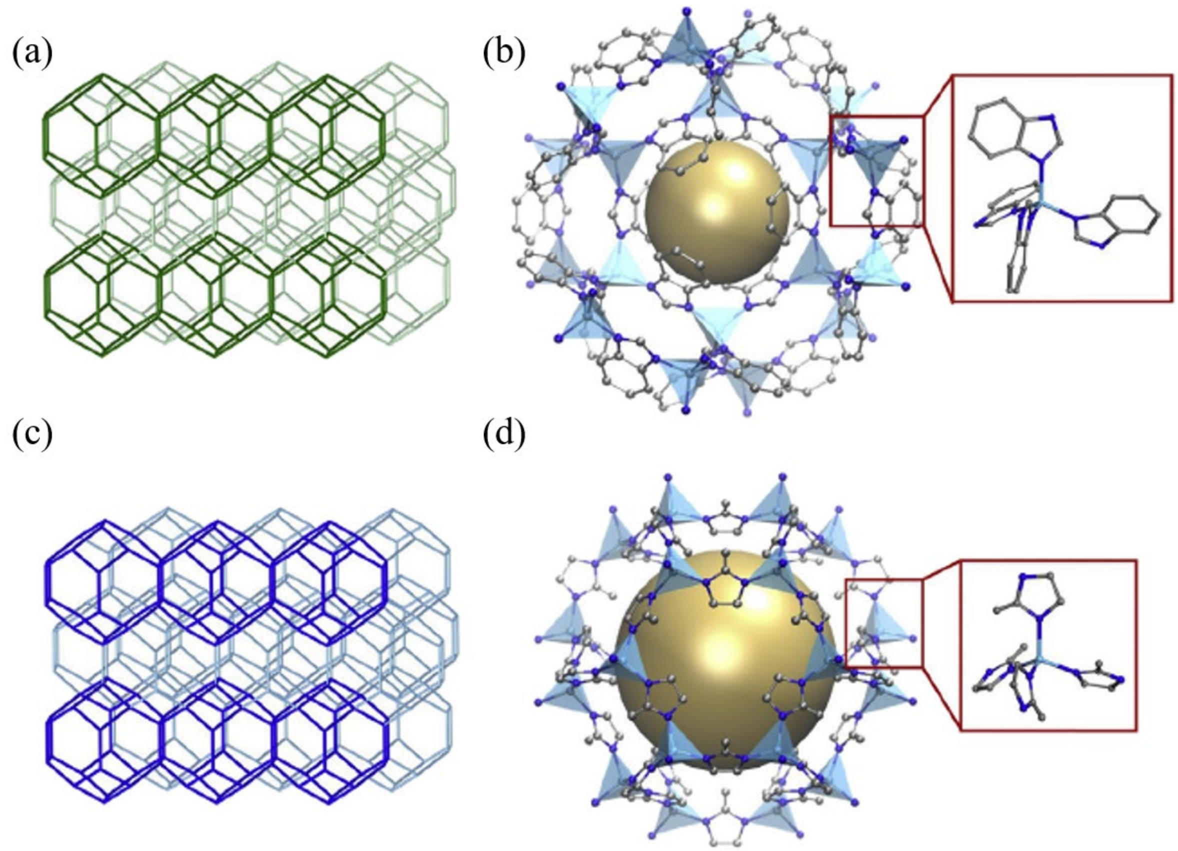

Fig. 2 Structural topology of (a) ZIF-7, (c) ZIF-8, and their corresponding molecular structure of (b) ZIF-7, (d) ZIF-8[83]. Copyright 2016, Elsevier Inc.

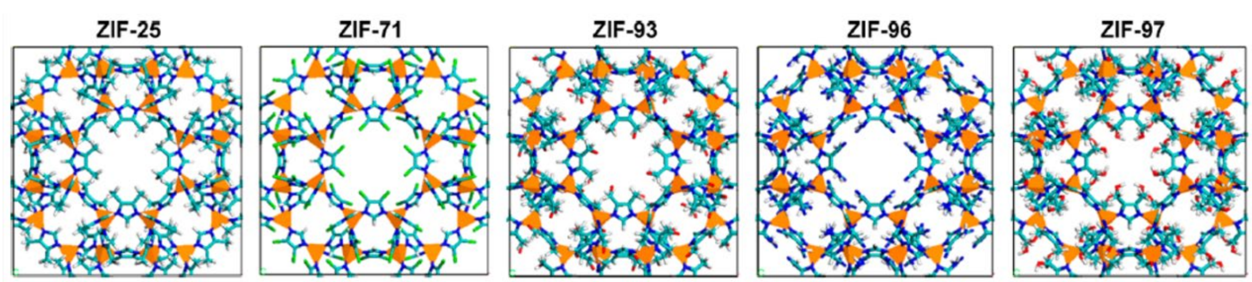

Fig. 3 Atomic structures of ZIF-25, ZIF-71, ZIF-93, ZIF-96 and ZIF-97, ZnN_4 cluster: orange polyhedra, C: cyan, O: red, N: blue, Cl: green, H: white[89]. Copyright 2015, American Chemical Society.

2.1.3 PCN series materials

PCN series materials are prepared by the coordination reaction between metal ions and porphyrin-like ligands. Tetrakis (4-carboxyphenyl) porphyrin (TCPP) is very popular because of its excellent stability and various functions. Some of these Zr-MOFs are prepared by the coordination reaction between $ZrCl_4$ and TCPP under different reaction conditions. For example, the planar tetracarboxylate compound TCPP is combined with twelve linked hexagonal Zr_6-SBUs and six linked hexagonal Zr_6-SBUs to obtain PCN-223 and PCN-224, respectively. Fig.4 demonstrates the preparation of different topological Zr-based porphyrin MOFs under similar solvothermal conditions[91]. MOF-545 having large pore channels is composed of Zr_6 flower clusters and TCPP. PCN series materials exhibited herein have good stability in air, boiling water and hydrochloric acid, which can be widely used in catalysts[92].

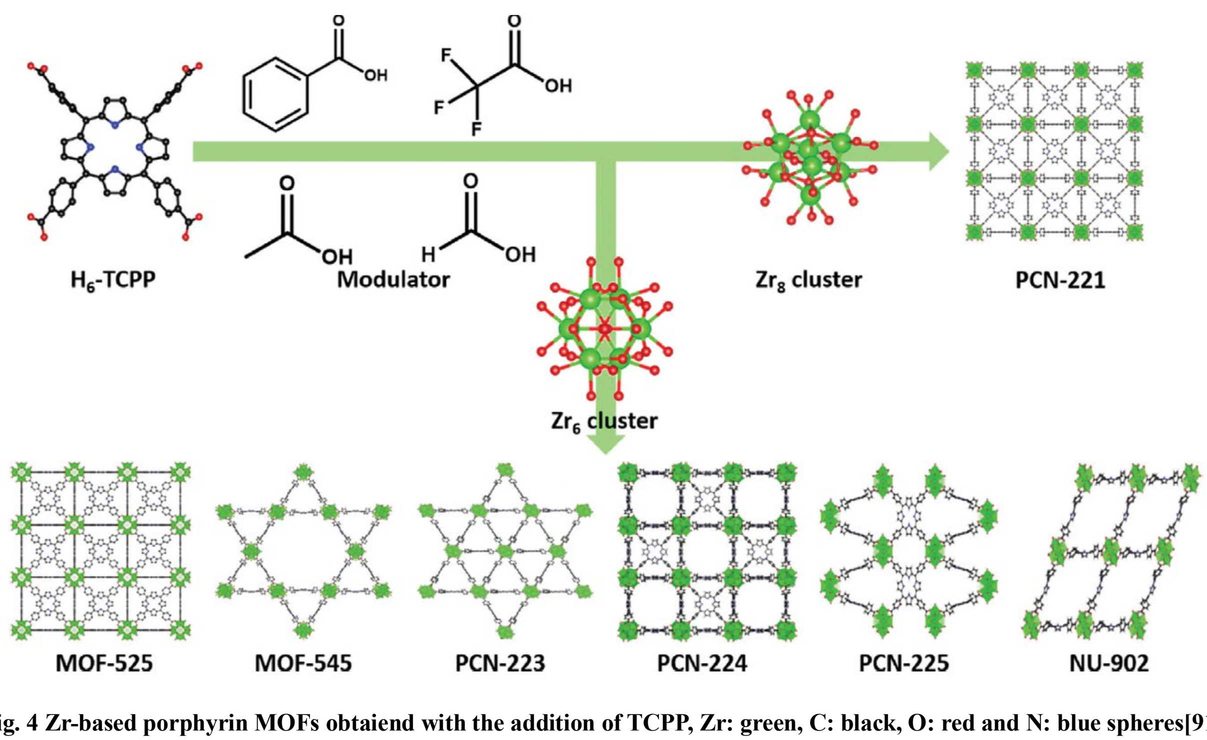

Fig. 4 Zr-based porphyrin MOFs obtaiend with the addition of TCPP, Zr: green, C: black, O: red and N: blue spheres[91].

2.1.4 CPL series materials

CPL series materials are composed of Cu^{2+}, 2,3-pyrazine dicarboxylic acid and neutral nitrogen-containing heterocycles of phenol, 4,4-bipyridine, pyrazine and 1,2 (or 2,2)-bis(4-pyridyl)ethylene. 2-bipyridine and other ligands are prepared by coordination reaction. CPL-MOFs are easily prepared and their pore size can be modified by changing the columnar ligands. Columnar layered MOFs can be considered as a type of Hofmann clathrates, which have a 3D porous framework directly utilizing the connection of 2D layered and columnar structures through metal nodes. Fig.5 shows an illustration of CPL-n prepared using various linker ligands [93]. CPL-2 and CPL-5 are typical MOFs in the family of CPL-MOFs series MOFs. The above two MOFs have mesoporous morphology, which can be widely used in the adsorption and separation of gases by loading metal nano-ions on them[94, 95].

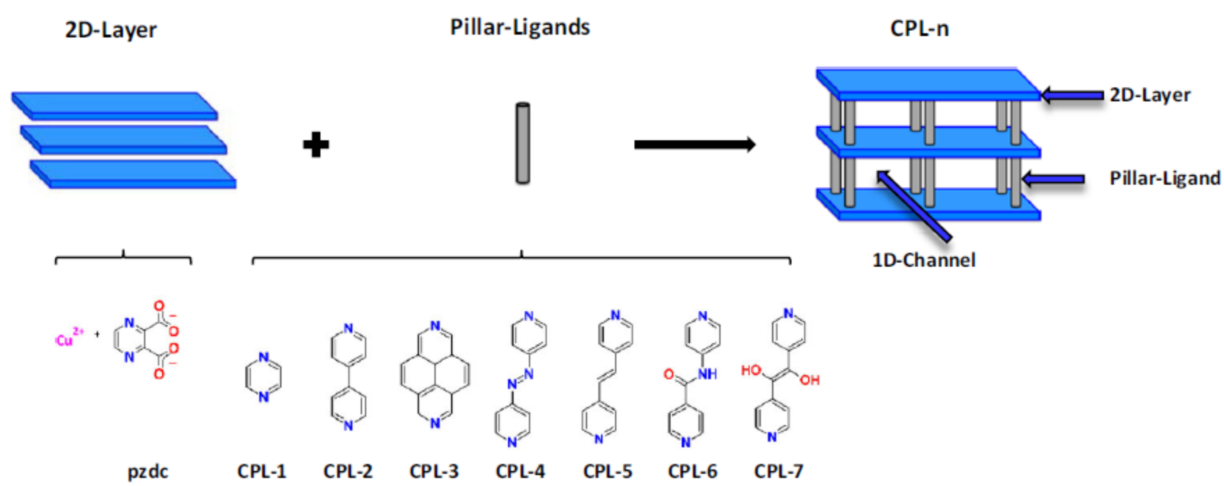

Fig. 5 illustraion of the CPL-n prepared using various linker ligands as pillars[93]. Copyright 2015, Springer Science+Business Media New York.

2.1.5 MIL series materials

MIL series materials can be divided into two categories. One is prepared by the coordination reaction of trivalent iron, vanadium, chromium and aluminum and other metals with trimesic acid or terephthalic acid. Another type is MIL-MOFs formed by the coordination of transition metals and lanthanide metals with succinic acid and glutaric acid, respectively. Fig.6 presents the structure diagram of two representative MIL-100 and MIL-101 MOFs[96]. Both of them exhibit large pore sizes, and have good application prospects in the preparation of catalysts to enhance pollutant adsorption[97] and to enhance visible light-driven photocatalysis[98, 99].

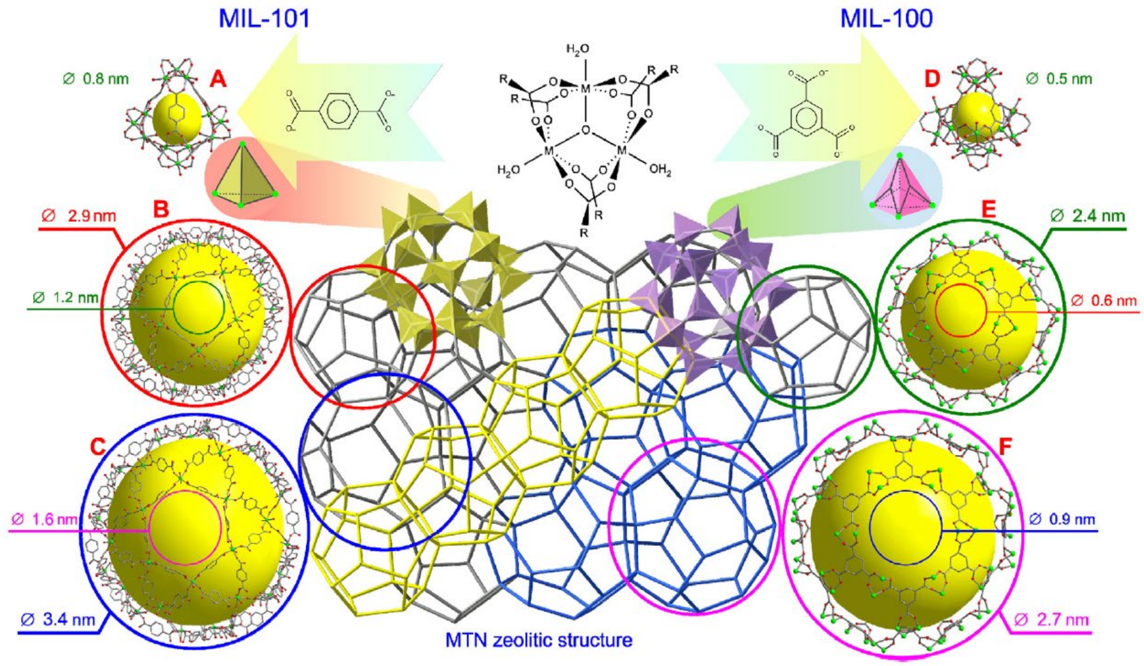

Fig. 6 Schematic representation of the MIL-101 and MIL-100 structures[96]. Copyright 2014, Elsevier B.V.

2.1.6 IRMOF series materials

IRMOF series materials are 3D stereo porous network MOFs consisting of Zn_4O^{6+} tetrahedra coordinated with aromatic carboxylic acid ligands. Fig.7 displays the characteristic maps of IRMOF-1, IRMOF-10 and IRMOF-14[100]. The first one is a microporous material having a large specific surface area, used to prepare electrode materials[101, 102] and gas adsorption[103].

IRMOF-14 also has a high specific surface area used for gas adsorption too[104].

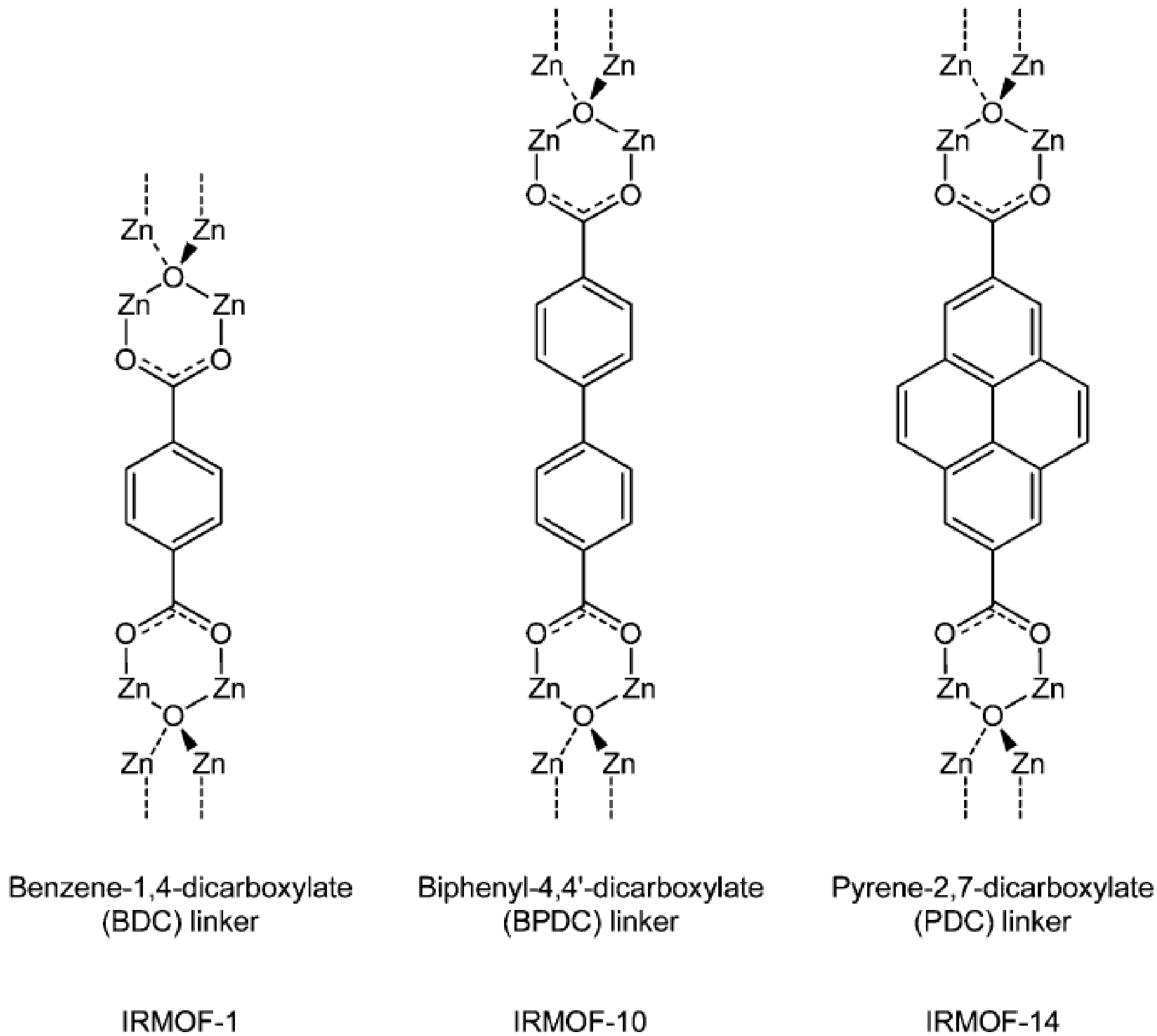

Fig. 7 Characterization maps of IRMOF-1, IRMOF-10 and IRMOF-14[100]. Copyright 2016, the Owner Societies.

2.1.7 Other series materials

NTU series materials are named after the abbreviation of Nanyang University of Technology, and the main representative materials includes NTU-Z30, NTU-Z31 and NTU-Z32. The synthesis process and reaction time of the above three MOFs are the same, but different ratios of raw materials are used, resulting in different coordination modes and the different morphologies. In addition, another MOFs named NTU-9-NS has great prospects for application in sensing field[105].

DUT series materials are named after the abbreviation of Dresden University of Technology. There are many kinds of materials and many ligands in this series. The main representatives are DUT-6, DUT-8, DUT-9, DUT-25, DUT-49, DUT-58, DUT-67, DUT-68 and DUT-69. For example, DUT-49 can be used for gas negative adsorption transitions[106]. HKUST series materials are synthesized by Chui in 1999 and named after the acronym of Hong Kong University of Science and Technology.

2.2 Preparation method of MOF materials

2.2.1 Solvothermal method

The solvothermal method is carried out under the conditions of high temperature and high pressure, which is beneficial to improve the dissolution rate of metal salts in organic solvents and accelerate the progress of the reaction. And the main driving force for the reaction is intermolecular contact. Li[107] et al. prepared ultrathin bimetallic Ni-Fe-MOFs nanoparticles by solvothermal reaction of $FeSO_4 \cdot 7H_2O$, $Ni(OAc)_2 \cdot 4H_2O$, 1,4-H_2BDC (molar ratio of 0.3:1:0.5), as shown in Fig.8(a). In this process, Fe^{2+} is spontaneously oxidized to Fe^{3+}. And MOFs with different morphologies are synthesized by changing the solvent. In Fig.8(b)(c), in the case of only water as solvent, nanoflowers are produced, and when only DMAC is employed, porous and fluffy powders are prepared. Wang[108] et al. prepared MIL-125 and NH_2-MIL-125 through using DMF and methanol mixed solvent, in the conditions of BDC and H_2ATA separately as ligands in Fig.8(d)-(f). The white sample is dominated by well-crystallized particles with a size of about 2 μm, while the yellow sampe is dominated by well-crystallized particles having 400-600 nm size. Pan et al. [109]prepared carbon quantum dots (CQD)/Ni MOFs composites using a mixture of DMF and deionized water with terephthalic acid as the ligand via a one-pot hydrothermal method. The preparation diagram, the sample morphology and the XRD patterns are separately displayed in Fig. 8(g)-(i).

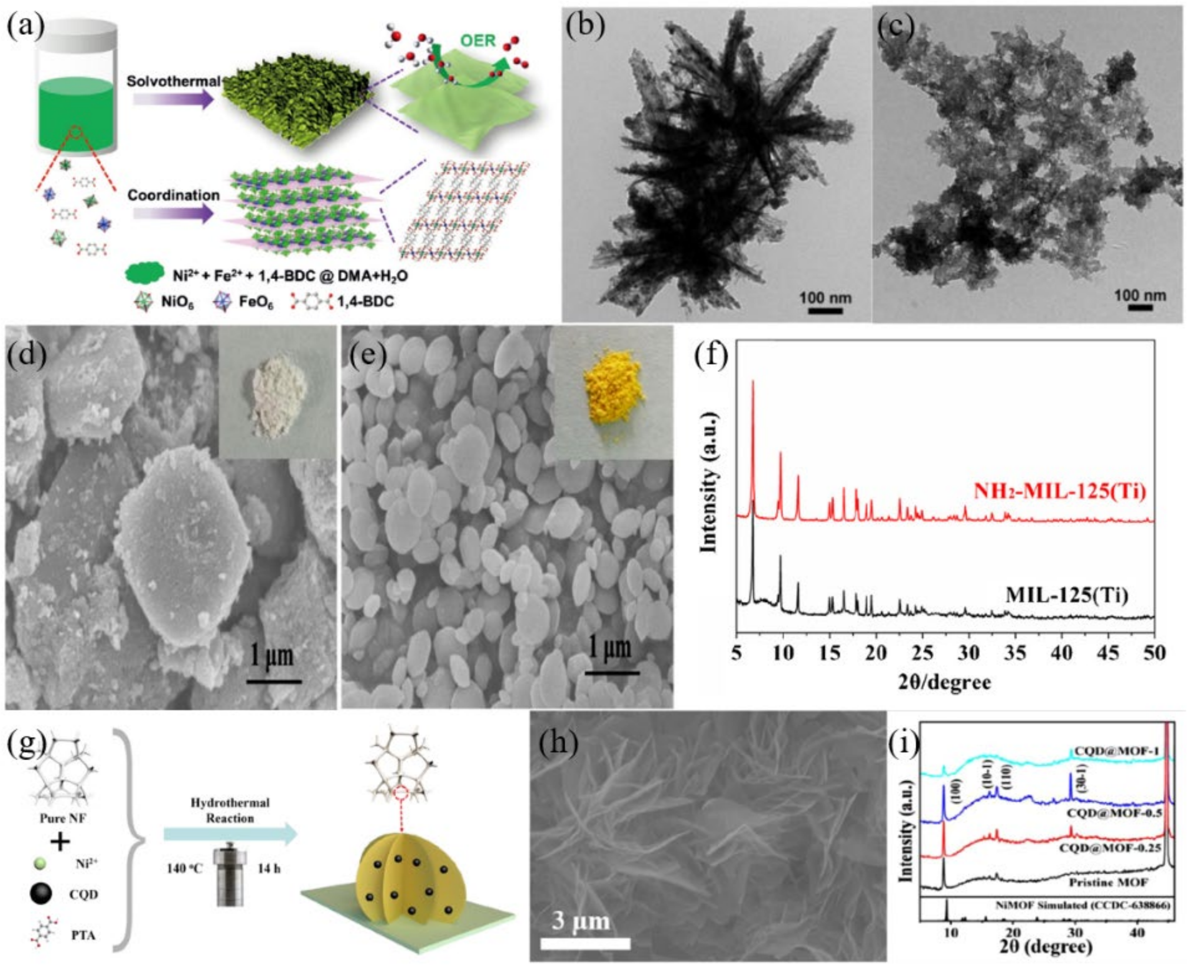

Fig. 8 (a) Ultrathin organometallic skeleton nanosheets prepared by solvothermal method, TEM images of Ni-Fe-MOFs synthesized with (b) water as solvent and (c) DMAC as solvent[107]. Copyright 2019, Wiley-VCH Verlag GmbH & Co. KGaA, Weinheim. SEM photos of (d) MIL-125(Ti), (e) NH_2-MIL-125(Ti) and their (f) XRD patterns[108]. Copyright 2019, Elsevier B.V. (g) schematic hydrothermal synthesis of CQD@Ni MOFs-0.5, and the corresponding (h) SEM image and (i) XRD patters[109]. Copyright 2022, Elsevier Ltd.

2.2.2 Microwave-assisted synthesis

The microwave-assisted preparation uses microwave radiation for providing energy, which can quickly heat the reactants to high temperature, accelerate the nucleation rate, shorten the reaction time, and improve the conversion rate. It is a green and environmentally friendly synthesis method. In Fig.9(a)-(c), Li et al.[110] synthesized trimetallic MOFs ($Ni_xCo_yFe_z$-UMOFNs, where xyz represent different ratios of metal precursors) using a microwave-assisted method. It is fund that the fabricated MOFs possess significantly improved OER activity. Chen et al.[111] used PTA as ligand to synthesize Zn-doped Ni-MOFs by microwave-assisted synthesis, and different microspheres can be seen in Fig.9(b)-(f). One can find that the size of the undoped microspheres is 1-3 mm, and each microsphere consists of a mass of nanosheets. However, for the doped microspheres, the diameter becomes smaller about 1.5 mm, and the size of the nanosheets also becomes smaller. Choi et al.[112] used terephthalic acid as a ligand to synthesise FeMo-MIL-88B in a hexagonal rod shape using a microwave-assisted synthesis in Fig. 9(g)-(i).

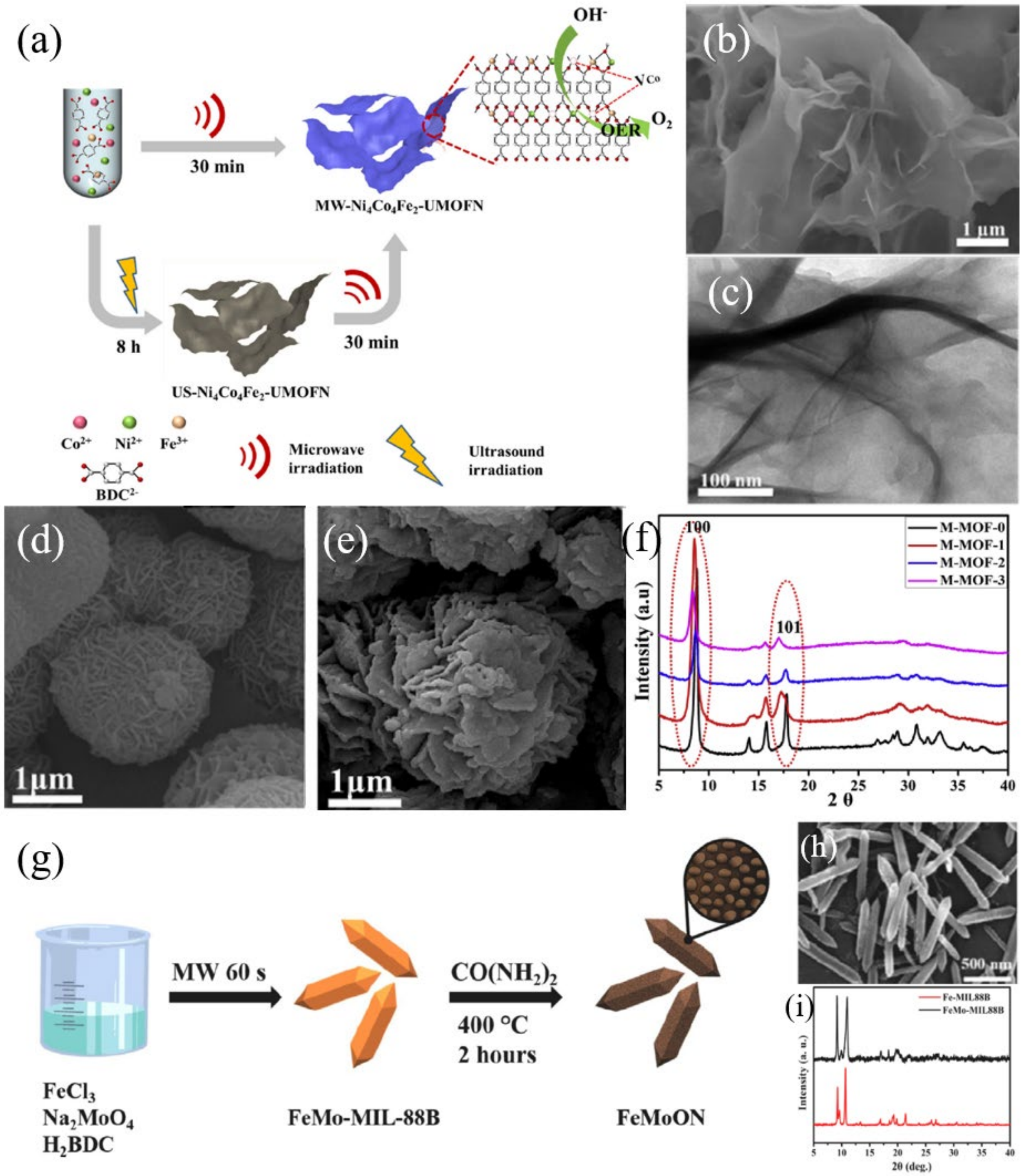

Fig. 9 (a) Schematic microwave-assisted synthesis of ultrathin trimetallic organometallic backbone nanosheets, (b) SEM and (c) TEM images of US-$Ni_4Co_4Fe_2$-UMOFN[110]. Copyright 2021, Elsevier Inc. SEM images of (d) with and (e) without Zn doping and (f) XRD patterns of Zn-doped Ni-MOFs[111]. Copyright 2018, Elsevier Ltd. (g) schematic synthesis of FeMo-MIL-88B and its (h) SEM images and (i) XRD patterns[112]. Copyright 2021, Elsevier Ltd.

2.2.3 Electrochemical synthesis

In 2005, the first case of electrochemically synthesized HKUST-1 was reported. In electrochemical synthesis, the yield and the structure of materials are constrained by electrolyte, solvent, voltage, density and temperature. Compared with traditional methods, this method has a faster reaction speed, lower temperature, and the metal source does not come from salt. Besides, it is a non-discontinuous process and is able to achieve higher yield. Aisha Asghar et al. [113] used 2,5-diaminoterephthalic acid as the ligand, and $NaNO_3$ aqueous solution as the electrolyte to prepare Mn-MOFs (Fig.10(a)). In comparison with that obtained by the solvothermal method (Fig.10(b)), the MOFs prepared herein have a better rod-like crystal structure, which is larger and more regular (Fig.10(c)). Liu et al. [114] successfully fabricated $Cu_3(HHTP)_2$ MOFs film onto Cu foil by employing electrochemical synthesis method (Fig.10(d)(e)). The conductivity and the mobility of the films are superior to those prepared by the liquid-liquid interface method. Qin et al. [115] prepared multilayer 3D MOFs ZIF-8 anti-protein structures by cathodic electrodeposition (Fig. 10(f)-(h)).

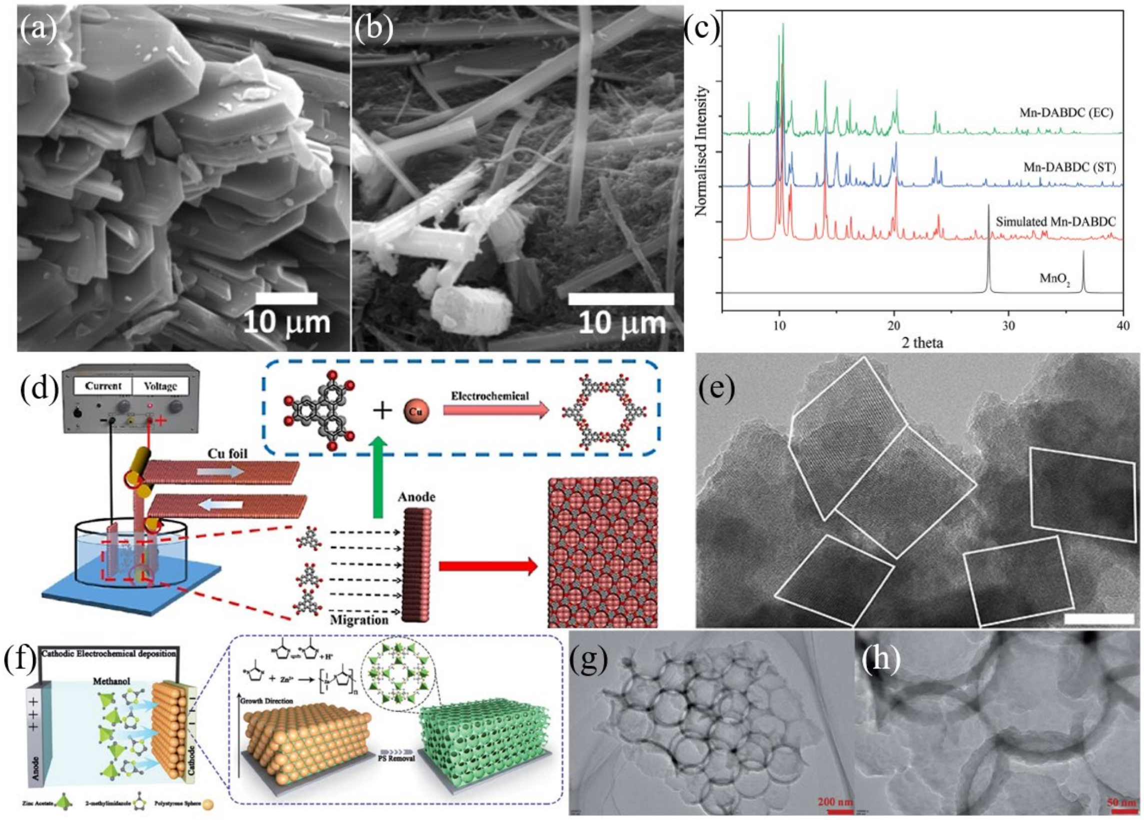

Fig. 10 SEM images of (a) Mn-MOFs synthesized by electrochemical synthesis and (b) solvothermal method, and (c) the corresponding XRD patterns[113]. Copyright 2021, The Royal Society of Chemistry. (d) schematic diagram of electrochemical reaction cell and coordination reaction between Cu^{2+} and HHTP ions for the preparation of $Cu_3(HHTP)_2$ films on copper foil, (e) TEM images of $Cu_3(HHTP)2$ films[114]. Copyright 2021, Wiley-VCH GmbH. (f) schematic diagram of electrochemical preparation of 3D ordered large microporous MOFs, (g) (h) TEM images of 3D MOFs ZIF-8[115]. Copyright 2022, The Royal Society of Chemistry.

2.2.4 Ultrasonic method

Ultrasonic method is a simple, inexpensive and effective method to prepare MOFs. The study finds that the frequency of 20 KHz-1 MHz can make the molecules in the solvent react chemically. During the sonication process, bubbles are formed, grown and collapsed. And this process results in local heating of the solution. The metal ions and the organic ligands are dissolved in an organic solvent, followed by the coordination of preparing MOFs in the presence of ultrasonic waves. Meghdad Karimi et al. [116] used 1,4-phthalic acid as ligand to prepare Ce-UiO-66 under high-density ultrasonic irradiation at 305 W. Fig.11(a)(b) shows the preparations by two different methods. It can be clearly seen that the Ce-UiO-66 synthesized by ultrasonic method has a more regular morphology. Li et al. [117] prepared CoFe-MOF using the ultrasonic method (Fig.11(c)), which can effectively promote the dispersion of particles compared with physical mixing and magnetic stirring methods, thus improving the charge transfer between Co and Fe ions. Shen et al. [118] successfully synthesized U-CD-MOF with the assistance of ultrasound and tuned the crystal morphology and size by varying the ultrasound power, as shown in Fig. 11(d-k).

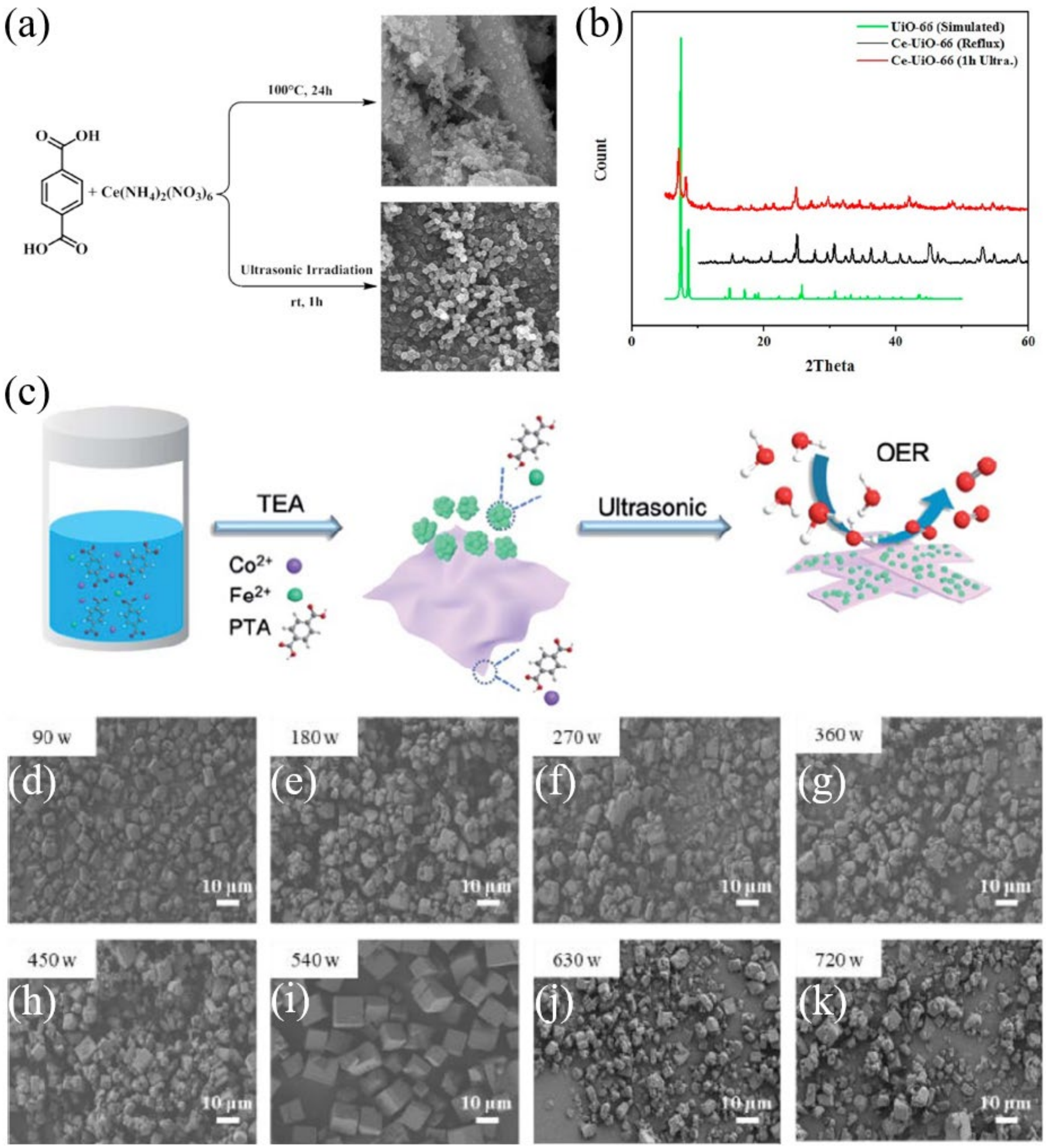

Fig. 11 (a) Preparation of Ce-UiO-66 by sonochemical route and the corresponding (b) XRD patterns[116]. Copyright 2021, Elsevier Inc. (c) schematic diagram of CoFe-BDC prepared by sonication[117]. Copyright 2021, The Royal Society of Chemistry. (d-k) SEM images of U-CD-MOF prepared at different sonication powers[118]. Copyright 2022, Elsevier B.V.

2.2.5 Mechanochemical synthesis

MOFs are thermodynamically more stable than other solid substances due to their structural characteristics. Unlike solvent-based reactions, in solids, metal ions are bound and need to be released by external forces. The metal cations released under external force undergo coordination reactions with available adjacent organic molecules to form MOFs. In the absence of solvent, the use of a small amount of solvent can provide the necessary mobile ions for metal ions and organic ligands to complete the coordination reaction. Without solvent, the reaction cannot proceed spontaneously, and the metal source and organic ligand cannot undergo coordination reaction. So in order to trigger the reaction, additional energy has to be applied in some way, such as by ball milling and extrusion. Wang et al[119] synthesized Im@NENU-3 by mechanochemical synthesis using homophthalic acid as the ligand (Fig.12(a)-(c)). And the synthesized samples shows a significant increase in proton conductivity over the normal NENU-3. Yi et al[120] synthesized PtZn-MOF-74 through applying 2,5-dihydroxyterephthalic acid as the ligand (Fig.12(d)-(f)). It is noteworthy that the metal ions are all able to cooperate with the ligand due to the limited diffusion coefficient, which can effectively avoid their agglomeration. Liu et al[121] prepared a series of HKUST-1 MOFs by mechanical grinding method (Fig.12(g)). It is found that this method can greatly shorten the preparation time and reduce the particle size of the prepared MOFs in comparison with those prepared by hydrothermal method, as shown in Fig.12(h)(i).

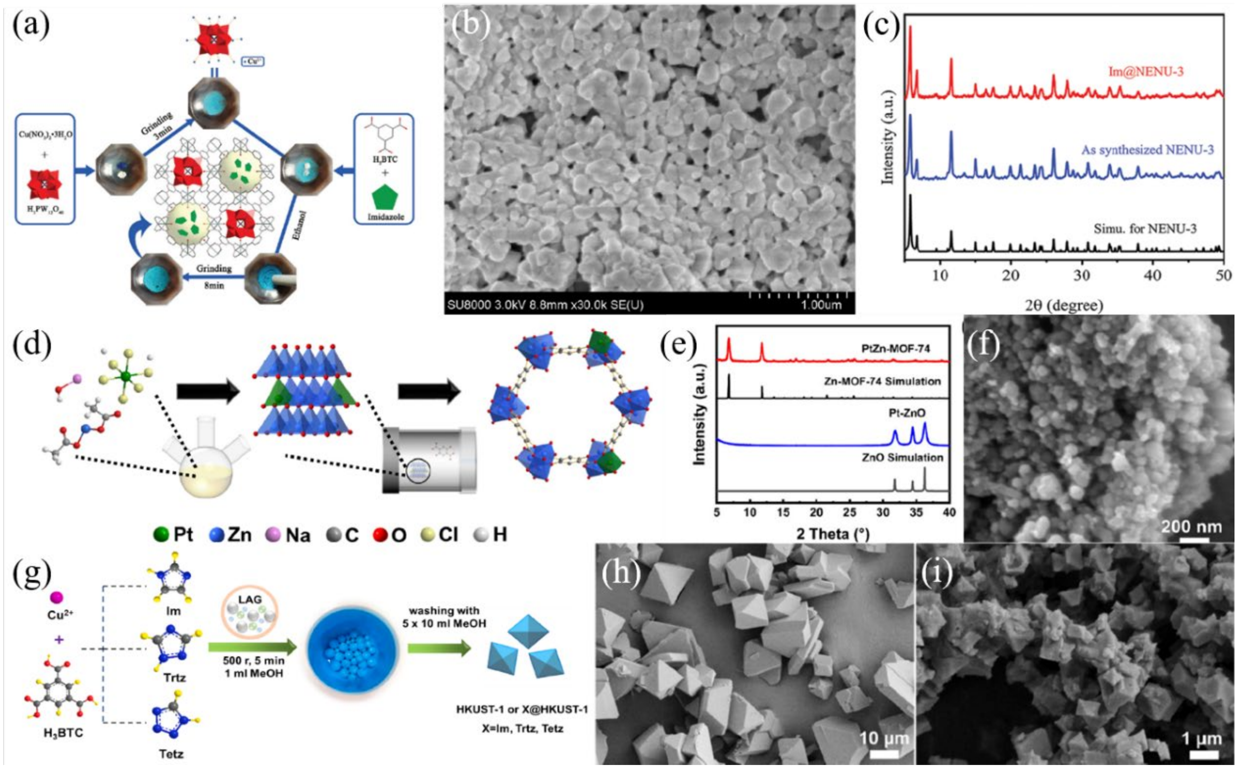

Fig. 12 (a) Synthesis processes of Im@NENU-3 by one-pot mechanochemical method, the corresponding (b) SEM image and (c) XRD patterns[119]. Copyright 2021, The Royal Society of Chemistry. (d) schematic diagram of the hydrothermal preparation of Pt-ZnO and PtZn-MOF-74, and the cprresponding (e) XRD patterns, (f) SEM images of PtZn-MOF-74[120]. Copyright 2021, Elsevier Ltd. (g) schematic diagram for praparing HKUST-1, SEM images of (h) HKUST-1 synthesized by hydrothermal method and (i) mechanical grinding method[121]. Copyright 2022, Elsevier B.V.

3. Electromagnetic wave absorption theory

According to Maxwell's electromagnetic wave theory, the electric and magnetic fields are perpendicular to each other and are alternately generated in the time-varying electromagnetic field. The electromagnetic wave absorbing materials are able to transform electromagnetic wave energy incident into other forms of energy via different losses including ohmic, dielectric and magnetic losses inside the material, thereby reducing the reflected echo signal of the electromagnetic wave.

When an incident electromagnetic wave comes into the absorbing material, three things can happen, as shown in Fig.13. Some of them is reflected by the material (reflected wave), part of them is absorbed by the material (absorbed wave), as well as the rest of the electromagnetic wave passes through the material (transmitted wave). The electromagnetic wave interacts with the material and is converted into different sorts of energy during the propagation process, or is consumed by interference cancellation, so as to achieve the purpose of stealth and loss of electromagnetic wave energy. When designing absorbing materials, researchers hope that incident electromagnetic waves are dissipated as much as possible inside the materials rather than be reflected and transmitted. Therefore, an excellent electromagnetic wave absorbing material commonly meet two requirements: one is excellent impedance matching; the other is powerful electromagnetic wave attenuation ability.

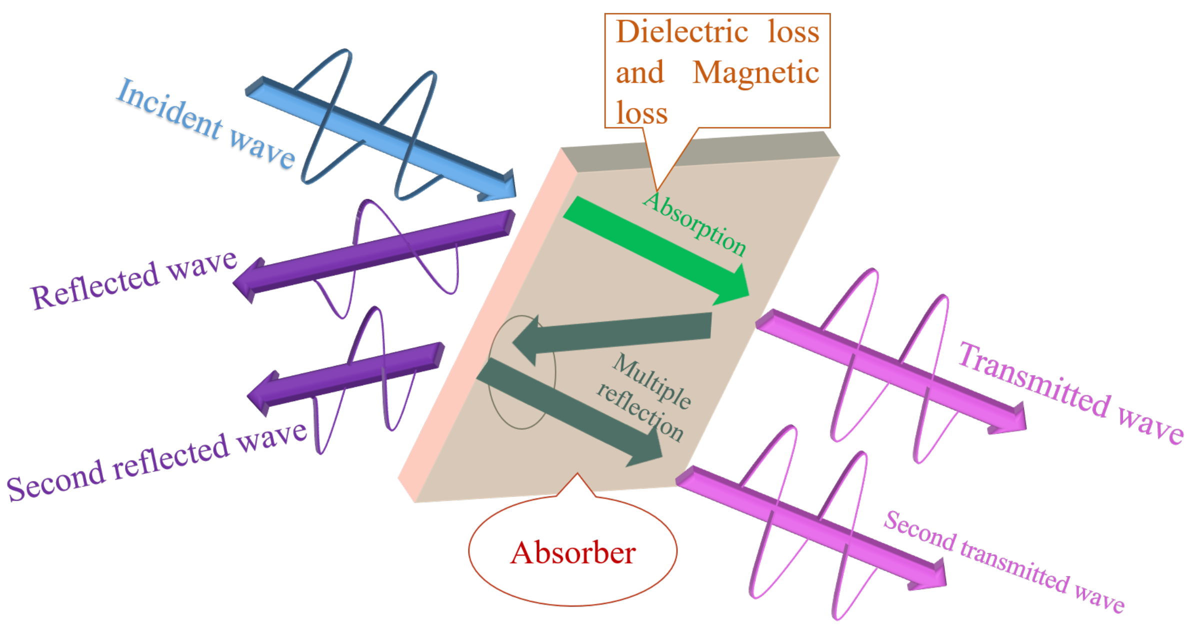

Fig. 13 Schematic diagram of the electromagnetic wave absorption principle.

3.1 Evaluation of absorbing properties of materials

Vector network analyzer is employed to measure four electromagnetic parameters of materials, namely complex permeability ($\mu_r = \mu' - j\mu''$) and complex permittivity ($\varepsilon_r = \varepsilon' - j\varepsilon''$), where μ' and ε' represent the storage of magnetic field energy and electric field energy, respectively, and μ'' and ε'' represent the energy dissipation capability[122, 123]. In general, the larger the values of μ'' and ε'' are, the stronger the dissipation of incident electromagnetic wave energy is. And the composition regulation in composite materials is also based on the improvement of μ'' and ε''. The magnetic loss tangent ($tan\delta_\mu = \frac{\mu''}{\mu'}$) and the dielectric loss tangent ($tan\delta_\varepsilon = \frac{\varepsilon''}{\varepsilon'}$) separately represent the magnetic and dielectric losses of the material to electromagnetic waves[124, 125].

According to transmission line theory, the reflection loss (RL) value is widely applied to assess the electromagnetic wave absorption characteristics of absorbing materials, and the value is calculated by the following formulas[126-129]:

$$Z_{in} = Z_0 \sqrt{\frac{\mu_r}{\varepsilon_r}} \tan h \left(\frac{j2\pi f d}{c} \times \sqrt{\mu_r \varepsilon_r}\right) \tag{1}$$

$$RL = 20log \left|\frac{Z_{in} - Z_0}{Z_{in} + Z_0}\right| \tag{2}$$

in which Z_{in} and Z_0 are separately the input impedances of absorbing material and free space, f is the electromagnetic wave frequency, d is the material thickness, as well as c is the light speed. If the RL value is below -10 dB, meaning that 90% electromagnetic wave is dissipated, and the related frequency range is called the EAB.

On the basis of equations (1) and (2), it can be known from the above theory that the reflected wave impedance is not only related to the complex permittivity and permeability, but also directly affected by the thickness of the material. Especially as the absorbing material thickness is equal to the odd multiple of 1/4 wavelength of the electromagnetic wave, the excellent impedance matching is obtained. The thickness *d* of the material satisfies[130, 131]:

$$d = \frac{\lambda_e}{4} = \frac{nc}{4f\sqrt{|\mu_r||\varepsilon_r|}} \tag{3}$$

At this time, the phase difference between the reflected wave onto the material and the reflected wave at material/substrate interface reaches π, which satisfies the condition of interference cancellation, resulting in a low electromagnetic wave reflectivity peak at this frequency. This is the so-called 1/4 wavelength of the thickness of the absorbing material matching theory. Under the matching thickness of 1/4 wavelength, the corresponding matching frequency generate a strong absorption wave, and part of the absorption is caused by the interference cancellation of the reflected waves on the upper and lower surfaces of the absorbing material. The final absorbing effect of the absorbing material is the result of the combined effect of the interference cancellation of 1/4 wavelength and the intrinsic loss of the material. In addition, the optimized electromagnetic wave absorption performance of materials needs to focus on two points: impedance matching characteristics and attenuation capability.

3.2 Impedance matching

From the reflectivity expression in formula (1), in order to achieve the ideal absorbing effect of electromagnetic waves with zero reflectivity, the impedance matching Z is required to satisfy the following formula[132]:

$$\mathrm{Z} = \frac{Z_{in}}{Z_0} \tag{4}$$

when Z is 1, the impedance of the absorbing material is in consistence with that of the free space, that is, the electromagnetic wave incident is able to completely access the absorbing material without reflection. In this case, the impedance matching is good, favoring the further electromagnetic wave attenuation. Conversely, impedance mismatching can lead to strong reflections and reduced absorption. Therefore, lower RL values occur as the absorbing material has excellent attenuation capabilities. Sometimes equation (4) is also written as $Z = \left|\frac{Z_{in}}{Z_0}\right|$, a revision to take into account the fact that in practice, the real and imaginary parts of Z_{in} and Z_0 can appear inconsistent[133].

According to equations (1) and (4), if Z = 1, and the input impedance Z_{in} is required to satisfy the following equation[134, 135]:

$$\left|\frac{Z_{in}}{Z_0}\right| = \sqrt{\frac{\mu_r}{\varepsilon_r}} \tan h \left(\frac{j2\pi f d}{c} \times \sqrt{\mu_r \varepsilon_r}\right) \tag{5}$$

Therefore, by calculating the $\left|\frac{Z_{in}}{Z_0}\right|$ value of the absorbing material under different thicknesses, the evaluation of the material's electromagnetic wave impedance matching can be achieved. However, Equation (5) is obviously a complex equation, and complex operations bring difficulties to the calculation and evaluation of the impedance matching degree. Therefore, based on equation (5), complex number equation theory removes the imaginary unit, and obtains the equivalent real number formulas as follows[136, 137]:

$$\sin h^2 \,(\mathrm{Kfd}) = \mathrm{M} \tag{6}$$

$$\mathrm{K} = \frac{4\pi\sqrt{\mu'\varepsilon'}}{c} \frac{\sin\left[\left(\delta_\varepsilon + \delta_\mu\right)/_2\right]}{\cos\delta_\varepsilon \cos\delta_\mu} \tag{7}$$

$$\mathrm{M} = \left[4\mu' \cos\delta_\varepsilon \varepsilon' \cos\delta_\mu\right]\left[\left(\mu' \cos\delta_\varepsilon - \varepsilon' \cos\delta_\mu\right)^2 + \left(\tan\frac{\delta_\mu - \delta_\varepsilon}{2}\right)^2 \left(\mu' \cos\delta_\varepsilon + \varepsilon' \cos\delta_\mu\right)^2\right]^{-1} \tag{8}$$

And the Δ (equation (9)) is further defined as a function of impedance matching degree[138]:

$$\Delta = \left|\sin h^2\,(\mathrm{Kfd}) - \mathrm{M}\right| \tag{9}$$

The Δ represents the degree of that the electromagnetic wave input impedance of the absorbing product deviates from the optimal matching state. With the decrease of Δ, the impedance of the product gets closer to that of the free space, and at the same time, a lower reflection coefficient is presented. Especially when Δ tends to 0, the product possesses the best impedance matching, and the reflectivity of electromagnetic waves is close to 0.

3.3 Electromagnetic wave loss mechanism

3.3.1 Interference cancellation

In the situation of that the thickness *d* is the odd multiple of the quarter wave of incident electromagnetic wave, there is phase difference π between the incident wave and the reflected wave. Because of the amplitude is equal, the interference phenomenon will occur. The basic principle can be based on the quarter wave, and the formula is described as follows[139-141]:

$$d_m = \frac{\lambda_e}{4} = \frac{nc}{4f\sqrt{|\mu_r||\varepsilon_r|}} \quad \text{（n=1，3，5···）} \tag{10}$$

in which d_m, f and c are matching thickness, frequency, and light speed in vacuum, respectively. The interference cancellation mechanism shows that the electromagnetic wave can also be attenuated by designing the structure of the material.

3.3.2 Absorption loss

Absorption loss mechanisms mainly include dielectric and magnetic losses, in which the former further includes conductivity and polarization losses.

(1) Conductivity loss

In the alternating electric field, conductivity loss is the dissipation of the induced current into other form of energy. As the electromagnetic wave enters the interior of the conductive medium, the electrons and holes form a microcurrent, which in turn consumes the energy of the electromagnetic wave. On the basis of the free electron theory ($\varepsilon'' \approx \sigma/(2\pi\varepsilon_0 f)$, σ: conductivity, ε_0: vacuum dielectric constant), it can be known that the value of ε'' increases with increasing the conductivity, followed by enhancing the conductivity loss.

(2) Dielectric loss

Polarization loss is mainly due to the polarization relaxation processes caused by alternating electric fields. These processes typically contains interfacial polarization, dipole polarization, ion polarization and electron polarization relaxations. The first relaxation is the result of defects, heterojunctions and non-homogeneous charge distribution in the phase interface. The polarization relaxation of dipoles is because of the generation of dipoles (e.g. functional groups) and defects, induced by the electric field. When the electric field disappears, the dipole returns to its original state and this dipole moment with the constant deflection or displacement of the alternating electric field can consume the electric field energy and thus dissipate the electromagnetic wave. However, ion and electron polarizations generally occur in the high frequency range (10^3-10^6 GHz). Hence they are often neglected. The mechanism of dielectric loss can be explained by the Debye polarization relaxation model, which defines the complex permittivity as follows[142-144]:

$$\varepsilon_r' = \varepsilon_\infty + \frac{\varepsilon_s - \varepsilon_\infty}{1 + (2\pi f)^2\tau^2} \tag{11}$$

$$\varepsilon_r'' = \frac{2\pi f\tau(\varepsilon_s - \varepsilon_\infty)}{1 + (2\pi f)^2\tau^2} + \frac{\sigma}{\varepsilon_0\omega} \tag{12}$$

Among them, ε_r', ε_r'', ε_∞ and ε_s are real and imaginary parts of the permittivity, relative permittivity at the high frequency limit, and static permittivity, respectively, f is the test frequency, and τ is the polarization relaxation time.

When ignoring electrical loss, the following equation can be obtained by combining the above two equations[145, 146]:

$$\left(\varepsilon_r' - \frac{\varepsilon_s + \varepsilon_\infty}{2}\right)^2 + \left(\varepsilon_r''\right)^2 = \left(\frac{\varepsilon_s - \varepsilon_\infty}{2}\right)^2 \tag{13}$$

Therefore, the Debye polarization relaxation is obtained via a semicircular ε'-ε'' curve (Cole-Cole curve). If the conductivity loss cannot be ignored, the upward tail of the curve can be regarded as the conductivity loss. And the longer the tail is, the stronger the conductance loss is.

(3) Magnetic loss

Magnetic loss originates from natural, alternating, eddy current, hysteresis effect and domain wall resonances. The hysteresis effect is caused by irreversible magnetization in the high frequency field, so it can be neglected in the low frequency range. Domain wall resonance commonly happens in the frequency below GHz and is also negligible. Natural resonance mainly occurs in 2-4 GHz, and exchange resonance mainly happens in 4-12 GHz. Eddy current loss is the energy loss caused by the closed-line current caused via the magnetic field of the electromagnetic wave ($C_0 = \mu''(\mu')^{-2}f^{-1} = 2\pi\sigma\mu_0 d^2$) [147, 148]. The value of C_0 is generally used to evaluate the eddy current loss. If C_0 is constant, the magnetic loss is ascribed to the eddy current loss. However, this loss will generate a lot of heat, which can reduce the service life of the absorbing material. The eddy current can be suppressed to improve the utilization rate of the wave absorber. In addition, in the GHz range, the magnetic permeability decreases due to the small Snoek limit, which can limit the application of magnetic materials. The Snoke limit is described as follows[149-152]:

$$(\mu_i - 1)f_r = \frac{1}{3\pi}\gamma M_s \tag{14}$$

in which γM_s, γ, M_s, μ_i and f_r separately denote to Snoek's constant, magnetic spin ratio, magnetization, initial permeability, and natural resonance frequency. According to formula (14), because the magnetic spin ratio and the saturation magnetization of the material are constant, μ_i is negatively correlated with f_r. As the frequency increases, the initial permeability inevitably decreases, which limits the applications in high frequency. Compared with other magnetic materials, typical soft magnetic materials including Fe, Co and Ni have higher Snoek limit, so they are more and more widely used for electromagnetic wave absorption. On the other hand, it is also a meaningful method to destory the Snoek limit by adjusting the anisotropy. The Snoek limit is described as follows[150]:

$$(\mu_i - 1)f_r = \frac{1}{3\pi}\gamma M_s\sqrt{\frac{H_\theta}{H_\emptyset}} \tag{15}$$

Among them, H_θ and $H_\emptyset$ separately represent the anisotropic equivalent magnetic field in the easy and hard magnetization directions. Therefore, as these values are large, magnetic permeability and resonant frequency simultaneously increase, which further enhance the magnetic loss at high frequencies, compared with magnetically anisotropic materials. According to Kittel's equation (16), the natural resonant frequency is determined by[153-155]:

$$f_r = \frac{\gamma|H_k|}{2\pi} \tag{16}$$

where γ is magnetic spin ratio and H_k is energy of magnetocrystalline anisotropy, which can be described as follows:

$$H_k = \frac{4|K_1|}{3\mu_0 M_s} \tag{17}$$

where K_1 is the anisotropy coefficient. In addition, K_1 is determined by:

$$K_1 = \frac{\mu_0 M_s H_c}{2} \tag{18}$$

where H_c is the coercivity. Therefore, according to the above three formulas, when H_c increases, the value of f_r moves to the high frequency. Accordingly, the magnetic loss at high frequency increases.

3.4 Decay constant

The attenuation capability of the absorbing material is usually evaluated by two points. On the one hand, dielectric and magnetic losses are evaluated by using the tangent of dielectric loss ($tan\delta_\varepsilon = \frac{\varepsilon''}{\varepsilon'}$) and the tangent of magnetic loss ($tan\delta_\mu = \frac{\mu''}{\mu'}$). On the other hand, the total loss capacity is evaluated by the attenuation constant (α)[156-158]:

$$\alpha = \frac{\sqrt{2}\Pi f}{c}\sqrt{(\mu''\varepsilon'' - \mu'\varepsilon') + \sqrt{(\mu''\varepsilon'' - \mu'\varepsilon')^2 + (\mu'\varepsilon'' + \mu''\varepsilon')^2}} \tag{19}$$

From equation (19), one can find the larger ε'' and μ'' are, the larger α is, and the stronger the attenuation ability of the absorbing material is. However, due to the limitation of matching characteristics, ε'' and μ'' should be in a moderate range.

4. MOF-derived absorbing materials

4.1 MOF-derived single metal absorbing materials

4.1.1 MOF-derived magnetic monometallic absorbing materials

Materials such as metal, carbon, ferrite and conductive polymers are used to adsorb electromagnetic waves. Metal and the corresponding alloys possess a power absorption intensity, however, the frequency range is generally narrow. Carbon materials contain carbon nanofibers, CNTs as well as graphene belong to well-light absorbing materials. If a single metal is combined with the carbon-based materials, the prepared material has advantages of high absorption strength, light texture and wide absorption frequency. MOFs synthesized by Fe, Co, Ni magnetic metal is a good precursor, which can be converted to a magnetic monolithic/carbon-based composite materials at different temperatures[159]. A comparison of the absorbing properties of the MOFs derived from magnetic metals is detailed in Table 1.

Xiang et al [160] used 1, 4-phthalic acid as the ligand to prepare Fe-MOFs precursor with regular octahedral shape, as shown in Fig 14(a)(b). Afterwards, the precursor was calcined at 700 °C to obtain Fe_3O_4@NPC composites (Fig 14(c)). The prepared sample (40 wt%) was evenly dispersed in a paraffin matrix, and the wave absorbing properties of the material are tested (Fig 14(d)(e)). At 9.8 GHz and 3 mm, the RL_{min} and the EAB can reach -65.5 dB and 4.5 GHz, respectively. And the EAB reaches 13.8 GHz in the case of 2-5 mm, covering 4.2~18 GHz. Fig 14(f) explains the wave absorption mechanism of the Fe_3O_4@NPC composite. After carbonization, Fe-MOF produces a porous carbon structure with a large number of mesopores producing dipole polarization, while Fe_3O_4 also produces magnetic losses such as natural resonance and exchange resonance. And after carbonization, a heterogeneous interface of Fe_3O_4/C is created, producing interfacial losses, so that the whole material has good absorption performances under the synergistic effect of Fe_3O_4 and porous carbon. Yang et al.[161] used fumaric acid as the ligand and prepared rod-like Fe-based MOFs precursor MIL-88A (Fig 14(g)(h)). Then, thiourea and MIL-

88A precursor were heated at 650 °C under nitrogen atmosphere to prepare Fe_7S_8/C composite, as shown in Fig 14(i). The prepared Fe_7S_8/C sample was uniformly combined with paraffin (filling rate of paraffin of 65 wt%) to test the absorbing performances (Fig 14(j)(k)). At 1.67 mm, the RL_{min} is -68.86 dB at 12.08 GHz. At 1.45 mm, the EAB reaches 4.56 GHz in the ragne of 12.32-16.88 GHz.

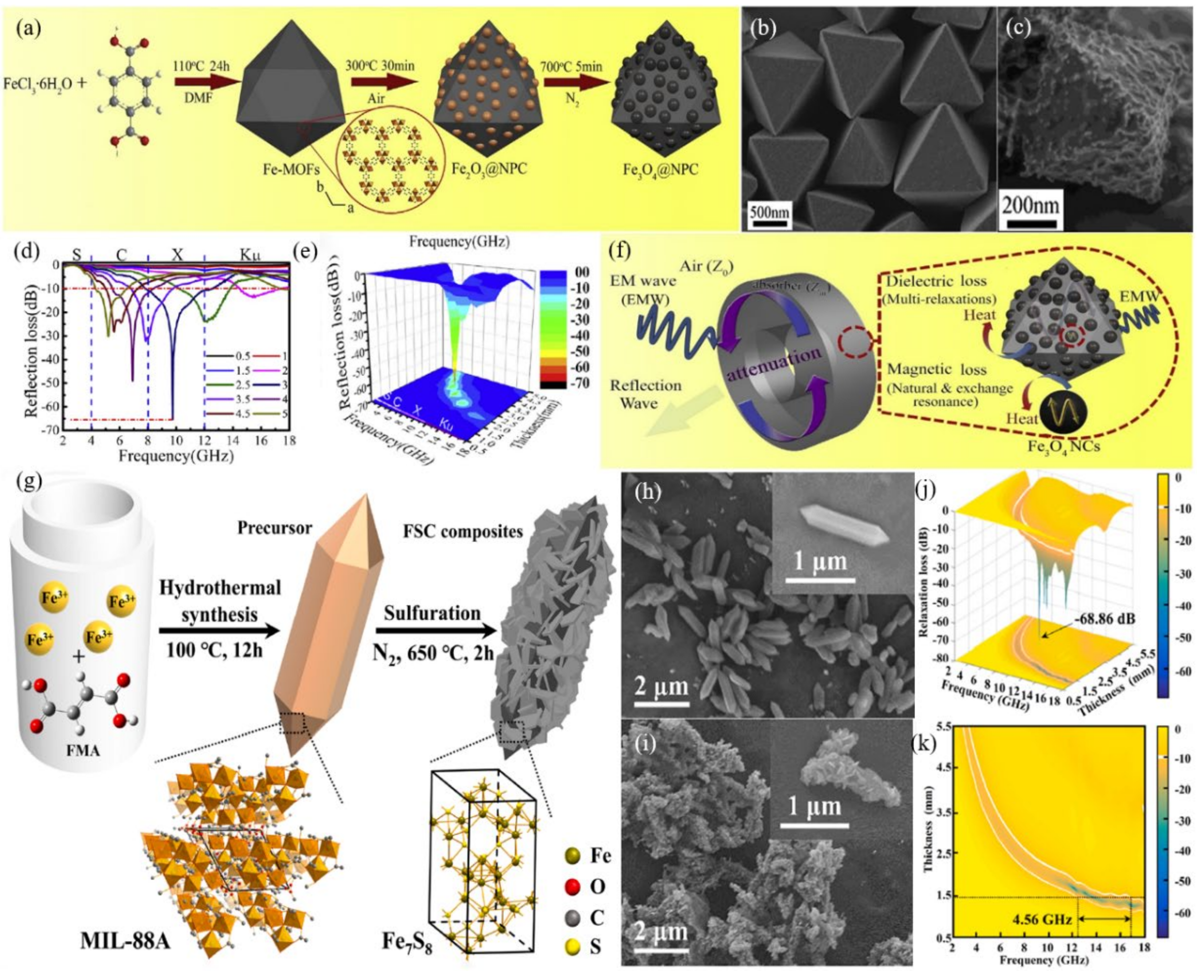

Fig. 14 (a) Preparation processes of Fe_3O_4@NPC composites. SEM images of (b) Fe-MOFs and (c) Fe_3O_4@NPC, (d) RL of Fe_3O_4@NPC composites at different thicknesses and (e) the corresponding 3D reflection image, (f) schematic diagram of the mechanism of Fe_3O_4@NPC composites[160]. Copyright 2018, Elsevier Ltd. (g) Flow chart of the preparation of Fe_7S_8/C composites, SEM images of (h) MIL-88A precursors and (i) Fe_7S_8/C, (j) 3D RL and (k) 2D RL of Fe_7S_8/C composites[161].

In Fig. 15(a)(b), Huang et al.[162] took 2-methylimidazole as the ligand to synthesize the eighteen face shape ZIF-67 precursor. After calcination at 500 °C, Co@NCNT composite was obtained (Fig. 15(c)). In Fig. 15(d)-(f), its RL_{min} can reach -53.0 dB at 16.8 GHz and 1.8 mm thickness. In the case of 2.0 mm, the EAB reaches 6.2 GHz (11.6-17.4 GHz). Fig 15(f) demonstrates the wave absorption mechanism of Co@NCNT. After carbonization, ZIF-67 produces a large number of Co/C heterogeneous interfaces generating interfacial polarization, and also a large number of ion transport channels making the material more conductive and more likely to dissipate electromagnetic waves. Wu et al. [163] used 2-methylimidazole as the ligand in Fig. 15(g) to prepare the ZIF-67 precursor with dodecahedral appearance. The precursor was calcinated at 400 °C to obtain Co_3O_4 particles (Fig. 15(h)). Then, the Co_3O_4 particles were reduced at different temperatures to obtain porous Co particles, which would be slowly passivated in air to produce CoO layer, thus obtaining porous Co/CoO particles (Fig. 15(i)). The prepared particles (50 wt%) was formed a mixture with paraffin to test wave absorption performances (Fig. 15(j)(k)). The RL_{min} of the Co/CoO particles reduced at 200 °C can reach -87.2 dB at 14.26 GHz and 1.0 mm. And at 1.0 mm, the EAB is 6.2 GHz (11.5-17.7 GHz).

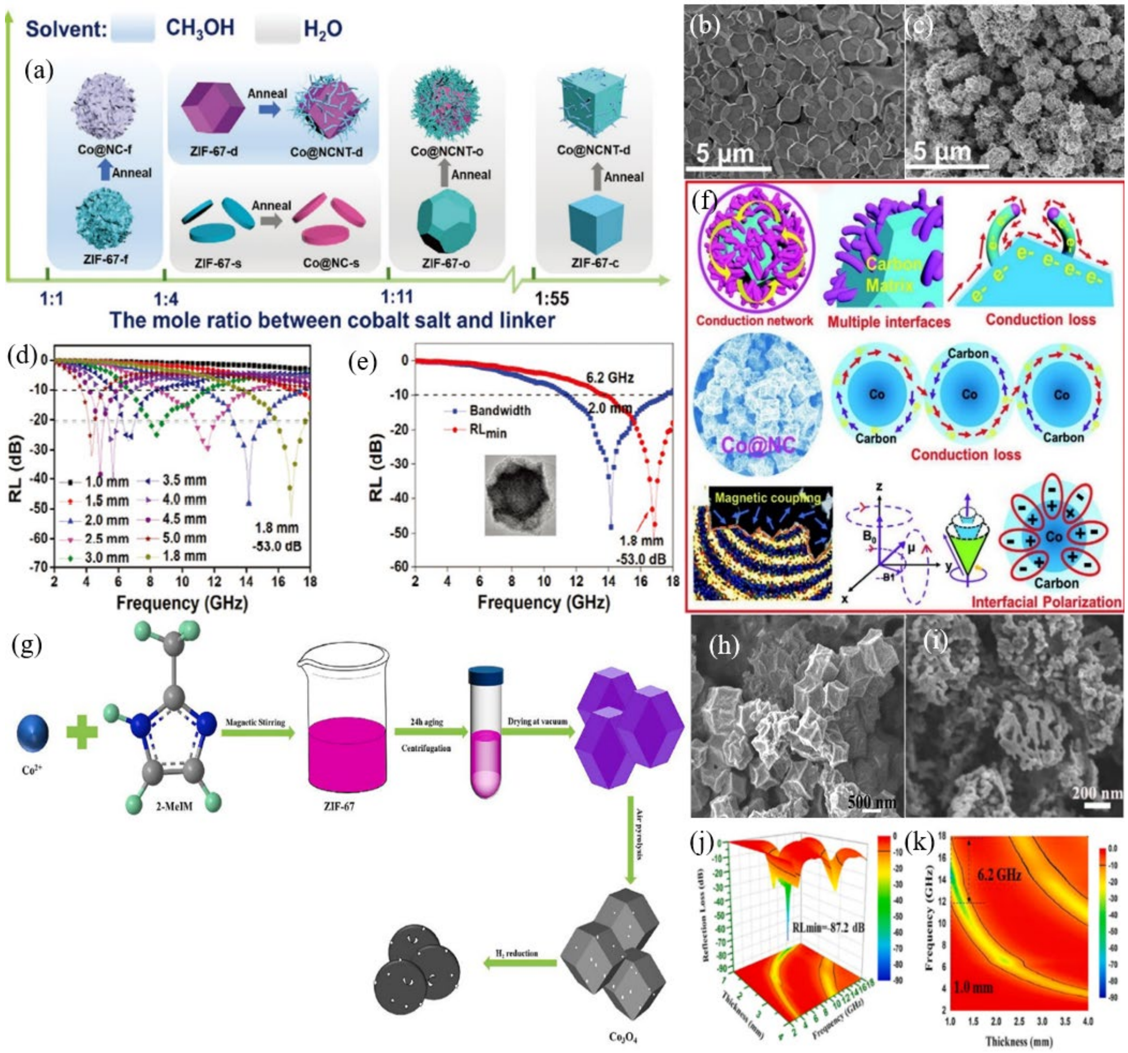

Fig. 15 (a) Flow chart of the preparation of Co@NCNT composites, SEM images of (b) ZIF-67 precursor and (c) Co@NCNT composite, (d) RL of Co@NCNT, (e) RL and EAB of Co@NCNT, (f) the absorbing mechanism of Co@NCNT[162]. Copyright 2020, WILEY-VCH Verlag GmbH & Co. KGaA, Weinheim. (g) Flow chart of the preparation of Co/CoO particles, SEM images of (h) Co_3O_4 particles and (i) Co/CoO particles, (j) 3D RL and (k) 2D RL of Co/CoO particles at different frequencies and thicknesses[163]. Copyright 2021, Elsevier B.V.

Jin et al[164] used terylene acid as the ligand and doped with pyridine (Fig 16(a)), and Ni-MOFs precursor with hexagonal sheet was prepared (Fig 16(b)). Afterwards, the N-doped Ni@NC nanoparticles were obtained by pyrolysis under argon at 650 °C (Fig.16 (c)). The prepared sample and paraffin wax were mixed evenly (sample filling rate of 30%), and the wave absorption performances are exhibited (Fig. 16(d)-(f)). It is found that the absorption performances are the best in the situation of 2 mL pyridine. At 17.28 GHz and 2.3 mm, RL_{min} can reach -37.29 dB, and the EAB is 6.21 GHz (11.79-18.0 GHz), covering the whole Ku band. Fig 16(f) shows the wave absorption mechanism of Ni@NC. The carbonization produces a heterogeneous structure, conductive network, carbon defects that can effectively generate conduction loss and polarization relaxation, and the dispersed Ni nanoparticles also provide some magnetic loss. Qiu et al[165] using homobenzoic acid as the ligand synthesized Ni-MOF hollow microspheres as precursor in the presence of PVP (Fig. 16(k)(g)). Then, the Ni/C composite was obtained by pyrolysis under Argon atmosphere at 600 °C, as shown in Fig. 16(h)-(j). 30 wt% Ni/C composite was mixed evenly with paraffin to test its absorbing performance (Fig. 16(l)(m)). At 16.1 GHz, the RL_{min} can reach -57.25 dB. In the situation of 1.8 mm, the EAB is 5.1 GHz.

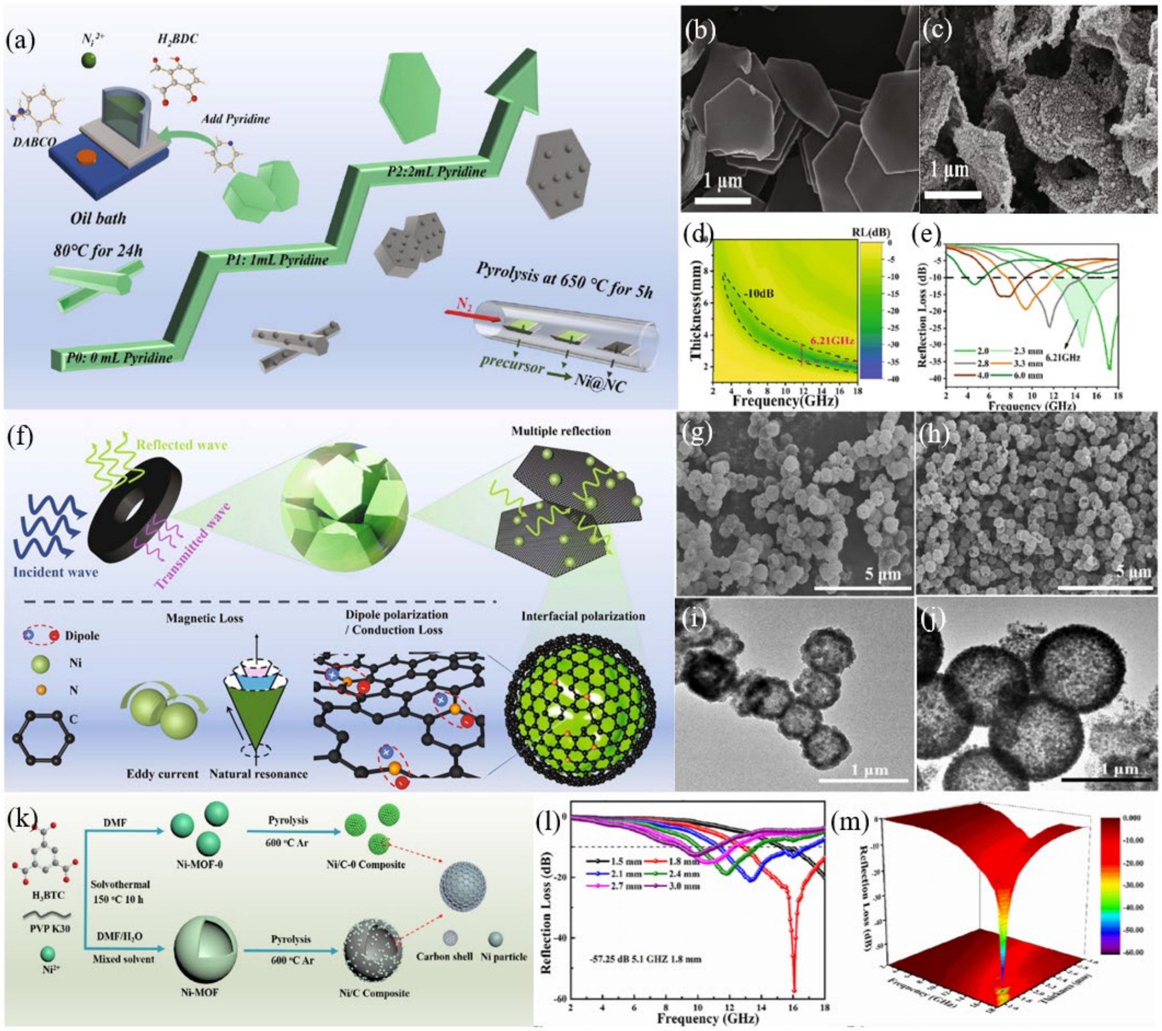

Fig. 16 (a) flow chart of the preparation of Ni@NC composites, SEM images of (b) Ni-MOF precursors and (c) Ni@NC, (d) 2D RL and (e) reflection curves at different thicknesses of Ni@NC composites, (f) absorption mechanism diagram of Ni@NC composites[164]. Copyright 2021, Elsevier B.V. SEM images of (g) Ni-MOF precursors and (h) Ni/C, (i) (j) TEM images of Ni/C, (k) flow chart of the preparation of Ni/C composites, (l) the reflection profile plots and (m) corresponding 3D RL of Ni/C at different thicknesses[165]. Copyright 2019, Elsevier B.V.

4.1.2 MOF-derived non-magnetic monometallic wave-absorbing materials

In recent years, non-magnetic metal-based MOFs such as Cu, Mn and Zr have also been attempted as precursors for wave-absorbing materials[166, 167], but they do not inherently have the same magnetic loss mechanism as magnetic metal-based MOFs. Therefore, the preparation of such precursors has mostly focused on the modulation of morphology and dielectric loss. A comparison of the absorbing properties of wave absorbing materials derived from MOFs from non-magnetic metals is detailed in Table 1. Li et al[168] synthesized the rod-like CU-MOF-74 precursor with 2,5-dihydroxy terephthalic acid as the ligand (Fig 17(a)(b)). Then, the precursor was treated in KOH solution for 180 min to transform it into a circular dodecahedron. After the calcination at 300 °C and the treatment in aqueous Na_2S solution, the final product with hollow dodecahedron shape with Cu_2S shell was obtained, as shown in Fig. 17(c). 20 wt% sample was mixed evenly with paraffin. In Fig. 17(e)(f). At 2.3 mm, the EAB can reach 6.2 GHz covering 11.8-18.0 GHz. Fig 17(g) shows the wave absorption mechanism of hollow Cu_2S. The material has a large number of defects and heterogeneous interfaces, which can effectively generate polarization relaxation. And the hollow structure can generate multiple reflections, which can effectively dissipate electromagnetic waves into thermal energy. Ma et al. [169] fabricated ZIF-67 precursor with 2-methylimidazole as the ligand (Fig. 17(h)). Afterwards, the precursor was carbonized at 700 °C for preparing Co@NPC composite. The composite was soaked in HF to remove Co atoms and only NPC was left. The resulting NPC was then combined with $Cu(NO_3)\cdot 3H_2O$ and calcined at different temperatures to obtain the final CuO@NPC composite, as shown in Fig. 17(i). The resulting composite (50 wt%) was mixed evenly with paraffin, and its absorbing performances were displayed in Fig. 17(j). One can find the RL_{min} can reach -57.5 dB at 14.9 GHz, and the EAB is 4.7 GHz (13-17.7 GHz) at 1.55 mm.

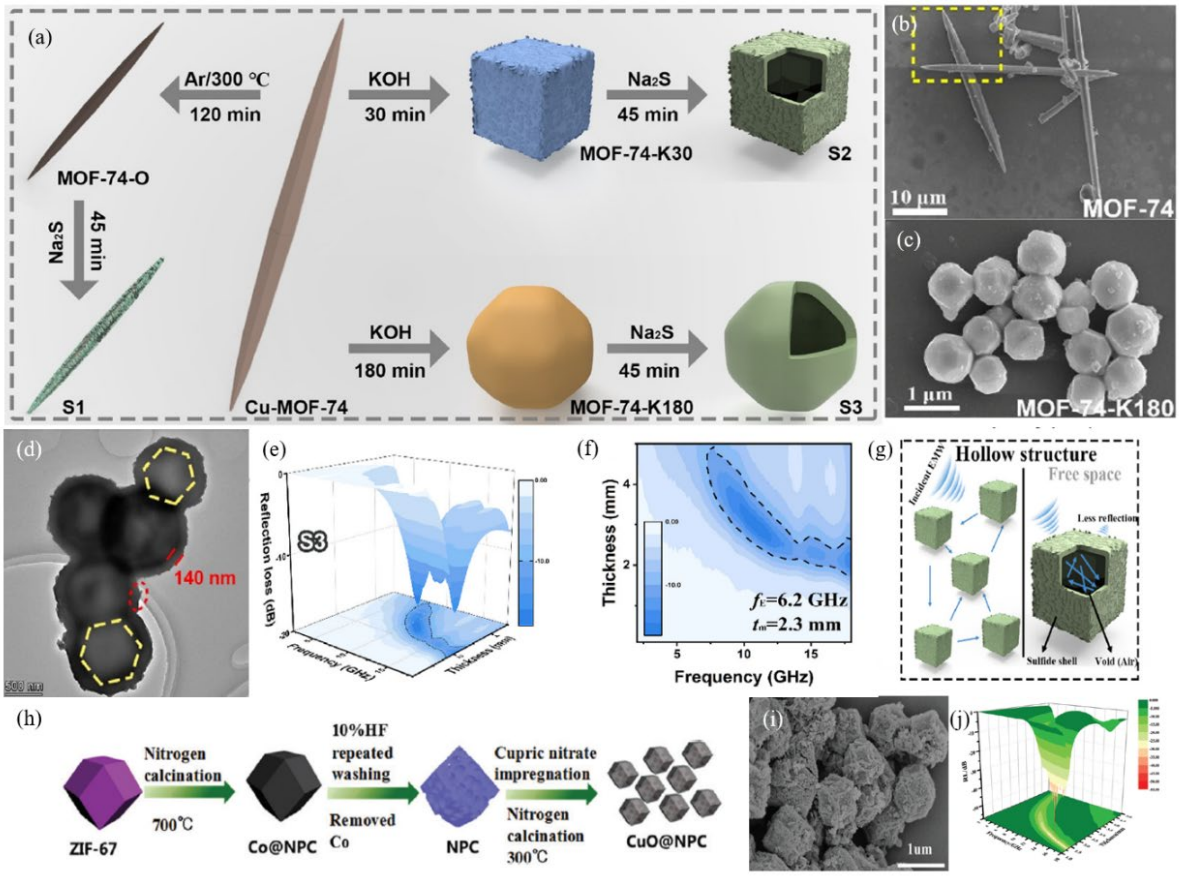

Fig. 17 (a) Fabrication flow chart of Cu-MOF-74-K180, SEM images of (b) MOF-74 and (c) MOF-74-K180, (d) TEM images of MOF-74-K180, (e) 3D RL diagram and (f) 2D mapping diagram of MOF-74-K180, (g) loss mechanism diagram of the MOF-74-K180[168]. Copyright 2021, Elsevier Inc. (h) preparation flow chart of CuO@NPC composite, (i) SEM image of the composite, (j) 3D RL diagram of the composite[169]. Copyright 2016, The Royal Society of Chemistry.

Yang et al. [170] took 2, 5-dihydroxy terephthalic acid as the ligand and prepared the MN-MOF-74 precursor, as shown in Fig.18(a)(b). Then, the prepared precursor was calcined at high temperature to obtain MnO@NPC composite (Fig.18(c)). After that, the MnO@NPC composite was oxidized with $KMnO_4$ in an acidic environment to obtain MnO_2@NPC composite (Fig.18(d)). The prepared MnO_2@NPC composite (50 wt%) was mixed evenly with paraffin to test its absorbing performances. From Fig.18(e)-(g), it can be seen that the RL_{min} and the EAB can separately reach -63.21 dB and 4.04 GHz at 12.48 GHz and the matching thickness is 2.05mm. Zhang et al[171] prepared the UIO-66 precursor with terylene acid as the ligand, which was calcined at different temperatures to obtain the ZrO_2/C composite (Fig.18(h)-(j)). 50 wt% composite was mixed evenly with paraffin to test its absorbing performances. Fig.18(k)(l) show that the RL_{min} can reach -58.7 GHz when the thickness is 1.5mm at 16.8 GHz, and the EAB is 5.5 GHz at 1.7mm.

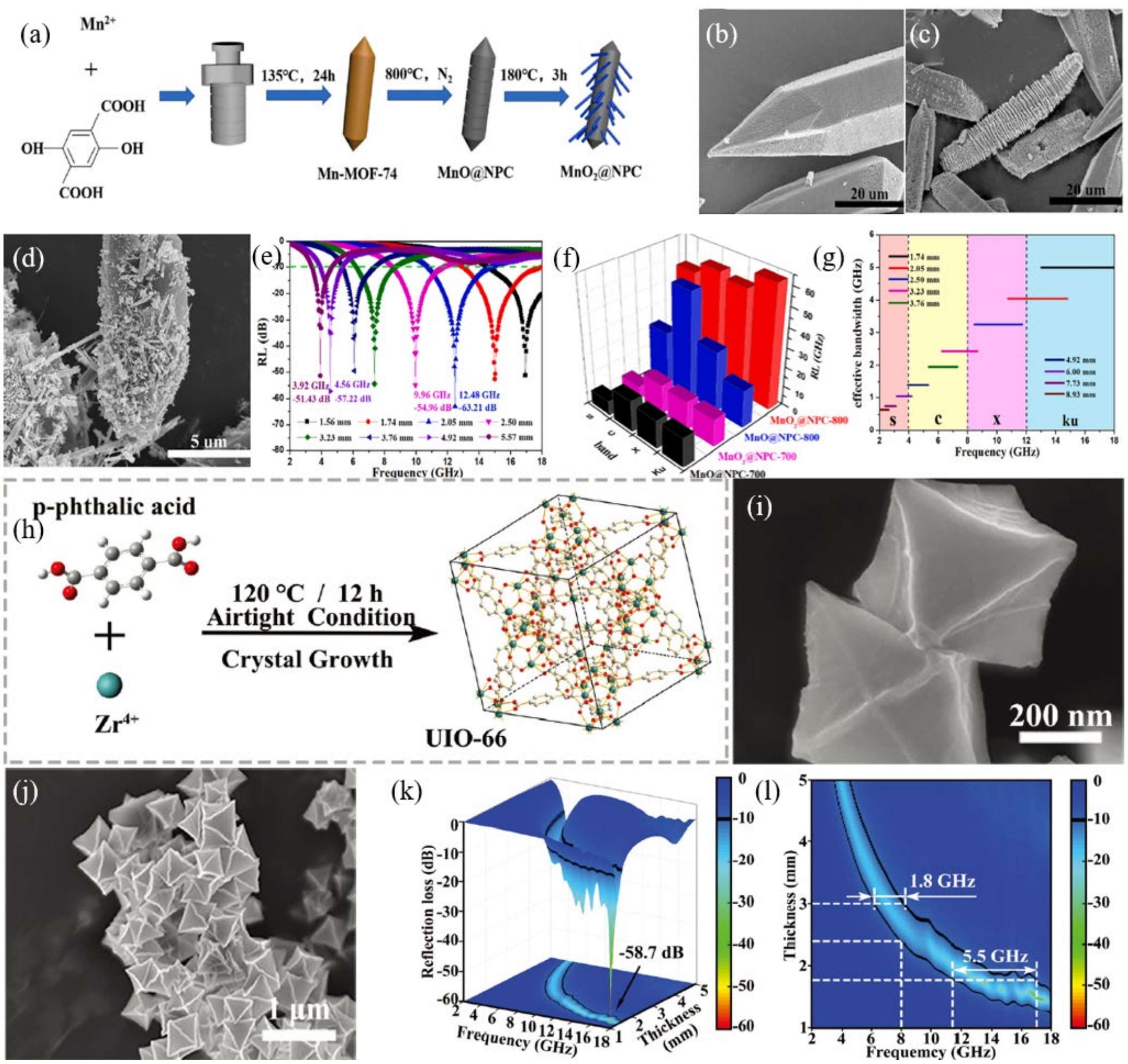

Fig. 18 (a) preparation flow chart of MnO_2@NPC composite, SEM image of (b) MN-MOF-74, (c) MnO@NPC and (d) MnO_2@NPC, (e) RL curve of MnO_2@NPC composite at different thicknesses, (f) 3D RL of all samples, (g) EAB plots of

MnO_2@NPC composite at different thicknesses[170]. Copyright 2020, Elsevier B.V. (h) synthesis schematic of UIO-66, (i) and (j) SEM images of ZrO_2/C, (k) 3D RL diagram and (l) 2D mapping diagram of ZrO_2/C composite[171]. Copyright 2019, the Partner Organisations.

Table 1 Wave absorption properties of monometallic MOF-derived absorbing materials.

Microwave absorbing materials	Loading (wt%)	RL_{min}			EAB			Ref
		Value (dB)	f_m (GHz)	Thickness (mm)	Value (GHz)	Range (GHz)	Thickness (mm)	
Ni@NC	30	-37.29	17.28	2.3	6.21	11.79-18.00	2.3	[164]
Cu-MOF-74-K180	20	-15.1	-	2.3	6.2	11.8-18.0	2.3	[168]
ML-Ni/C	20	-65.33	-	2.4	7.6	10.4-18	2.8	[172]
Co/C	25	-30.31	11.03	3	4.93	8.31-13.24	3	[173]
Co@C	30	-62.12	11.85	2.4	13.9	4.1-18	3	[174]
MOF-160	30	-73.5	13.8	3.3	6.1	9.8-15.9	3.3	[175]
Fe_3O_4@NPC	60	-65.5	9.8	3	4.5	-	3.0	[160]
Ni@C-ZIF	40	-86.8	7.25	2.7	7.4	4-11.4	2.7	[176]
Fe_7S_8/C	65	-68.86	12.08	1.67	4.56	12.32-16.88	1.45	[161]
Co-LDHs	5	-40.4	-	2	6.5	-	2.1	[90]
Co/C	40	-35.3	5.8	4	5.8	8.4-14.2	2.5	[177]

Ni/C	30	-57.25	16.1	1.8	5.1	12.9-18	1.8	[165]
ZrO_2/C	50	-58.7	16.8	1.5	5.5	-	1.7	[171]
Co/C	50	-59.8	-	3.0	5.7	8.7-14.4	3.0	[178]
H-Ni/C	30	-32.3	-	1.61	4.4	13.6-18.0	1.61	[179]
Co@NCNT	-	-53	16.8	1.8	6.2	11.6-17.4	2.0	[162]
CuO@NPC	50	-57.5	14.9	1.55	4.7	13-17.7	1.55	[169]
MnO_2@NPC	50	-63.21	12.48	2.05	4.04	-	2.05	[170]
Ni-MOF	50	-58	6	4.2	6.2	5-11.2	4.6	[180]
Ni@C	50	-46.9	-	3.3	6.8	-	-	[181]
HFNC	25	-59.38	-	3.0	6.4	11.6-18	2.4	[182]
Co/CoO	50	-87.2	14.26	1.0	6.2	11.5-17.7	1.0	[163]
Co/CNTs	30	-49.16	-	2.5	4.2	12.4-16.6	2.5	[183]
CNC	15	-27.2	3.4	6.68	5.97	12.0-18.0	1.88	[184]
Ni@C	80	-51.9	10.5	2.5	5.6	8.9	14.5	[185]
Co/C-HS	30	-66.5	17.6	1.53	4.4	11.0-15.4	2.0	[186]

Fe_4N@C	40	-42.0	-	2.5	6.7	10.8-17.5	2.5	[187]
MOF-74	40	-33.5	-	2.3	7.6	10.4-18.0	2.3	[188]

4.2 MOF-derived multi-metal absorbing materials

4.2.1 MOF-derived bimetallic absorbing materials

Compared with monometallic MOFs, bimetallic MOFs with various topologies in the center of metals with different electronic configurations are easier to adjust the microwave absorption properties. And their electromagnetic parameters can be easily optimized by reasonably controlling temperature. A comparison of the absorbing properties of absorbing materials derived from MOFs from polymetals is detailed in Table 2. Miao et al[189] synthesized Fe-Mn PBA and Fe-Co PBA MOFs prec ursors with hollow cage and solid box morphology, respectively (Fig.19(a)(b)). Fe/Co/C and Fe/Mn/C composites were obtained by annealing two precursors at different temperatures (Fig.19(c)(d)). Their absorbing properties were tested by mixing them evenly with paraffin (33 wt% filling). In Fig.19(e)(f), the RL_{min} of Fe/Co/C-900 composite at 16.1 GHz and 2.0 mm is -54.6 dB, and the EAB at 2.5 mm is 8.8 GHz. The EAB of Fe/Mn/C-800 composite is 6.7 GHz at 2.5 mm after treating at 800 ℃. Fig 19(b) demonstrates the wave absorption mechanism of the Fe/Co/C composite, where the graphitic carbon or nanorods in the complex provide additional interfaces and enhanced interfacial polarization, in addition to the magnetic loss provided by the FeCo core. And the combined effect of interfacial polarization and magnetic loss results in excellent electromagnetic wave attenuation. Pan et al. [190] synthesized rod-shaped CoZn-ZIF precursor with 2-methylimidazole as the ligand (Fig.19(g)). Afterwards, the precursor was returned at high temperature to obtain Co/NC composite (Fig.19(h)). The 15 wt% composite was mixed evenly with paraffin to test the wave absorption performances, as shown in Fig.19(j)(k). The composite prepared with the ratio of Co:Zn=3:1 has the best absorption performances. The

RL_{min} can reach -53.2 dB at 2.5 mm at 10.1 GHz. And in the case of 2.0 mm, the EAB is 5.0 GHz, which can cover the frequency range of 11.1-16.1 GHz.

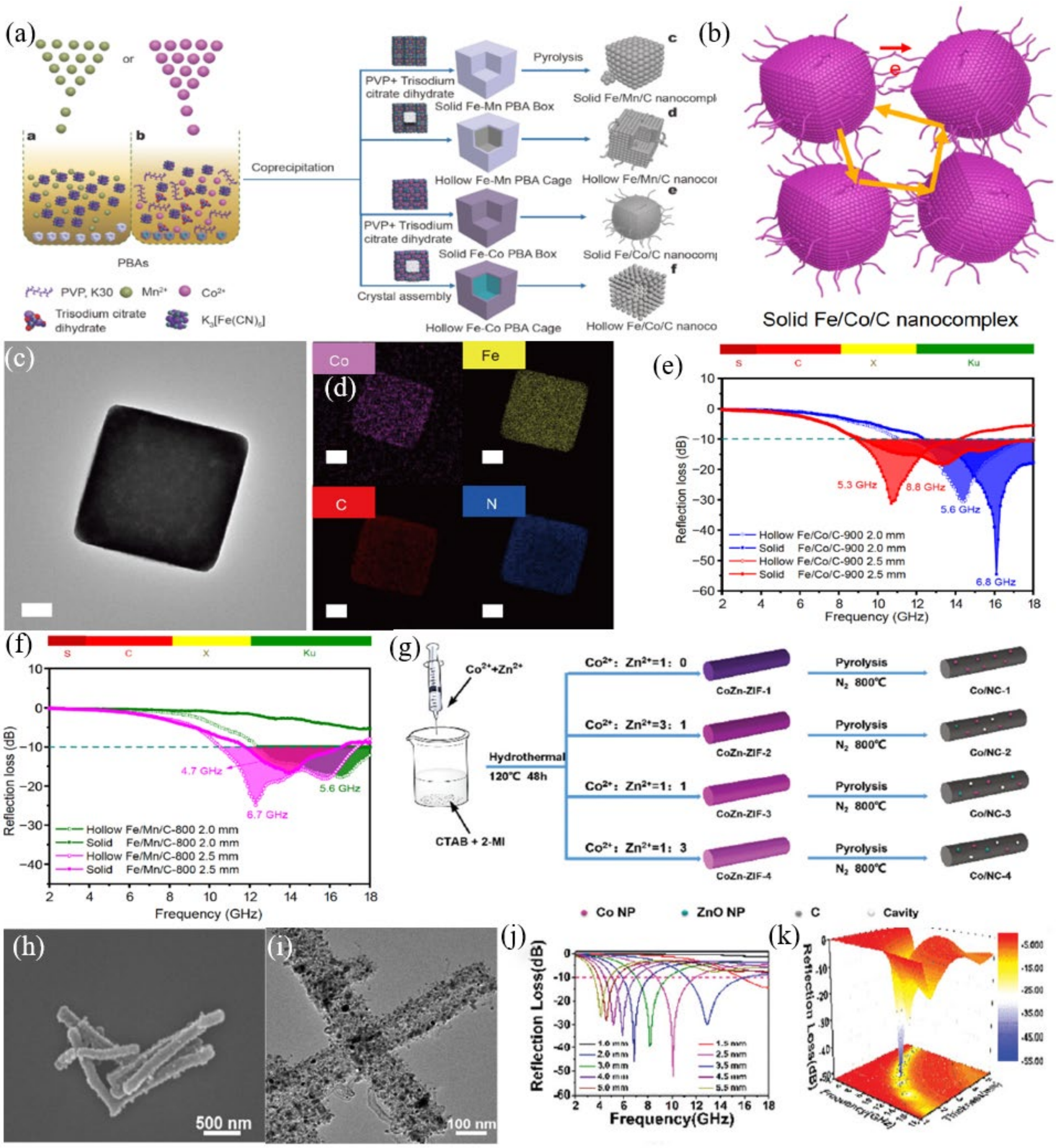

Fig. 19 (a) preparation flow diagram of solid box Fe/Co/C composites, (b) absorption mechanism diagram, (c) TEM images and (d) elemental mapping of solid box Fe/Co/C, (e) RL curves of solid box Fe/Co/C composites as well as (f) hollow cage Fe/Mn/C composites[189]. Copyright 2020, Science China Press and Springer-Verlag GmbH Germany, part of Springer

Nature. (g) preparation flow diagram of Co/NC composites, (h) SEM image and (i) TEM image of Co/NC composites, (j) RL diagram and (k) 3D RL diagram of Co/NC composites at different thicknesses[190]. Copyright 2021, The Royal Society of Chemistry.

Qiao et al. [191] synthesized PCN-415 (TiZr-MOFs) precursor with octahedral structure using terephoric acid as the ligand (Fig.20(a)-(c)). After high temperature annealing, $TiO_2/ZrTiO_4/C$ composite was obtained in Fig.20(b)-(e). 35 wt% composite was mixed evenly with paraffin to test its wave absorption performances (Fig.20(f)(g)). When the matching thickness of is 2.16 mm at 13.0 GHz, the RL_{min} can reach -67.8dB. When the thickness is 2.7 mm, the EAB covers 5.9 GHz. Wang et al[192] used 2, 5-dihydroxy terephthalic acid as the ligand (Fig.20(h)). By changing the ratio of Co^{2+} and Fe^{3+} ions, CoFe-MOF-74 precursors with different morphologies were fabricated (Fig.20(i)). After high temperature pyrolysis of CoFe-MOF-74 precursor, CoFe@C composite was obtained (Fig.20(j)). The CoFe@C composite material with bird's nest morphology only needs a filling ratio of 10 wt% to have good wave absorbing performances. In Fig.20(k)-(m), at 12.7 GHz and 2.8mm, the RL_{min} can reach -61.8 dB, and the EAB reaches 9.2 GHz (8.8-18 GHz).

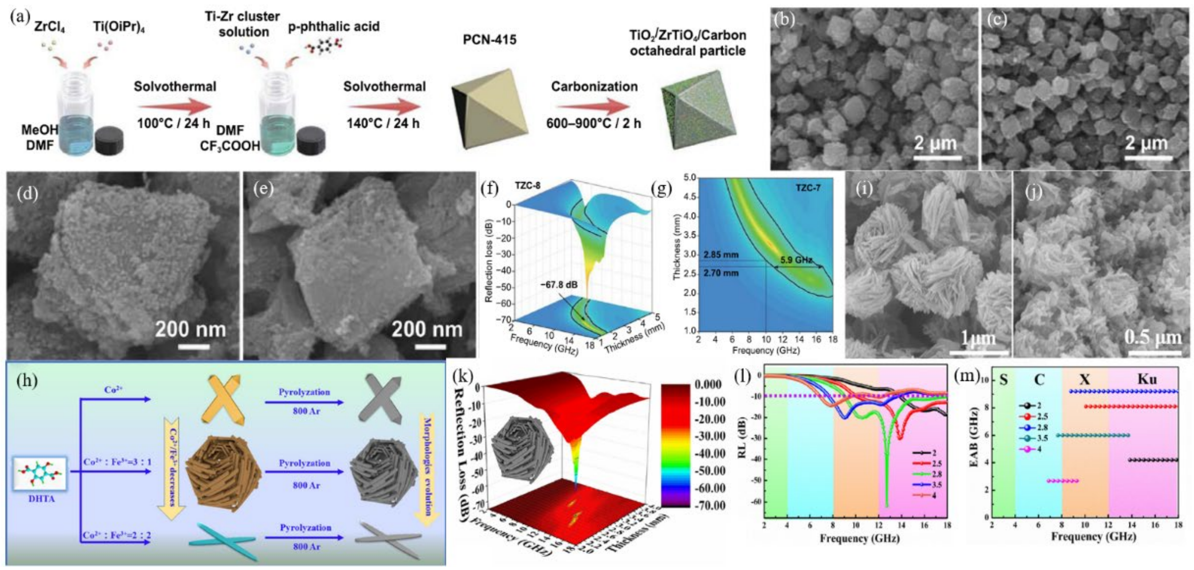

Fig. 20 (a) Flow diagram of fabrication of $TiO_2/ZrTiO_4/C$ composites, SEM images of $TiO_2/ZrTiO_4/C$ carbonized at (b) (c) 700 and (d) (e) 800 °C, (f) 3D RL images of $TiO_2/ZrTiO_4/C$-800, (g) 2D RL of $TiO_2/ZrTiO_4/C$-700[191].Copyright 2021,Springer. (h) flow chart of the preparation of CoFe@C composites with bird's nest morphology, SEM image of (i) CoFe-MOF-74 precursor and (j) CoFe@C, (k) 3D RL image of CoFe@C composites, (l) the RL of CoFe@C composites at different thicknesses, (m) the EAB of CoFe@C composites[192]. Copyright 2020, Elsevier Ltd.

Wen et al. [15] synthesized MOF precursors with different morphologies (Co-MOF-11, CoCd-MOF-11 and CoZn-MOF-11) by hydrothermal method (Fig.21(a)). Then, the precursors were treated by annealing at high temperature. Among them, the Co@CNTs composite obtained by CoCd-MOF-11 precursor has the best absorbing performances. In Fig.21(e)-(g), at 2.0 mm, the RL_{min} can reach -76.6 dB, and the EAB is 6.2 GHz, which can cover 11.76-18 GHz. Yang et al[193] prepared CoZn-MOF precursors with hexagonal morphology (Fig.21(h)-(j)), with 2-methylimidazole as the ligand. Then, the prepared precursors were processed at high temperature to obtain Co@ZnO@NC composites (Fig.21(k)(l)). The composite has good absorbing properties at 30 wt% filling rate. In Fig.21(m)-(o), at 8.7 GHz, the RL_{min} can reach -61.9 dB at 3.4 mm. As the thickness is 2.3 mm, the EAB can reach 5.5 GHz (11.6-17.1 GHz).

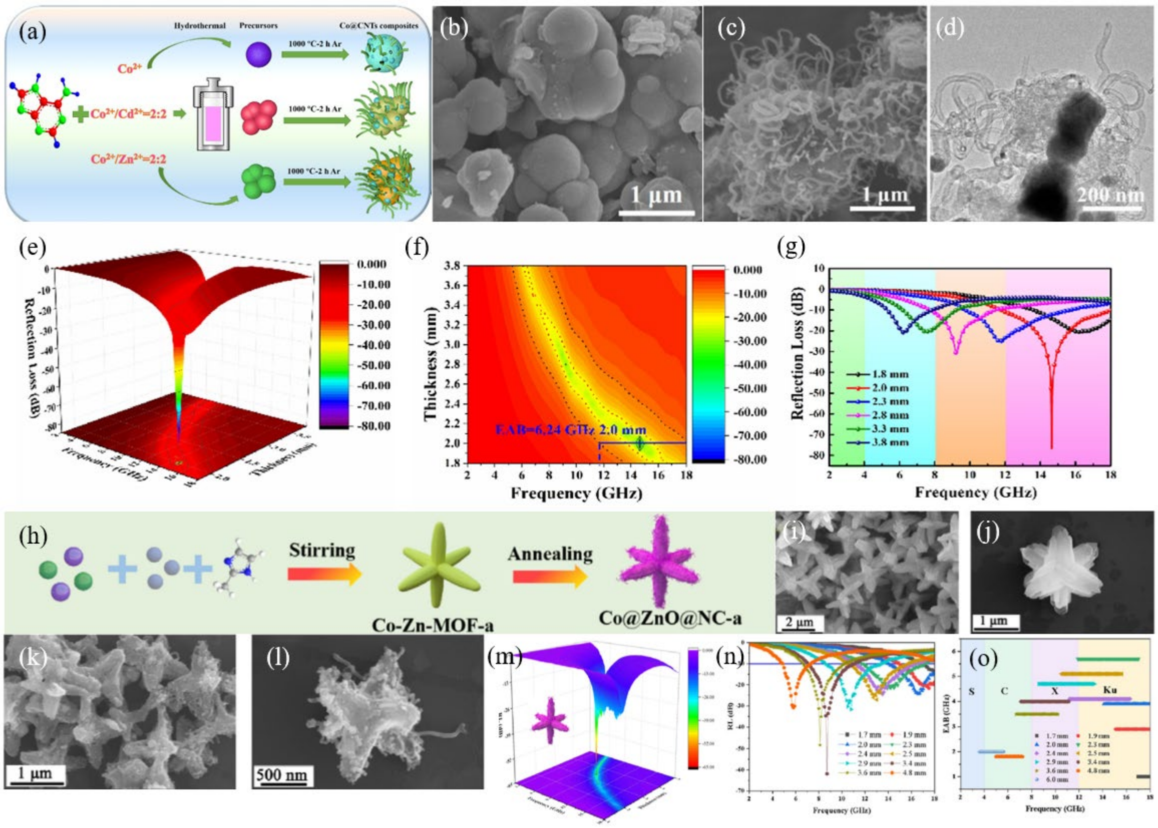

Fig. 21 (a) Flow chart of the fabrication of Co@CNTs composites, SEM images of (b) CoCd-MOF-11 precursors and (c) Co@CNTs composites, (d) TEM images of Co@CNTs composites, (e) 3D RL, (f) 2D contour maps and (g) RL at different thicknesses of Co@CNTs composites[194]. Copyright 2021, Elsevier Inc. (h) schematic illustration of Co@ZnO@NC composites, (i)(j) SEM images of CoZn-MOF precursors, (k)(l) SEM images of Co@ZnO@NC composites, (m) 3D RL, (n) RL at different thicknesses and (o) EAB of of Co@ZnO@NC composites[193]. Copyright 2022, Elsevier Ltd.

4.2.2 MOF-derived trimetal absorbing materials

Cui et al.[195] using 2-methylimidazole as the ligand fabricated ZIF-67@ZIF-8 precursor (Fig.22(a)-(c)). After adding $Ni(NO_3)_2 \cdot 6H_2O$, the ZIF-67@ZIF-8/Ni^{2+} precursor was prepared, as shown in Fig.22(d)(e). Finally, the Co@ZnO/Ni@NC composite was obtained at 600 °C

(Fig.22(f)-(n)). 27% wt% composite was mixed evenly with paraffin wax, and its absorbing performances were measured, as displayed in Fig.22(o)(p). The composite at 4.1 mm and 8.2 GHz has the RL_{min} up to -55.0 dB and the EAB up to 12.6 GHz (5.4-18 GHz). In Fig.22(q)(r), Ouyang et al.[196] used 2, 5-dihydroxyterephoric acid as the ligand and fabricated FeCoNi-MOF-74 precursor. After pyrolysis at high temperature, the FeCoNi@C composite was obtained (Fig.22(s)-(x)). 38 wt% composite material was mixed with paraffin wax evenly, and the wave absorption performances were presented in Fig.22(y)(z). The RL_{min} and the EAB of FeCoNi@C composite can reach -64.75 dB and 8.08 GHz at 15.44 GHz and 2.1 mm covering 9.92-18 GHz.

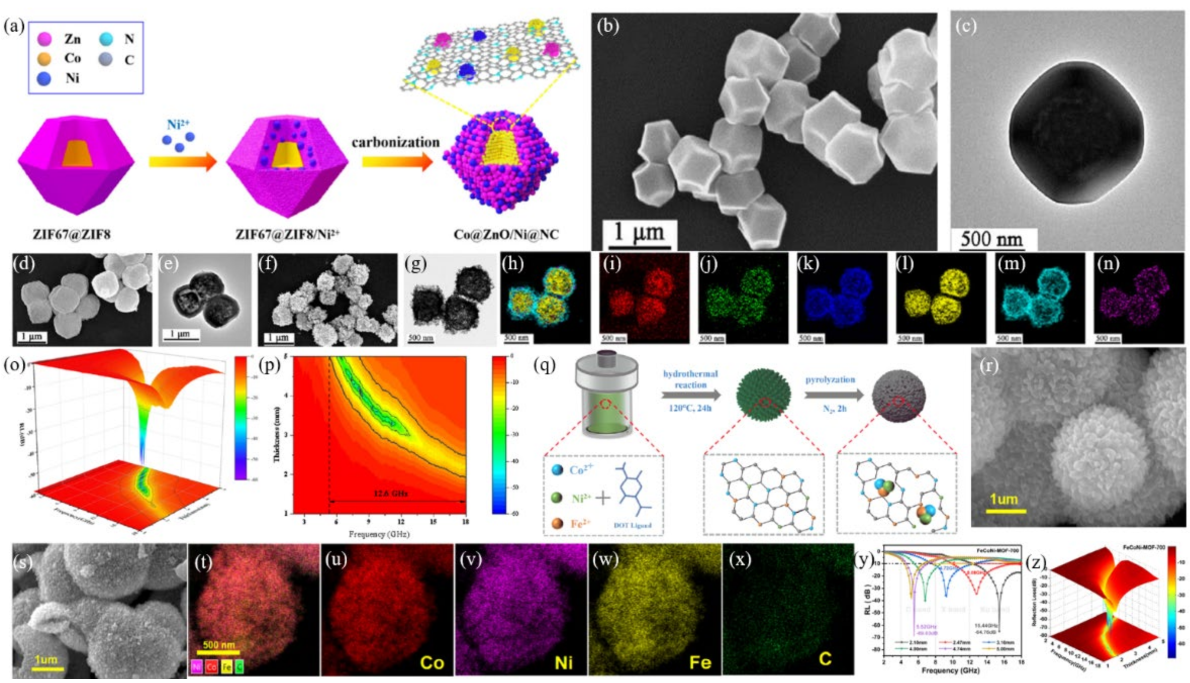

Fig. 22 (a) Flow chart of the preparation of Co@ZnO/Ni@NC composites, (b) SEM and (c) TEM images of ZIF-67@ZIF-8 precursors, (d) SEM and (e) TEM images of ZIF-67@ZIF-8/Ni^{2+}, (f) SEM and (g) TEM images of Co@ZnO/Ni@NC, (h-n) elemental mapping images, (o)(p) 3D RL maps and corresponding contour maps[195]. Copyright 2021, Elsevier Inc. (q) preparation flow diagram of FeCoNi@C composites, SEM image of (r) FeCoNi-MOF-74 precursors and (s) FeCoNi@C

composites images and (t-x) corresponding elemental energy spectra, (y) the RL and (z) 3D RL of FeCoNi@C composites[196]. Copyright 2019, American Chemical Society.

Wu et al. [197] prepared a DUT-52@Co-doped MIL-88B (UM) precursor using terephthalic acid as the ligand (Fig.23(a)-(c)). Then, this precursor was become DM-700 composite at 700 °C (Fig.23(d)-(f)). DM-700 was mixed with paraffin wax (42.5 wt% filling) and its absorbing properties and mechanism were displayed in Fig.23(g)-(i). DM-700 achieves an RL_{min} of -65.2 dB at 13.0 GHz and 2.0 mm and an EAB of 4.8 GHz. Fig 23(i) shows the wave absorption mechanism of DM-700. The synergistic effect of multiple metals and the excellent magnetic loss optimize the impedance matching. The porous carbon structure and the rich heterojunction surface can increase the dipole polarization. And the special structure makes the material have a 3D conductive network, which increases the conduction loss, making DM-700 have excellent wave absorption performances. Yan et al. [198] faricated BMOFs Zn_xCo_yFe precursor using 2-methylimidazole as ligand (Fig. 23(j)). This precursor was treated in a mixed atmosphere of H_2 and N_2 at 800 °C to obtain Zn_xCo_yFe composites (Fig. 23(k)-(n)). The composite was mixed well with paraffin (15 wt% filling) and tested for its wave absorption properties. In Fig. 23(o)(p), the final sample of Zn_6CoFe exhibiting the best performances with the RL_{min} up to -66.0 dB at 9.43 GHz and 2.8 mm and the EAB of 4.79 GHz.

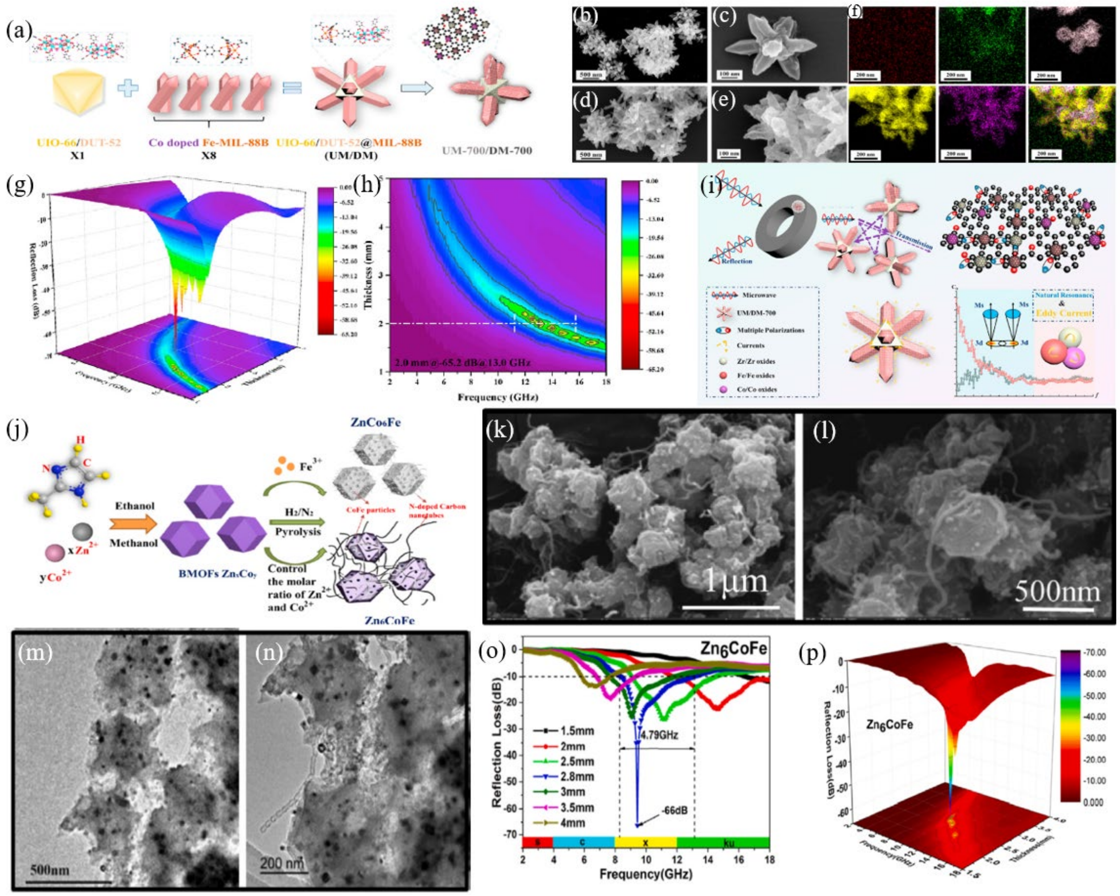

Fig. 23 (a) Flow chart of the preparation of DM(DUT-52@Co-MIL-88B)-700 composite, SEM images of (b)(c) DUT-52@Co-doped MIL-88B (UM) precursor and (d)(e) DM-700, (f) elemental mapping diagrams of DM-700, (g) 3D and (h) 2D RL of DM-700, (i) absorption mechanism map of DM-700[199]. Copyright 2021, Elsevier Ltd. (j) preparation flow chart of Zn_xCo_yFe composite, (k) (l) SEM and (m) (n) TEM images of Zn_6CoFe, (o) RL map and (p) 3D RL of Zn_6CoFe[198]. Copyright 2022, Elsevier Ltd.

Table 2. Wave absorption properties of polymetallic MOF-derived absorbing materials.

Microwave absorbing materials	Loading (wt%)	RL_{min}			EAB			Ref
		Value (dB)	f_m (GHz)	Thickness (mm)	Value (GHz)	Range (GHz)	Thickness (mm)	
NiCo@C	20	-55.4	15.3	2.5	7.2	11.8-18	2.5	[200]
Co@ZnO/Ni@NC	27	-55	8.2	4.1	12.6	5.4-18	4.1	[195]
Fe-ZnO	-	-33.22	14	2.6	4.24	13.76-18	2.6	[201]
Ni/NiO/Cu@C	10	-38.1	-	3.2	-	-	-	[202]
Cu/C	40	-52.44	6.76	4.2	6.8	11.2-18	2.3	[203]
CoFe alloys@ZnO@C	30	-40.63	-	2.2	5.84	-	2.2	[197]
Co/ZnO/C	30	-52.6	12.1	3.0	4.9	-	3.0	[204]
Co/Ni/C	40	-49.8	-	2.6	7.8	-	2.6	[205]
ZnO/Fe_3C/C	60	-30.4	14.5	1.5	4.96	-	1.5	[206]
Cu/Co/C	40	-25	13.72	1.95	5.68	-	1.85	[207]

Fe/Co/C	33	-54.6	16.1	2.0	8.8	-	2.5	[189]
FeCoNi@C	38	-64.75	15.44	2.1	8.08	9.92-18	2.1	[196]
Co/NC	15	-53.2	10.1	2.5	5.0	11.1-16.1	2.0	[190]
$TiO_2/ZrTiO_4/C$	35	-67.8	13.0	2.16	5.9	-	2.7	[191]
Co@C@MnO	20	-64.4	13.5	4.0	6.7	-	4.0	[208]
FeCo/MnO@NPC	50	-54.07	12.00	2.37	7.72	10.28-18	1.63	[209]
N-Ni-Co_xS_y/Ni_xS@C	25	-48.3	11.7	2.0	3.95	13.99-17.94	1.5	[210]
Co@NC-ZnO	25	-69.6	17.5	1.9	6.8	11.2-18	2.4	[211]
$Ni_{1-x}Co_x$@C	25	-59.5	-	4.5	4.7	9.9-14.6	2.5	[212]
CoFe@C	10	-61.8	12.7	2.8	9.2	8.8-18	2.8	[192]
Ni@C@ZnO	25	-55.8	-	2.5	4.1	-	2.5	[213]
CoMn@CN	25	-39.9	-	2.5	5.24	-	2.0	[214]
CoNi/C	10	-61.02	13.68	2.0	5.2	-	2.0	[215]
CoFe@C	40	-44.1	4.08	5.8	5.2	9.7-14.9	2.3	[216]
Co@CNTs	-	-76.6	-	2.0	6.2	11.76-18	2.0	[194]

DM(DUT-52@Co-MIL-88B)-700	42.5	-65.2	13.0	2.0	4.8	-	2.0	[199]
CoNC/CNTs	20	-15.37	15.49	1.5	4.5	13.5-18.0	1.5	[217]
Zn_xCo_yFe	15	-66	9.43	2.8	4.79	-	2.8	[198]
Co@ZnO@NC	30	-61.9	8.7	3.4	5.5	11.6-17.1	2.3	[193]
Co/ZrO_2/C	50	-57.2	15.8	3.3	11.9	6.1-18	3.3	[218]
Cu/NC@Co/NC	35	-54.13	9.84	3.0	5.19	10.18-15.37	2.5	[219]
Zn_6CoFe	15	-66	9.43	2.8	4.79	-	2.8	[198]
Zn@Co-C	30	-34.99	-	3.3	5.52	12.48-18.0	2.0	[220]

4.3 MOF-based composite absorbing materials

4.3.1 MOF-carbon composite absorbing materials

After carbonization MOFs form a composite of metal or metal oxide and carbon with good dielectric and magnetic losses, but there is an inherent disadvantage in that they do not have a good conductive network of their own. Therefore, although MOFs have excellent electrical conductivity after carbonization, the absence of a conductive network limits the ion transfer rate and prevents further enhancement of their wave absorption performances. Carbon-based materials with good attenuation properties for electromagnetic waves, good stability and low density can effectively improve this disadvantage when compounded with MOFs[221]. Common carbon materials include carbon black[222], carbon fibers[35, 223], CNTs[224-226], and graphene[227-230], as well as derivatives. The introduction of carbon materials not only forms a conductive network and increases ion transport channels, but the defects in its own structure and the heterogeneous interfaces formed with MOFs also increase the dielectric loss, further enhancing the wave absorption properties of the overall material. A comparison of the absorbing properties of the absorbing materials prepared by combining MOFs with carbon materials is shown in Table 3.

4.3.1.1 MOF-CNTs composite absorbing materials

Fang et al. [231] prepared CNTs with adsorbed metal Co^{2+} using floating catalyst CVD. The prepared CNTs were then mixed with 2-methylimidazole as ligand to obtain ZIF-67/CNTs precursors, and the precursors were heat-treated at high temperature to obtain Co-CNTs composites. The resulting Co-CNTs composites were mixed with paraffin wax at 20 wt% in order to test their wave absorption properties. The composite prepared at 500 °C declares the optimal performances, with an RL_{min} of -30 dB at 14.2 GHz and an EAB of 7.8 GHz (10.2-18.0 GHz) at 1.5 mm. The absorbing material can even maintain its good performances at -40 °C. Hu et al [232] synthesized Fe filled CNTs using a CVD process, which was mixed with $C_{10}H_{10}O_4$ ligand to prepare the CNT/FeCoNi-MOF precursors (Fig.24(a)). The prepared precursors were charred at high temperature under argon atmosphere to obtain CNT/FeCoNi@C composites (Fig. 24(c)(d)). The CNT/FeCoNi@C composite (30 wt% filling) was mixed well with paraffin wax and tested for its wave absorption properties. In Fig.24(i), the composite obtained at 700 °C shows the best absorption performances, with the RL_{min} up to -51.7 dB at 3.0 mm, as well as the EAB up to 6.0 GHz at 1.0 mm. Li et al [233] prepared MOF-5@MWCNTs precursors by using terephthalic acid as the ligand and adding multi-walled carbon nanotubes (MWCNTs) (Fig. 24(e)). Then, the precursors were calcined at 500 °C for different times to obtain ZnO@MWCNTs composites (Fig. 24(g)(h)). 20 wt% ZnO@MWCNTs composites were mixed with paraffin to test their wave absorption properties (Fig. 24(j)(k)). The sample obtained at 500 °C for 4 h displays the optimal performances, with an RL_{min} of -47.4 dB at 7.68 GHz at 2.7 mm and an EAB of 3.7 GHz at 1.5 mm. Fig 24(f) demonstrates the wave absorption mechanism of ZnO@MWCNTs. The introduction of MWCNTs forms a conductive network, which enhances the conduction loss, and a heterogeneous interface between ZnO and MWCNTs, which enhances the polarization relaxation and facilitates the dielectric loss. The multidimensional structure also increases the multiple reflection loss of electromagnetic waves, which is conducive to improving the wave absorption performances of the material.

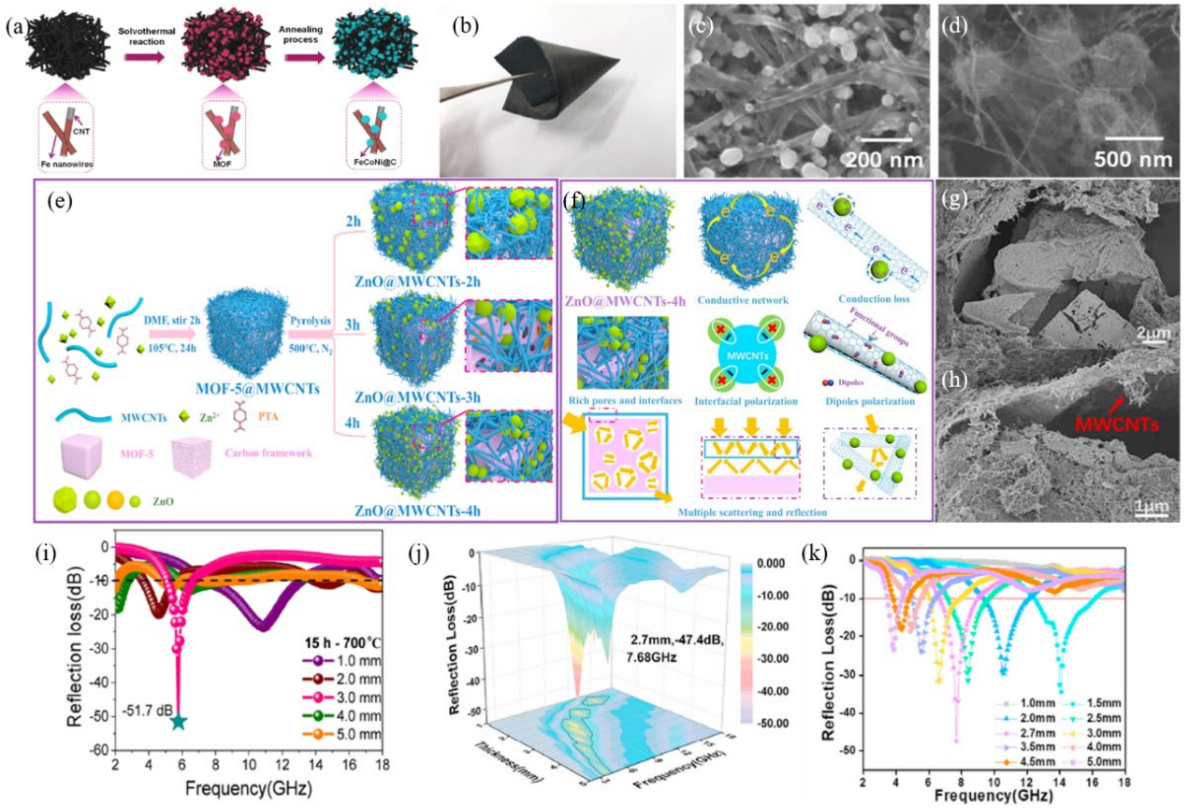

Fig. 24 (a) Flow diagram of preparation of CNT/FeCoNi@C composites, (b) digital photograph of a flexible iron-filled CNT sponge, (c) (d) SEM image of CNT/FeCoNi@C[232]0. Copyright 2021, American Chemical Society. (e) flow diagram of the preparation of ZnO@MWCNTs composites, (f) the wave absorption mechanism of ZnO@MWCNTs composites, (g)(h) SEM images of ZnO@MWCNTs SEM[233]. Copyright 2020, Elsevier Ltd. (i) RL plot of CNT/FeCoNi@C composites[232]. Copyright 2021, American Chemical Society. (j) 3D RL and (k) RL plot of ZnO@MWCNTs[233]. Copyright 2020, Elsevier Ltd.

4.3.1.2 MOF-carbon fibers composite absorbing materials

Chen et al.[234] prepared Fe^{III}-MOF-5 using terephthalic acid as the ligand. Afterwards, FeIII-MOF-5 and PAN were mixed in different ratios to obtain electrostatic spinning solutions and spun using an electrostatic spinning device, and finally the spun product was annealed at 700 °C to obtain the final product Fe^{III}-MOF-5-derived/carbon fibers composites (FMCFs). The prepared

FMCFs mixed with paraffin wax (40 wt% filling ratio) were tested their absorbing properties. The RL_{min} reaches -39.2 dB at 1.4 mm and the EAB was 4.44 GHz (13.56-18 GHz). Guo et al.[235] prepared hollow loofah fibres (HLF) from loofah sponges, and then grew ZIF-67 on HLF using a hydrothermal method with 2-methylimidazole as the ligand to prepare HLF@ZIF-67(Fig.25(a)-(c)). And finally high temperature calcination was carried out in N_2 environment to obtain HCF@NC/Co, as shown in Fig.25(d). HCF@NC/Co was mixed well with paraffin wax to test its wave absorption performance (14 wt% filling rate), and the results are shown in Fig.25(e)(f). At 2.25 mm thickness, the RL_{min} at 17.04 GHz can reach -50.14 dB, and at 2.7 mm, the EAB is 7.36 GHz (10.64-18 GHz). Tao et al.[236] used 2-methylimidazole as a ligand to prepare ZIF-67 onto the treated CF, and the CF@C/Co composite was obtained after a one-step high temperature calcination treatment (Fig.25(g)-(i)). The CF@C/Co composites mixed well with paraffin (20 wt% filling rate) were measured the performances (Fig.25(j)(k)). The results show that the composite achieves an RL_{min} of -71.95 dB at 1.78 mm and an EAB of 6.25 GHz at 1.71 mm.

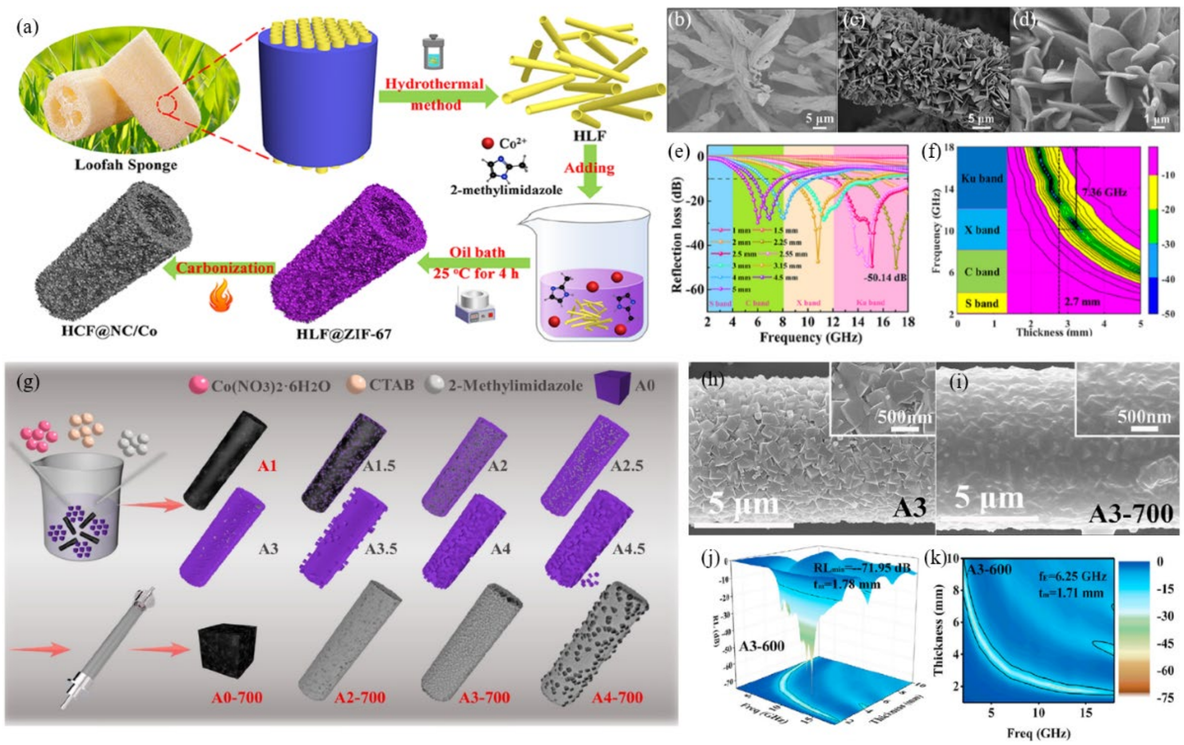

Fig. 25 (a) Flow chart of preparation of HCF@NC/Co composites, SEM images of (b) hollow lucerne fibres, HLF@ZIF-67 and (d) HCF@NC/Co, (e) RL curves and (f) 2D RL[235]. Copyright 2021, American Chemical Society. (g) flow chart of preparation of CF@C/Co composites, SEM image of (h) CF@ZID-67 precursor and (i) CF@C/Co, (j) 3D RL and (k) 2D RL of CF@C/Co composite[236]. Copyright 2021, Elsevier Ltd.

4.3.1.3 MOF-graphene (GO) composite absorbing materials

Li et al.[237] prepared the Ce-MOF using 2-aminoterephthalic acid as the ligand (Fig.26(a)(b)). The prepared graphene oxide (GO) was mixed with Ce-MOF and calcined at 500 °C to prepare accordion-like CeO_{2-x}/RGO composite nanosheets (Fig. 26(c)). The CeO_{2-x}/RGO composite nanosheets were mixed with paraffin wax (50 wt% filling rate) and the absorption properties were tested in Fig. 26(e)(f). It is found that the EAB is up to 5.84 GHz, covering 12.16-18 GHz. Fig 26(g) demonstrates the wave absorption mechanism of CeO_{2-x}/RGO composites. Firstly, CeO_{2-x} generates a large number of contact interfaces with the RGO surface, which enhances the interfacial polarization. Secondly, CeO_{2-x}/RGO composites have a good conductive network with good dipole polarization. Finally, the accordion-like RGO also effectively enhances the dielectric loss, and the synergistic effect of CeO_{2-x} and RGO makes CeO_{2-x}/RGO has good wave absorption properties Wang et al.[238] prepared multistage porous-like ZIF-67 precursors in the presence of GO using 2-methylimidazole as ligand (Fig.26(h)), after which the precursors were pyrolyzed in situ at high temperature to prepare honeycomb-like Co/C composites (Fig.26(i)). The prepared Co/C composites were mixed well with paraffin (10% mass ratio). And the results in Fig.26(k) display that the Co/C composites achieve an RL_{min} of -50.7 dB at 2.9 mm and an EAB of 4.6 GHz (8.6-13.2 GHz).

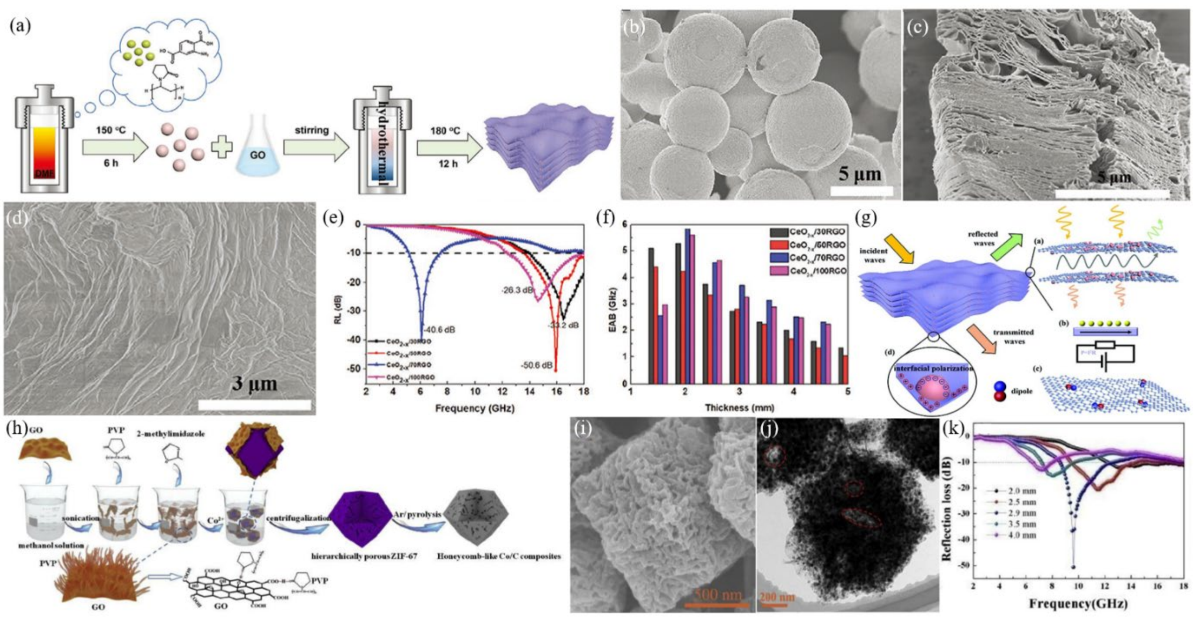

Fig. 26 (a) Flow chart of the preparation of Ce_{2-x}/RGO composite nanosheets, SEM images of (b) Ce-MOF, (c) Ce_{2-x}/RGO (d) GO, (e) RL profile of Ce_{2-x}/RGO, (f) EAB of Ce_{2-x}/RGO composite nanosheets at different RGO contents, (g) absorption mechanism of Ce_{2-x}/RGO composite nanosheets[237]. Copyright 2020, Wiley-VCH GmbH. (h) flow chart of the preparation of Co/C composites, (i) SEM images and (j) TEM images of Co/C composites, (k) RL curve plots of Co/C composites[238].

In Fig. 27(a), Wang et al.[239] fabricated Fe-doped Co-MOF/rGO precursors in the presence of rGO using 2-methylimidazole as the ligand, in Fig. 27(b), after which the precursors were calcined at high temperature to obtain graded porous Fe-Co/NC/rGO composites. The prepared composite was mixed well with paraffin (25% mass ratio) and its wave absorption properties were tested in Fig. 27(d)-(f). The RL_{min} at 11.28 GHz at 2.5 mm can reach -43.26 and the EAB can reach 9.29 GHz at 2.63 mm (8.71-18 GHz). Zhao et al [240] prepared a ZIF-67@CoNi LDHs-GO precursor by using 2-methylimidazole as the ligand (Fig. 27(g)), where ZIF-67 was formed on the periphery of GO with different contents and CoNi LDHs were fabricated on ZIF-67 (Fig. 27(h)(i)). This precursor was then annealed at 600 °C under argon to obtain the final product CoNi@NCPs-rGO (Fig. 27(j)(k)). 30 wt% CoNi@NCPs-rGO was mixed well with paraffin and the related properties was exhibited in Fig. 27(n)-(p). At 2.5 mm and 10.62 GHz, the RL_{min} is up to -58.2 dB with the EAB of 4.03 GHz (8.80-12.83 GHz).

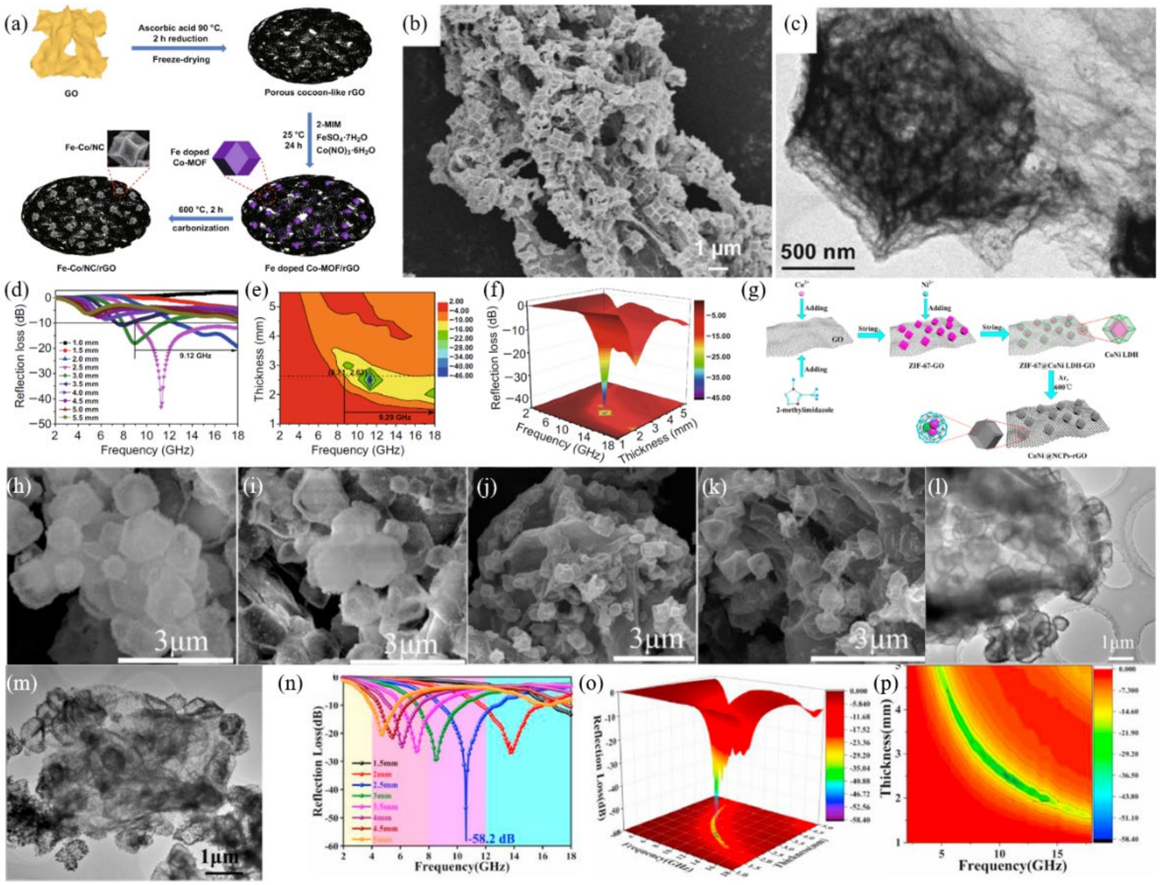

Fig. 27 (a) Preparation diagram of Fe-Co/NC/rGO composites, (b) SEM and (c) TEM images of Fe-Co/NC/rGO, (d) RL profile, (e) 2D projection and (f) 3D RL[239]. Copyright 2019, Springer. (g) illustration of preparation of CoNi@NCPs-rGO, SEM images of (h)(i) ZIF-67@CoNi LDHs-GO precursors and (j)(k) CoNi@NCPs-rGO, (l)(m) TEM images of CoNi@NCPs-rGO, (n) RL profiles of CoNi@NCPs-rGO, (o) 3D RL maps and (p) 2D projection maps[240]. Copyright 2020, Elsevier Ltd.

4.3.1.4 MOF-other carbon composite absorbing materials

Liu et al.[241] synthesized CC@NPC/CoS_2 composites using 2-plus-methylimidazole as the ligand on the surface of CC (Fig.28(a),(c)-(e)). 30 wt% composite was mixed with paraffin as well as tested for its wave absorption properties. In Fig.28(f)(g), at 2.5 mm the composite has a 9.2 GHz EAB, covering 8.8-18 GHz. Xiong et al.[242] obtained FeCo/C@WC composites through using 2-

methylimidazole as ligand by growing ZIF-67 on the surface of the now-prepared degreased wood aerogel embedded with Fe_3O_4 particles and charring the sample at 800 °C under argon atmosphere (Fig. 28(h)-(l)). The prepared composites achieved an RL_{min} of -47.6 dB at 1.5 mm and 15.7 GHz, and an EAB of 8.9 GHz (9.1-18 GHz) at 1.96 mm, as shown in Fig. 28(m)(n). And the absorbing mechanism is presented in Fig. 28(b). The excellent dielectric loss of FeCo/C@WC composites is ascribed to the dipole polarization from the introduction of FeCo/C and the interfacial polarization generated by the heterogeneous interface among FeCo/C, FeCo/C and WC. Besides, WC retains its original porous structure, and the excellent porous conductive network is more conducive to the transmission of electrons, allowing the electromagnetic waves to be dissipated quickly. Zhang et al.[243] prepared $NiCo_2S_4$@C/PC composites by growing ZIF-67 on the surface of porous carbon (PC) using 2-methylimidazole as ligand and after carbonization, introduction of Ni elements and sulfidation. The RL_{min} of the prepared composites can reach -59.36 dB at thickness of 2.1mm and 15.28 GHz, and the EAB can reach 6.8 GHz (10.96-17.76 GHz).

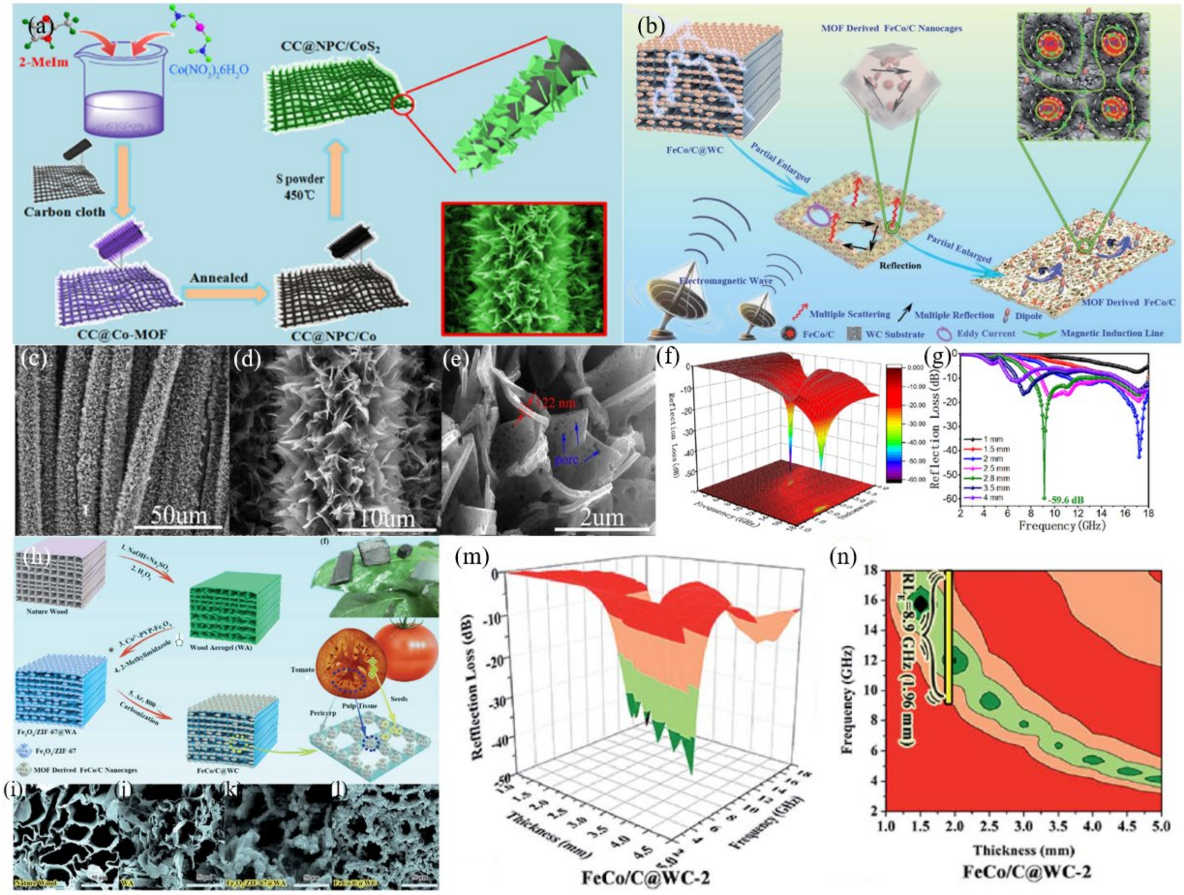

Fig. 28 (a) preparation diagram of CC@NPC/CoS_2[241], Copyright 2020, Elsevier Ltd. (b) absorbing mechanism diagram of FeCo/C@WC[242], Copyright 2020, The Royal Society of Chemistry. (c)-(e) SEM images of CC@NPC/CoS_2, (f) 3D loss diagram and (g) RL curve of CC@NPC/CoS_2[241]. Copyright 2020, Elsevier Ltd. (h) flow diagram of the preparation of FeCo/C@WC, (i-l) SEM images of natural wood, WA, Fe_3O_4/ZIF-67@WA and FeCo/C@WC, (m) 3D RL diagram and (n) EAB diagram of FeCo/C@WC[242]. Copyright 2020, The Royal Society of Chemistry.

4.3.2 MOF- MXene composite absorbing materials

MXene is a new 2D nanomaterial discovered in recent years, prepared by etching an A-layer from the former phase MAX[244-247]. The 2D layered structure and the abundance of surface functional groups, as well as having a controlled layered structure and the high electrical conductivity makes it have strongly dielectric and polarization loss, which exhibits a huge potential in microwave absorption[248-251]. The introduction of MXene into MOFs effectively improves the impedance matching and increases the polarization sites of the material, and the multilayer structure of MXene increases the multiple reflection loss of electromagnetic waves. A comparison of the absorbing properties of the absorbing materials prepared by combining MOFs with MXene is shown in Table 3. Chen et al. [252] prepared CoFe-MIL-88A spindle precursors using fumaric acid as the ligand, and a MXene sheet layer was grown on its surface by electrostatic self-assembly, and finally the whole composite was charred at high temperature to obtain CoFe/C@TiO_2/C composites (Fig. 29(a)-(f)). The composite was mixed well with paraffin wax (5 wt% mass ratio) and tested for the wave absorption properties (Fig. 29(g)(h)). The results show that the composite can achieve an RL_{min} of -20 dB at 2.5 mm and an EAB of 6.1 GHz at 2.0 mm, which can cover 11.9-18 GHz. Wang et al.[253] prepared flower-like CoNi-MOF precursors as using 2-methylimidazole as the ligand (Fig. 29(i)(j)). Afterwards, a layer of $Ti_2C_3T_x$ MXene was coated on its surface by electrostatic self-assembly and annealed at 350 °C under argon to obtain CoO/$NiCo_2O_4$/$Ti_2C_3T_x$ composites (Fig. 29(k)). The CoO/$NiCo_2O_4$/$Ti_2C_3T_x$ composites were mixed well with PVDF (5 wt% mass ratio). In Fig.29(l)(m), the results show that the composite realizes an RL_{min} of -47.17 dB at 2.9 mm and a 5.44 GHz EAB. Figure 29(n) shows the absorption mechanism of the CoO/$NiCo_2O_4$/$Ti_2C_3T_x$ composite. The good absorption performances rely on the multiple reflections of electromagnetic waves by the porous structure and the optimization of the impedance matching throughout the material, which is rich in heterogeneous interfaces and defects that enhance interfacial polarization and dipole polarization, and a good conductive network that facilitates conductive losses.

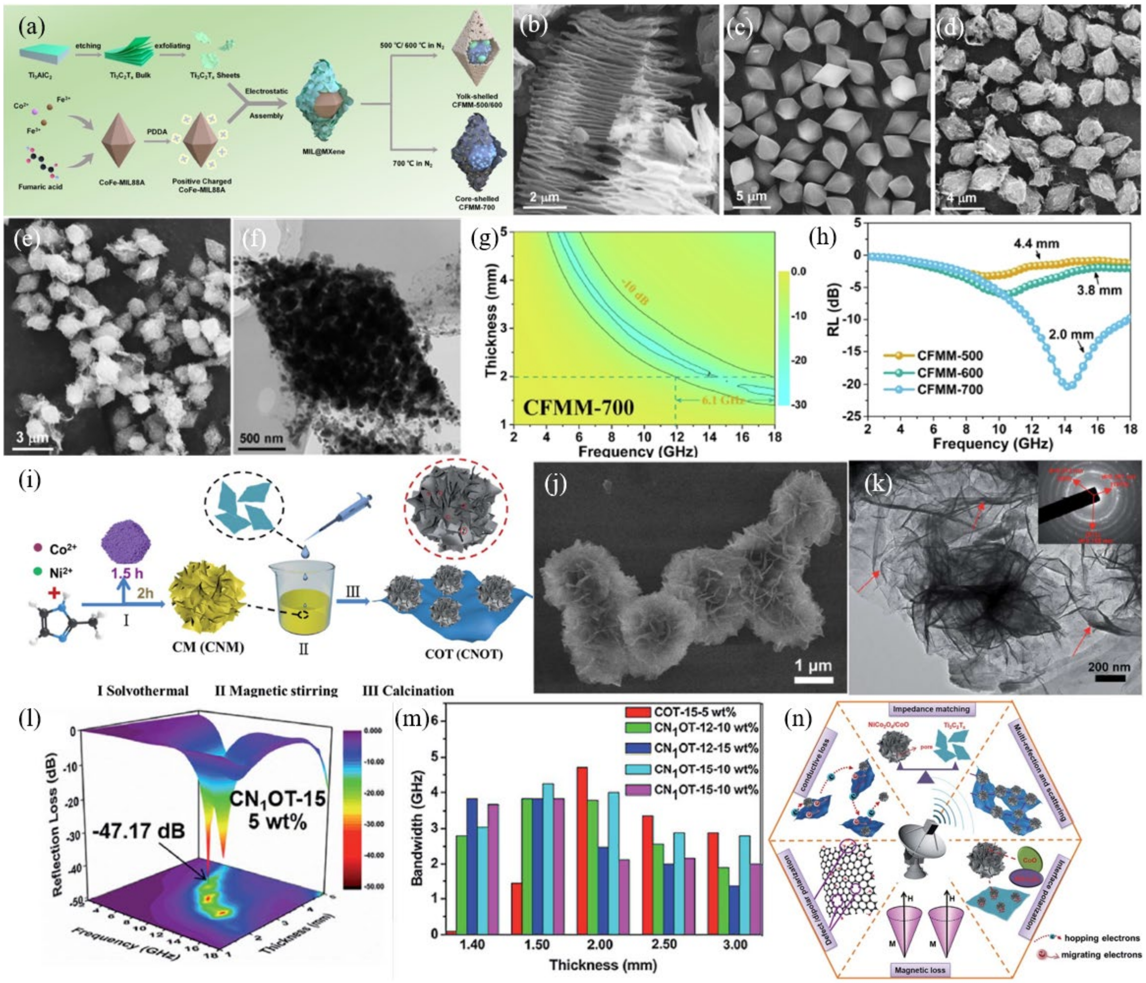

Fig. 29 (a) preparation diagram of $CoFe/C@TiO_2/C$, (b-e) SEM images of $Ti_2C_3T_x$ MXene, CoFe-MIL-88A, CoFe-MIL-88A/MXene precursors and $CoFe/C@TiO_2/C$, (f) TEM images of $CoFe/C@TiO_2/C$, (g) 2D RL of $CoFe/C@ TiO_2/C$, (h) RL profiles of $CoFe/C@TiO_2/C$ at different carbonization temperatures[252]. Copyright 2021, Elsevier B.V. (i) preparation diagram of $CoO/NiCo_2O_4/Ti_2C_3T_x$ composite, (j) SEM image of CoNi-MOF precursors, (k) TEM image of $CoO/NiCo_2O_4/Ti_2C_3T_x$, (l) 3D RL of $CoO/NiCo_2O_4/Ti_2C_3T_x$, (m) EAB of different samples, (n) absorbing mechanism of $CoO/NiCo_2O_4/Ti_2C_3T_x$[253]. Copyright 2021, The Royal Society of Chemistry.

In Fig.30(a)-(d), Deng et al.[254] prepared $Fe\&TiO_2@C$ composites at high temperature by using terephthalic acid as the ligand to prepare Fe-MOF on the periphery of $Ti_2C_3T_x$ MXene. 40 wt% composites were mixed well with paraffin and tested for their wave absorption properties. In

Fig. 30(e), the results show that the composite can reach an RL_{min} of -51.8 dB at 6.6 GHz at 3 mm, as well as the EAB is 6.5 GHz (11.5-18 GHz) at 1.6 mm. Fig 30(f) shows the wave absorption mechanism of Fe&TiO_2@C composites. The sandwich-like structure is conducive to the multiple reflection loss of electromagnetic waves, the large number of heterojunction surfaces can produce huge interfacial polarization, and Fe&TiO_2 is able to produce certain natural resonance and exchange resonance. Moreover, the introduction of magnetic loss also optimizes the impedance matching of the material to a certain extent, which makes the composites have good wave absorption performances. Wu et al.[255] fabricated MXene/CoNi/CNTs composites at high temperature by applying terephthalic acid as the ligand to prepare CoNi-MOF on the surface of MXene fibers (Fig. 30(g)-(j)). In Fig. 30(k)(l), the MXene/CoNi/CNTs composites at 1.6 mm achieve an -51.6 dB RL_{min} at 15.1 GHz and a 4.5 GHz EAB (13.2-17.7 GHz).

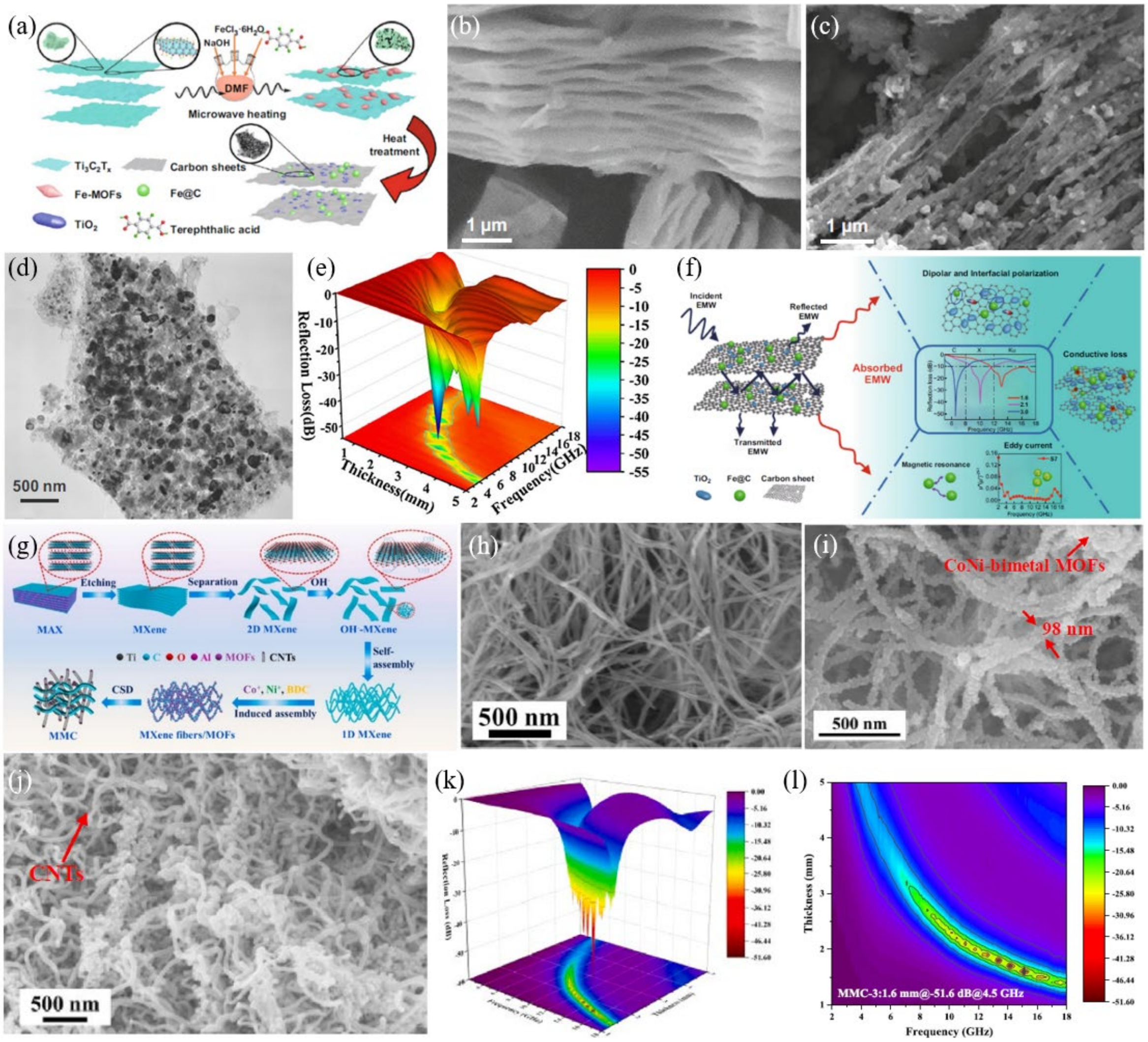

Fig. 30 (a) Flow chart for preparing Fe&TiO$_2$@C, (b) SEM image of Ti$_2$C$_3$T$_x$ MXene, (c) SEM and (d) TEM images of Fe&TiO$_2$@C, (e) 3D RL, (f) wave absorption mechanism of Fe&TiO$_2$@C[254]. Copyright 2020, Springer. (g) Flow chart of the preparation of MXene/CoNi/CNTs, SEM images of (h) MXene fibers, (i) MXene@CoNi-MOF and (j) MXene/CoNi/CNTs, (k) 3D RL and (l) 2D RL of MXene/CoNi/CNTs[255]. Copyright 2021, Elsevier B.V.

4.3.3 MOF-conductive polymer composite absorbing materials

Conductive polymers[256] are also commonly compounded with MOFs as excellent absorbers due to their high dielectric, low density, flexibility, corrosion resistance, low cost and tunable absorbing frequency width properties[257-259]. Conductive polymers such as polyaniline

(PANI)[260-263] and polypyrrole (PPy)[264, 265] are usually used. Conductive polymers with adjustable conductivity when compounded with MOFs can modulate the electromagnetic parameters of the material so that the absorber can move towards lower fill rates and thinner thicknesses while still ensuring a good EAB. A comparison of the absorbing properties of wave absorbing materials prepared from MOFs compounded with conductive polymers is shown in Table 3. Bi et al.[266] prepared CoZn-MOF precursors using 2-methylimidazole as the ligand in Fig.31(a)(b), and the precursors were subjected to high temperature carbonization and then grown with MoS_2 and PPy successively to obtain CoZn/C@MoS_2@PPy composites (Fig.31(c)). The prepared material was mixed well with paraffin wax (30 wt% mass ratio). The results in Fig.31(d)-(f) indicate that the prepared composite has an RL_{min} at 15.88 GHz of -49.18 dB and its EAB of 4.56 GHz (13.44-18 GHz). Sun et al.[267] obtained Co/C@PPy composite by using 2-methylimidazole as the ligand to grow PPy on the surface of ZIF-67 precursors (Fig. 31(g)-(j)). The composite was mixed well with paraffin (10 wt% mass ratio) and its wave absorption properties are presented in Fig.31(k)(l). The results show that the RL_{min} at 17.32 GHz is up to -44.76 dB at 2.0 mm and the EAB is 6.56 GHz (11.04-17.6 GHz) at 2.5 mm. Wang et al.[268] prepared Fe-MOF precursors using terephthalic acid as the ligand, followed by PANI grown on the surface of them to prepare Fe-MOF@PANI composites. 30 wt% Fe-MOF@PANI composites were mixed with paraffin as well as their absorbing properties were tested. It is found that at 2.0 mm, the RL_{min} at 11.6 GHz is -41.4 dB and the EAB is 5.5 GHz, covering 9.8-15.3 GHz.

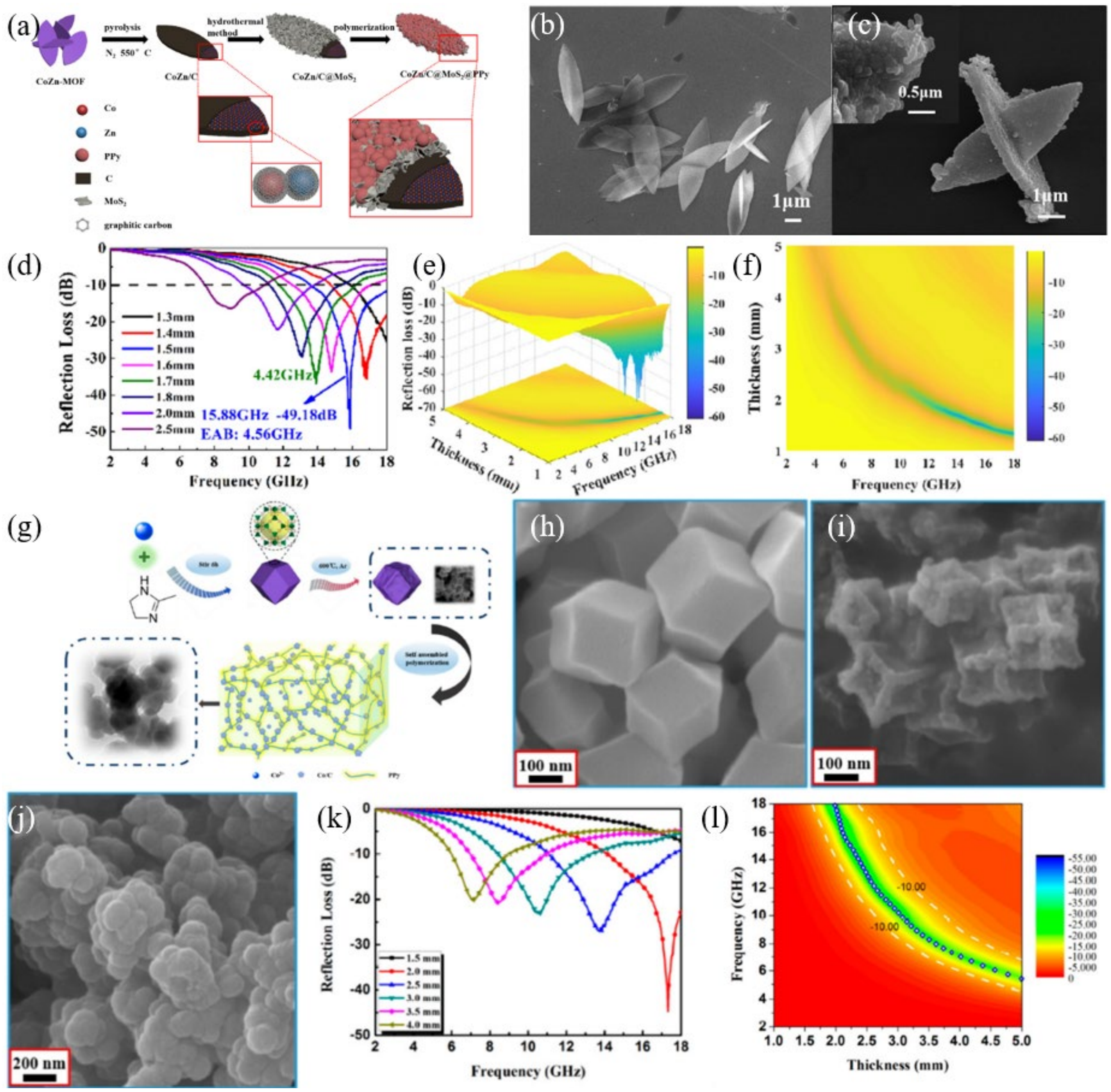

Fig. 31 (a) flow chart of the preparation of CoZn/C@MoS$_2$@PPy composites, SEM images of (b) CoZn-MOF precursors and (c) CoZn/C@MoS$_2$@PPy, (d) RL profile, (e) 3D RL and (f) 2D RL of CoZn/C@MoS$_2$@PPy composites[266]. Copyright 2021, Elsevier Inc. (g) flow chart of Co/C@PPy aerogel, (h-j) SEM images of ZIF-67, Co/C and Co/C@PPy, respectively, (k) RL profile and (l) 2D RL of Co/C@PPy[267]. Copyright 2018, MDPI.

Table 3 Wave absorption properties of MOF-based composite absorbing materials.

Microwave absorbing materials	Loading (wt%)	RL$_{min}$			EAB			Ref
		Value (dB)	f_m (GHz)	Thickness (mm)	Value (GHz)	Range (GHz)	Thickness (mm)	
CoZn/C@MoS_2@PPy	30	-49.18	15.88	1.5	4.56	13.44-18	1.5	[266]
CoFe/C@TiO_2/C	50	-20	-	2.5	6.1	11.9-18	2.0	[252]
FMCFs	40	-39.2	-	1.4	4.44	13.56-18	1.4	[234]
Fe&TiO_2@C	40	-51.8	6.6	3	6.5	11.5-18	1.6	[254]
Co-CNTs	20	-30	14.2	1.5	7.8	10.2-18	1.5	[231]
HCF@NC/Co	14	-50.14	17.04	2.25	7.36	10.64-18	2.7	[235]
MXene/Co-CZIF	50	-60.09	7.36	2.7	9.3	-	2.7	[269]
CNT/FeCoNi@C	30	-51.7	-	3.0	6.0	-	1.0	[232]
PPy/ZIFs	30	-31	-	2.6	7.24	10.76-18	2.6	[270]
CeO_{2-x}/RGO	50	-50.6	15.9	1.5	5.84	12.16-18	1.5	[237]
ZnO@MWCNTs	20	-47.4	7.68	2.7	3.7	-	1.5	[233]

$CoFe_2O_4$@CNTs	40	-34.6	13.4	2.5	7.1	10-17.1	2.5	[271]
CC@NPC/CoS_2	30	-59.6	9.1	2.8	9.2	8.8-18	2.5	[241]
Co_3O_4/CF	40	-46.58	10.72	3.3	5.4	-	3.3	[272]
CNT/Ni@N-C	30	-55.1	10.56	2.5	11.2	6.0-17.2	1.5-4.0	[273]
Co/C@PPy	10	-44.76	17.32	2.0	6.56	11.04-17.60	2.5	[267]
CF@C/Co	20	-71.95	-	1.78	6.25	-	1.71	[236]
CoO/$NiCo_2O_4$/$Ti_3C_2T_x$	5	-47.17	-	2.9	5.44	-	2.9	[253]
Co/C	10	-50.7	-	2.9	4.6	8.6-13.2	2.9	[238]
Fe-Co/NC/rGO	25	-43.26	11.28	2.5	9.29	8.71-18.0	2.63	[239]
CoO@N/C-Co/Ni-NCO	30	-52.45	14.77	1.66	5.3	-	1.66	[274]
CNT-CoFe@C	10	-40.00	9.86	3.0	5.62	-	2.0	[275]
Fe-MOF@PANI	30	-41.4	11.6	2.0	5.5	9.8-15.3	2.0	[268]
Co@SC@MNC	20	-72.3	-	2.6	6.0	-	2.3	[276]
MXene/CoNi/CNTs	-	-51.6	15.1	1.6	4.5	13.2-17.7	1.6	[255]
Ti_3CNT_X/Ni@C	8	-65.7	-	1.5	5.4	12.6-18	1.5	[277]

FeCo/C@WC	85	-47.6	15.7	1.5	8.9	9.1-18	1.96	[242]
CoNi@NC/rGO	25	-68.0	10.9	-	6.7	-	2.5	[278]
FeNi@CNTs/CNRs	20	-47.0	-	2.3	4.5	-	1.6	[279]
Co/MnO/CNTs	35	-58.0	-	2.65	5.36	10-15.36	1.97	[280]
CoS_2/NCNTs	50	-65.0	-	1.6	6.2	13.8-18.0	1.6	[281]
HCF@CZ-CNTs	10	-53.5	7.8	2.9	8.02	9.98-18	2.0	[282]
SiC/Ni/NiO/C	20	-50.52	13.24	4.0	2.96	14.76-17.72	2.5	[283]
NiFe@CNC@GO	30	-51.0	7.7	2.8	3.97	8.30-12.27	2.2	[284]
NBC@GN	10	-53.99	-	3.9	4.39	-	1.4	[285]
Co-C/MWCNTs	15	-48.9	-	2.99	-	-	-	[286]
$NiCo_2S_4$@PC	20	-59.36	15.28	2.1	6.8	10.96-17.76	2.1	[243]
$NiFe_2S_4$@PC	25	-51.41	-	1.8	4.08	-	1.9	[287]
CoAl-LDO@Co-C	30	-38.18	-	2.6	8.48	9.16-18.0	2.6	[288]
CoNi@NPCs-rGO	30	-58.2	10.62	2.5	4.03	8.80-12.83	2.5	[240]
ZnO-Co@N/C	30	-62.7	5.98	4.05	5.75	-	2.0	[289]

Ni/NC/C	16	-63.1	13.84	2.0	5.12	11.28-16.40	2.0	[290]
ZIF-7@CNTs	10	-62.5	6.19	3.6	5.78	-	2.4	[291]
HCoZnNC@MX	20	-76.40	7.50	2.92	3.9	-	2.92	[292]
CZIF-PPy	40	-40.0	16.0	1.8	-	-	-	[293]

5. Conclusions and prospect

In recent decades, MOFs and MOF-based absorbers have continued to demonstrate their advantages in electromagnetic wave absorption, due to simple preparation process, low cost, high thermal stability, high specific surface area and porosity. The high absorption and loss of incident electromagnetic waves can be achieved by adjusting the microstructure and composition. At present, MOF-based absorbing materials have made great breakthroughs, opening up a new path for the pursuit of "thin, light, wide and strong".

Although some results for the research and development of MOF-derived absorbing materials have been demonstrated, a number of significant challenges remain at this stage. Firstly, as the research continues, the traditional routes for the preparation of carbon materials faces many new issues when MOFs are directly severed as templates or precursors. Due to the inherent characteristics of MOFs, the carbon materials obtained are predominantly microporous, which is not conducive to mass/electron transfer. Moreover, the structure of carbon materials obtained by direct carbonization of MOFs has a single morphology and is not easily adjustable, and the carbonization process requires strict temperature control. Therefore, the parameters of various synthetic MOFs need to be further investigated. Secondly, because the absorption capacity is attributed to different mechanisms such as dielectric and magnetic losses, multiple reflections and impedance matching, etc., the quantitative estimation of the effect of various mechanisms still lacks sufficient theoretical support. Hence, the microwave absorption mechanism of MOF-derived absorbing materials needs to be further clarified.

In addition, many researchers currently pursue the RL and EAB of absorbers too much, making the development of MOF absorbing materials detached from practical applications. Finally, there are still many MOF composites that need more experimentation and exploration, and more structural shapes to be designed. In conclusion, there is still a long way to explore for MOF-based absorbing materials to industrial applications.

In summary, MOF-based materials have infinite possibilities in the field of microwave absorption, although there are still many problems and most of the research is still at the experimental development stage. MOF-based materials as a new star, is a very promising high-efficiency electromagnetic wave absorption material at present and in the future. It will certainly continue to drive scientific and technological progress and industrial upgrade, and achieve the continued prosperity of human society.

Acknowledgement

We gratefully appreciate the support of the Natural Science Foundation of Shandong (ZR2019BB063). The author gratitude the environmental and function material team, supported by the Project of Shandong Province Higher Educational Young Innovative Talent Introduction and Cultivation. The authors would like to thank the Deanship of Scientific Research at Umm Al-Qura University for supporting this work by Grant Code: (22UQU4320141DSR71).

Conflict of Interest

The authors declare that they have no conflict of interest.

References

[1] Z. Cai, L. Su, H. Wang, M. Niu, L. Tao, Lu, L. Xu, M. Li, H. Gao, Alternating Multilayered Si_3N_4/SiC Aerogels for Broadband

and High-Temperature Electromagnetic Wave Absorption up to 1000 degrees C, ACS Appl. Mater. Inter. 13(14) (2021) 16704-16712, https://doi.org/10.1021/acsami.1c02906.

[2] H. Cheng, Y. Pan, X. Wang, C. Liu, C. Shen, D.W. Schubert, Z. Guo, X. Liu, Ni Flower/MXene-Melamine Foam Derived 3D Magnetic/Conductive Networks for Ultra-Efficient Microwave Absorption and Infrared Stealth, Nano-Micro Lett. 14(1) (2022) 63, https://doi.org/10.1007/s40820-022-00812-w.

[3] W. Chu, K. Wang, H. Li, Y. Chen, H. Liu, Harvesting yolk-shell nanocomposites from Fe-MIL-101 self-template in NaCl/KCl molten salt environment for high-performance microwave absorber, Chem. Eng. J. 430 (2022) 133112, https://doi.org/10.1016/j.cej.2021.133112.

[4] L. Deng, R. Shu, J. Zhang, Fabrication of ultralight nitrogen-doped reduced graphene oxide/nickel ferrite composite foams with three-dimensional porous network structure as ultrathin and high-performance microwave absorbers, J. Colloid Interf. Sci. 614 (2022) 110-119, https://doi.org/10.1016/j.jcis.2022.01.104.

[5] Y. Ma, Z. Zhuang, M. Ma, Y. Yang, W. Li, J. lin, M. Dong, S. Wu, T. Ding, Z. Guo, Solid polyaniline dendrites consisting of high aspect ratio branches self-assembled using sodium lauryl sulfonate as soft templates: Synthesis and electrochemical performance, Polymer 182 (2019) 121808, https://doi.org/10.1016/j.polymer.2019.121808.

[6] Y. Liu, X. Liu, X. E, B. Wang, Z. Jia, Q. Chi, G. Wu, Synthesis of Mn_xO_y@C hybrid composites for optimal electromagnetic wave absorption capacity and wideband absorption, J. Mater. Sci. Technol. 103 (2022) 157-164, https://doi.org/10.1016/j.jmst.2021.06.034.

[7] J. Qiao, X. Zhang, D. Xu, L. Kong, L. Lv, F. Yang, F. Wang, W. Liu, J. Liu, Design and synthesis of TiO_2/Co/carbon nanofibers with tunable and efficient electromagnetic absorption, Chem. Eng. J. 380 (2020) 122591, https://doi.org/10.1016/j.cej.2019.122591.

[8] G. Cao, S. Cai, H. Zhang, Y. Tian, High-performance conductive adhesives based on water-soluble resins for printed circuits, flexible conductive films, and electromagnetic interference shielding devices, Adv. Compos. Hybrid Mater. 5 (2022) 1730-1742, https://doi.org/10.1007/s42114-021-00402-1.

[9] Z. Ma, X. Xiang, L. Shao, Y. Zhang, J. Gu, Multifunctional Wearable Silver Nanowire Decorated Leather Nanocomposites for Joule Heating, Electromagnetic Interference Shielding and Piezoresistive Sensing, Angew. Chem. Int. Ed. 61(15) (2022) e202200705, https://doi.org/10.1002/anie.202200705.

[10] L. Wang, Z. Ma, H. Qiu, Y. Zhang, Z. Yu, J. Gu, Significantly Enhanced Electromagnetic Interference Shielding Performances of Epoxy Nanocomposites with Long-Range Aligned Lamellar Structures, Nano-Micro Lett. 14(1) (2022) 224,

https://doi.org/10.1007/s40820-022-00949-8.

[11] L. Liang, Q. Li, X. Yan, Y. Feng, Y. Wang, H.B. Zhang, X. Zhou, C. Liu, C. Shen, X. Xie, Multifunctional Magnetic Ti_3C_2Tx MXene/Graphene Aerogel with Superior Electromagnetic Wave Absorption Performance, ACS Nano 15(4) (2021) 6622-6632, https://doi.org/10.1021/acsnano.0c09982.

[12] Z. Liao, M. Ma, Z. Tong, Y. Bi, K.L. Chung, M. Qiao, Y. Ma, A. Ma, G. Wu, Z. Li, Y. Zhang, Fabrication of one-dimensional $ZnFe_2O_4$@carbon@MoS_2/FeS_2 composites as electromagnetic wave absorber, J. Colloid Interf. Sci. 600 (2021) 90-98, https://doi.org/10.1016/j.jcis.2021.04.142.

[13] H. Cheng, L. Xing, Y. Zuo, Y. Pan, M. Huang, A. Alhadhrami, M.M. Ibrahim, Z.M. El-Bahy, C. Liu, C. Shen, Constructing nickel chain/MXene networks in melamine foam towards phase change materials for thermal energy management and absorption-dominated electromagnetic interference shielding, Adv. Compos. Hybrid Mater. 5 (2022) 755-765, https://doi.org/10.1007/s42114-022-00487-2.

[14] R. Tang, P. Xu, J. Dong, H. Gui, T. Zhang, Y. Ding, V. Murugadoss, N. Naik, D. Pan, M. Huang, Z. Guo, Carbon foams derived from emulsion-templated porous polymeric composites for electromagnetic interference shielding, Carbon 188 (2022) 492-502, https://doi.org/10.1016/j.carbon.2021.12.026.

[15] R. Guo, D. Su, F. Chen, Y. Cheng, X. Wang, R. Gong, H. Luo, Hollow Beaded Fe_3C/N-Doped Carbon Fibers toward Broadband Microwave Absorption, ACS Appl. Mater. Inter. 14(2) (2022) 3084-3094, https://doi.org/10.1021/acsami.1c21272.

[16] C. Jin, Z. Wu, C. Yang, L. Wang, R. Zhang, H. Xu, R. Che, Impedance amelioration of coaxial-electrospun TiO_2@Fe/C@TiO_2 vesicular carbon microtubes with dielectric-magnetic synergy toward highly efficient microwave absorption, Chem. Eng. J. 433 (2022) 133640, https://doi.org/10.1016/j.cej.2021.133640.

[17] Y. Ma, C. Hou, H. Zhang, Q. Zhang, H. Liu, S. Wu, Z. Guo, Three-dimensional core-shell Fe_3O_4/Polyaniline coaxial heterogeneous nanonets: Preparation and high performance supercapacitor electrodes, Electrochim. Acta 315 (2019) 114-123, https://doi.org/https://doi.org/10.1016/j.electacta.2019.05.073.

[18] Y. Ma, C. Hou, H. Zhang, M. Qiao, Y. Chen, H. Zhang, Q. Zhang, Z. Guo, Morphology-dependent electrochemical supercapacitors in multi-dimensional polyaniline nanostructures, J. Mater. Chem. A 5(27) (2017) 14041-14052, https://doi.org/10.1039/c7ta03279j.

[19] F. Chu, S. Cheng, Z. Ye, F. Wu, H. Zhuang, W. Dong, A. Xie, In situ etching by released proton in aniline polymerization to form network VO_2 doped polyaniline composites with variable infrared emissivity for electromagnetic absorption application, Adv.

Compos. Hybrid Mater. 5 (2022) 2760–2771, https://doi.org/10.1007/s42114-022-00566-4.

[20] Y. Dong, X. Zhu, F. Pan, B. Deng, Z. Liu, X. Zhang, C. Huang, Z. Xiang, W. Lu, Mace-like carbon fiber/ZnO nanorod composite derived from typha orientalis for lightweight and high-efficient electromagnetic wave absorber, Adv. Compos. Hybrid Mater. 4(4) (2021) 1002-1014, https://doi.org/10.1007/s42114-021-00277-2.

[21] Y. Wu, K. Huang, X. Weng, R. Wang, P. Du, J. Liu, S. Lin, K. Huang, H. Yang, M. Lei, PVB coating efficiently improves the high stability of EMI shielding fabric with Cu/Ni, Adv. Compos. Hybrid Mater. 5(1) (2022) 71-82, https://doi.org/10.1007/s42114-021-00401-2.

[22] Y. Zhang, J. Kong, J. Gu, New generation electromagnetic materials: harvesting instead of dissipation solo, Sci. Bull. 67(14) (2022) 1413-1415, https://doi.org/10.1016/j.scib.2022.06.017.

[23] B. Du, D. Zhang, J. Qian, M. Cai, C. He, P. Zhou, A. Shui, Multifunctional carbon nanofiber-SiC nanowire aerogel films with superior microwave absorbing performance, Adv. Compos. Hybrid Mater. 4(4) (2021) 1281-1291, https://doi.org/10.1007/s42114-021-00286-1.

[24] J. Guo, Z. Chen, X. Xu, X. Li, H. Liu, S. Xi, W. Abdul, Q. Wu, P. Zhang, B.B. Xu, J. Zhu, Z. Guo, Enhanced electromagnetic wave absorption of engineered epoxy nanocomposites with the assistance of polyaniline fillers, Adv. Compos. Hybrid Mater. 5(3) (2022) 1769-1777, https://doi.org/10.1007/s42114-022-00417-2.

[25] B. Li, J. Xu, H. Xu, F. Yan, X. Zhang, C. Zhu, X. Zhang, Y. Chen, Grafting thin N-doped carbon nanotubes on hollow N-doped carbon nanoplates encapsulated with ultrasmall cobalt particles for microwave absorption, Chem. Eng. J. 435 (2022) 134846, https://doi.org/10.1016/j.cej.2022.134846.

[26] Q. Li, X. Zhao, Z. Zhang, X. Xun, B. Zhao, L. Xu, Z. Kang, Q. Liao, Y. Zhang, Architecture Design and Interface Engineering of Self-assembly VS_4/rGO Heterostructures for Ultrathin Absorbent, Nano-Micro Lett. 14(1) (2022) 67, https://doi.org/10.1007/s40820-022-00809-5.

[27] X. Dai, Y. Du, J. Yang, D. Wang, J. Gu, Y. Li, S. Wang, B.B. Xu, J. Kong, Recoverable and self-healing electromagnetic wave absorbing nanocomposites, Compos. Sci. Technol. 174 (2019) 27-32, https://doi.org/10.1016/j.compscitech.2019.02.018.

[28] Y. Guo, D. Wang, T. Bai, H. Liu, Y. Zheng, C. Liu, C. Shen, Electrostatic self-assembled $NiFe_2O_4$/Ti_3C_2Tx MXene nanocomposites for efficient electromagnetic wave absorption at ultralow loading level, Adv. Compos. Hybrid Mater. 4(3) (2021) 602-613, https://doi.org/10.1007/s42114-021-00279-0.

[29] B. Jain, A. Hashmi, S. Sanwaria, A.K. Singh, M. Susan, A.B. Hasan, A. Singh, Zinc oxide nanoparticle incorporated on

graphene oxide: an efficient and stable photocatalyst for water treatment through the Fenton process, Adv. Compos. Hybrid Mater. 3(2) (2020) 231-242, https://doi.org/10.1007/s42114-020-00153-5.

[30] C. Liu, Y. Lin, Y. Dong, Y. Wu, Y. Bao, H. Yan, J. Ma, Fabrication and investigation on Ag nanowires/TiO_2 nanosheets/graphene hybrid nanocomposite and its water treatment performance, Adv. Compos. Hybrid Mater. 3(3) (2020) 402-414, https://doi.org/10.1007/s42114-020-00164-2.

[31] Y. Guo, H. Qiu, K. Ruan, Y. Zhang, J. Gu, Hierarchically Multifunctional Polyimide Composite Films with Strongly Enhanced Thermal Conductivity, Nano-Micro Lett. 14(1) (2021) 26, https://doi.org/10.1007/s40820-021-00767-4.

[32] W. Xie, F. Yao, H. Gu, A. Du, Q. Lei, N. Naik, Z. Guo, Magnetoresistive and piezoresistive polyaniline nanoarrays in-situ polymerized surrounding magnetic graphene aerogel, Adv. Compos. Hybrid Mater. 5 (2022) 1003-1016, https://doi.org/10.1007/s42114-021-00413-y.

[33] Q. Men, S. Wang, Z. Yan, B. Zhao, L. Guan, G. Chen, X. Guo, R. Zhang, R. Che, Iron-encapsulated CNTs on carbon fiber with high-performance EMI shielding and electrocatalytic activity, Adv. Compos. Hybrid Mater. 5(3) (2022) 2429-2439, https://doi.org/10.1007/s42114-022-00457-8.

[34] L. Wang, H. Qiu, C. Liang, P. Song, Y. Han, Y. Han, J. Gu, J. Kong, D. Pan, Z. Guo, Electromagnetic interference shielding MWCNT-Fe_3O_4@Ag/epoxy nanocomposites with satisfactory thermal conductivity and high thermal stability, Carbon 141 (2019) 506-514, https://doi.org/10.1016/j.carbon.2018.10.003.

[35] X. Xu, F. Yao, O.A.A. Ali, W. Xie, S.F. Mahmoud, P. Xie, S.M. El-Bahy, M. Huang, C. Liu, R. Fan, Adjustable core-sheath architecture of polyaniline-decorated hollow carbon nanofiber nanocomposites with negative permittivity for superb electromagnetic interference shielding, Adv. Compos. Hybrid Mater. 5(3) (2022) 2002-2011, https://doi.org/10.1007/s42114-022-00538-8.

[36] Y. Han, K. Ruan, J. Gu, Janus (BNNS/ANF)-(AgNWs/ANF) thermal conductivity composite films with superior electromagnetic interference shielding and Joule heating performances, Nano Res. 15(5) (2022) 4747-4755, https://doi.org/10.1007/s12274-022-4159-z.

[37] F. Yao, W. Xie, C. Ma, D. Wang, Z.M. El-Bahy, M.H. Helal, H. Liu, A. Du, Z. Guo, H. Gu, Superb electromagnetic shielding polymer nanocomposites filled with 3-dimensional p-phenylenediamine/aniline copolymer nanofibers@copper foam hybrid nanofillers, Compos. Part B-Eng. 245 (2022) 110236, https://doi.org/10.1016/j.compositesb.2022.110236.

[38] S. Li, X. Tang, X. Zhao, S. Lu, J. Luo, Z. Chai, T. Ma, Q. Lan, P. Ma, W. Dong, Z. Wang, T. Liu, Hierarchical graphene@MXene

composite foam modified with flower-shaped FeS for efficient and broadband electromagnetic absorption, J. Mater. Sci. Technol. 133 (2023) 238-248, https://doi.org/10.1016/j.jmst.2022.06.018.

[39] B. Wen, H. Yang, Y. Lin, L. Ma, Y. Qiu, F. Hu, Controlling the heterogeneous interfaces of S, Co co-doped porous carbon nanosheets for enhancing the electromagnetic wave absorption, J. Colloid Interface. Sci. 586 (2021) 208-218, https://doi.org/10.1016/j.jcis.2020.10.085.

[40] Z. Zhang, Y. Zhao, Z. Li, L. Zhang, Z. Liu, Z. Long, Y. Li, Y. Liu, R. Fan, K. Sun, Synthesis of carbon/SiO_2 core-sheath nanofibers with Co-Fe nanoparticles embedded in via electrospinning for high-performance microwave absorption, Adv. Compos. Hybrid Mater. 5(1) (2022) 513-524, https://doi.org/10.1007/s42114-021-00350-w.

[41] T. Gao, H. Rong, K.H. Mahmoud, J. Ruan, S.M. El-Bahy, A.A. Faheim, Y. Li, M. Huang, M.A. Nassan, R. Zhao, Iron/silicon carbide composites with tunable high-frequency magnetic and dielectric properties for potential electromagnetic wave absorption, Adv. Compos. Hybrid Mater. 5 (2022) 1158-1167, https://doi.org/10.1007/s42114-022-00507-1.

[42] D. Pan, G. Yang, H.M. Abo-Dief, J. Dong, F. Su, C. Liu, Y. Li, B. Bin Xu, V. Murugadoss, N. Naik, S.M. El-Bahy, Z.M. El-Bahy, M. Huang, Z. Guo, Vertically Aligned Silicon Carbide Nanowires/Boron Nitride Cellulose Aerogel Networks Enhanced Thermal Conductivity and Electromagnetic Absorbing of Epoxy Composites, Nano-Micro Lett. 14(1) (2022) 118, https://doi.org/10.1007/s40820-022-00863-z.

[43] Q. Cao, J. Zhang, H. Zhang, J. Xu, R. Che, Dual-surfactant templated hydrothermal synthesis of $CoSe_2$ hierarchical microclews for dielectric microwave absorption, J. Adv. Ceram. 11(3) (2022) 504-514, https://doi.org/10.1007/s40145-021-0545-3.

[44] S. Zheng, Z. Zeng, J. Qiao, Y. Liu, J. Liu, Facile preparation of C/MnO/Co nanocomposite fibers for High-Performance microwave absorption, Compos. Part A-Appl. S. 155 (2022) 106814, https://doi.org/10.1016/j.compositesa.2022.106814.

[45] X. Cao, Z. Jia, D. Hu, G. Wu, Synergistic construction of three-dimensional conductive network and double heterointerface polarization via magnetic FeNi for broadband microwave absorption, Adv. Compos. Hybrid Mater. 5(2) (2022) 1030-1043, https://doi.org/10.1007/s42114-021-00415-w.

[46] Q. Jiang, Y. Qiao, C. Xiang, A. Uddin, L. Wu, F. Qin, Metacomposite based on three-dimensional ferromagnetic microwire architecture for electromagnetic response, Adv. Compos. Hybrid Mater. 5 (2022) 3190-3200, https://doi.org/10.1007/s42114-021-00394-y.

[47] S. Zhang, Z. Jia, B. Cheng, Z. Zhao, F. Lu, G. Wu, Recent progress of perovskite oxides and their hybrids for electromagnetic wave absorption: a mini-review, Adv. Compos. Hybrid Mater. 5(3) (2022) 2440-2460, https://doi.org/10.1007/s42114-022-00458-

7.

[48] Y. Han, M. He, J. Hu, P. Liu, Z. Liu, Z. Ma, W. Ju, J. Gu, Hierarchical design of FeCo-based microchains for enhanced microwave absorption in C band, Nano Res. (2022), https://doi.org/10.1007/s12274-022-5111-y.

[49] P. Hu, S. Dong, F. Yuan, X. Li, C. Hong, Hollow carbon microspheres modified with $NiCo_2S_4$ nanosheets as a high-performance microwave absorber, Adv. Compos. Hybrid Mater. 5(1) (2022) 469-480, https://doi.org/10.1007/s42114-021-00318-w.

[50] Y. Li, Y. Qing, W. Li, M. Zong, F. Luo, Novel Magnéli Ti_4O_7/Ni/poly (vinylidene fluoride) hybrids for high-performance electromagnetic wave absorption, Adv. Compos. Hybrid Mater. 4(4) (2021) 1027-1038, https://doi.org/10.1007/s42114-021-00297-y.

[51] K. Liu, W. Liu, W. Li, Y. Duan, K. Zhou, S. Zhang, S. Ni, T. Xu, H. Du, C. Si, Strong and highly conductive cellulose nanofibril/silver nanowires nanopaper for high performance electromagnetic interference shielding, Adv. Compos. Hybrid Mater. 5(2) (2022) 1078-1089, https://doi.org/10.1007/s42114-022-00425-2.

[52] Z. Zhou, X. Yang, D. Zhang, H. Zhang, J. Cheng, Y. Xiong, Z. Huang, H. Wang, P. Zhang, G. Zheng, Achieving superior GHz-absorption performance in VB-group laminated VS_2 microwave absorber with dielectric and magnetic synergy effects, Adv. Compos. Hybrid Mater. 5 (2022) 2317-2327, https://doi.org/10.1007/s42114-022-00416-3.

[53] Z. Shan, S. Cheng, F. Wu, X. Pan, W. Li, W. Dong, A. Xie, G. Zhang, Electrically conductive Two-dimensional Metal-Organic frameworks for superior electromagnetic wave absorption, Chem. Eng. J. 446 (2022) 137409, https://doi.org/10.1016/j.cej.2022.137409.

[54] L. Wang, S. Zhu, J. Zhu, Constructing ordered macropores in hollow Co/C polyhedral nanocages shell toward superior microwave absorbing performance, J. Colloid Interf. Sci. 624 (2022) 423-432, https://doi.org/10.1016/j.jcis.2022.05.158.

[55] F. Luo, D. Liu, T. Cao, H. Cheng, J. Kuang, Y. Deng, W. Xie, Study on broadband microwave absorbing performance of gradient porous structure, Adv. Compos. Hybrid Mater. 4(3) (2021) 591-601, https://doi.org/10.1007/s42114-021-00275-4.

[56] P. Xie, Y. Liu, M. Feng, M. Niu, C. Liu, N. Wu, K. Sui, R.R. Patil, D. Pan, Z. Guo, Hierarchically porous Co/C nanocomposites for ultralight high-performance microwave absorption, Adv. Compos. Hybrid Mater. 4(1) (2021) 173-185, https://doi.org/10.1007/s42114-020-00202-z.

[57] E. Chamanehpour, M.H. Sayadi, M. Hajiani, A hierarchical graphitic carbon nitride supported by metal–organic framework and copper nanocomposite as a novel bifunctional catalyst with long-term stability for enhanced carbon dioxide photoreduction

under solar light irradiation, Adv. Compos. Hybrid Mater. 5 (2022) 2461-2477, https://doi.org/10.1007/s42114-022-00459-6.

[58] Y. Guo, H. Liu, D. Wang, Z.M. El-Bahy, J.T. Althakafy, H.M. Abo-Dief, Z. Guo, B.B. Xu, C. Liu, C. Shen, Engineering hierarchical heterostructure material based on metal-organic frameworks and cotton fiber for high-efficient microwave absorber, Nano Res. 15 (2022) 6841-6850, https://doi.org/10.1007/s12274-022-4533-x.

[59] Z. Sun, M. Wang, J. Fan, R. Feng, Y. Zhou, L. Zhang, TiO_2@ MIL-101 (Cr) nanocomposites as an efficient photocatalyst for degradation of toluene, Adv. Compos. Hybrid Mater. 4(4) (2021) 1322-1329, https://doi.org/10.1007/s42114-021-00337-7.

[60] W. Cheng, Y. Wang, S. Ge, X. Ding, Z. Cui, Q. Shao, One-step microwave hydrothermal preparation of Cd/Zr-bimetallic metal–organic frameworks for enhanced photochemical properties, Adv. Compos. Hybrid Mater. 4(1) (2021) 150-161, https://doi.org/10.1007/s42114-020-00199-5.

[61] H. Yang, C. Yang, N. Zhang, K. Mo, Q. Li, K. Lv, J. Fan, L. Wen, Drastic promotion of the photoreactivity of MOF ultrathin nanosheets towards hydrogen production by deposition with CdS nanorods, Appl. Catal. B-Environ. 285 (2021) 119801, https://doi.org/10.1016/j.apcatb.2020.119801.

[62] M. Yuan, Y. Fei, H. Zhang, B. Qiu, L. Shen, X. He, M. Liang, S. Zhou, Y. Chen, H. Zou, Electromagnetic asymmetric films comprise metal organic frameworks derived porous carbon for absorption-dominated electromagnetic interference shielding, Compos. Part B-Eng. 233 (2022) 109622, https://doi.org/10.1016/j.compositesb.2022.109622.

[63] B. Yuan, M. Guo, V. Murugadoss, G. Song, Z. Guo, Immobilization of graphitic carbon nitride on wood surface via chemical crosslinking method for UV resistance and self-cleaning, Adv. Compos. Hybrid Mater. 4(2) (2021) 286-293, https://doi.org/10.1007/s42114-021-00235-y.

[64] X. Xie, H. Gao, X. Luo, Y. Zhang, Z. Qin, H. Ji, Polyethyleneimine-modified magnetic starch microspheres for Cd (II) adsorption in aqueous solutions, Adv. Compos. Hybrid Mater. 5 (2022) 2772-2786, https://doi.org/10.1007/s42114-022-00422-5.

[65] P. Sun, S. Zhou, Y. Yang, S. Liu, Q. Cao, Y. Wang, T. Wågberg, G. Hu, Artificial chloroplast-like phosphotungstic acid—iron oxide microbox heterojunctions penetrated by carbon nanotubes for solar photocatalytic degradation of tetracycline antibiotics in wastewater, Adv. Compos. Hybrid Mater. 5 (2022) 3158-3175, https://doi.org/10.1007/s42114-022-00462-x.

[66] C. Jing, Y. Zhang, J. Zheng, S. Ge, J. Lin, D. Pan, N. Naik, Z. Guo, In-situ constructing visible light CdS/Cd-MOF photocatalyst with enhanced photodegradation of methylene blue, Particuology 69 (2022) 111-122, https://doi.org/10.1016/j.partic.2021.11.013.

[67] P. Zhang, X. Zhang, B. Li, L. Xu, F. Dang, B.-W. Li, Enhanced microwave absorption performance in an ultralight porous single-atom Co-N-C absorber, Adv. Compos. Hybrid Mater. 4(4) (2021) 1292-1301, https://doi.org/10.1007/s42114-021-00308-y.

[68] Z. Zhang, Z. Cai, Z. Wang, Y. Peng, L. Xia, S. Ma, Z. Yin, Y. Huang, A Review on Metal-Organic Framework-Derived Porous Carbon-Based Novel Microwave Absorption Materials, Nano-Micro Lett. 13(1) (2021) 56, https://doi.org/10.1007/s40820-020-00582-3.

[69] X. Zhang, J. Qiao, Y. Jiang, F. Wang, X. Tian, Z. Wang, L. Wu, W. Liu, J. Liu, Carbon-Based MOF Derivatives: Emerging Efficient Electromagnetic Wave Absorption Agents, Nano-Micro Lett. 13(1) (2021) 135, https://doi.org/10.1007/s40820-021-00658-8.

[70] S.-Q. Zhu, J.-C. Shu, M.-S. Cao, Tailorable MOF architectures for high-efficiency electromagnetic functions, Mater. Chem. Front. 5(17) (2021) 6444-6460, https://doi.org/10.1039/d1qm00659b.

[71] K. Vasanth Kumar, G. Charalambopoulou, M. Kainourgiakis, A. Stubos, T. Steriotis, Insights on the physical adsorption of hydrogen and methane in UiO series of MOFs using molecular simulations, Comput. Theor. Chem. 1061 (2015) 36-45, https://doi.org/10.1016/j.comptc.2015.03.007.

[72] X. Peng, L. Ye, Y. Ding, L. Yi, C. Zhang, Z. Wen, Nanohybrid photocatalysts with $ZnIn_2S_4$ nanosheets encapsulated UiO-66 octahedral nanoparticles for visible-light-driven hydrogen generation, Appl. Catal. B-Environ. 260 (2020) 118152, https://doi.org/10.1016/j.apcatb.2019.118152.

[73] A.B. Ali Baig, V. Rathinam, V. Ramya, Facile fabrication of Zn-doped SnO_2 nanoparticles for enhanced photocatalytic dye degradation performance under visible light exposure, Adv. Compos. Hybrid Mater. 4(1) (2021) 114-126, https://doi.org/10.1007/s42114-020-00195-9.

[74] J. Zheng, Y. Zhang, C. Jing, H. Zhang, Q. Shao, R. Ge, A visible-light active p-n heterojunction ZnO/Co_3O_4 composites supported on Ni foam as photoanode for enhanced photoelectrocatalytic removal of methylene blue, Adv. Compos. Hybrid Mater. 5(3) (2022) 2406-2420, https://doi.org/10.1007/s42114-022-00448-9.

[75] S. Jamshidifard, S. Koushkbaghi, S. Hosseini, S. Rezaei, A. Karamipour, A. Jafari Rad, M. Irani, Incorporation of UiO-66-NH_2 MOF into the PAN/chitosan nanofibers for adsorption and membrane filtration of Pb(II), Cd(II) and Cr(VI) ions from aqueous solutions, J. Hazard. Mater. 368 (2019) 10-20, https://doi.org/10.1016/j.jhazmat.2019.01.024.

[76] C.C. Lee, C.I. Chen, Y.T. Liao, K.C. Wu, C.C. Chueh, Enhancing Efficiency and Stability of Photovoltaic Cells by Using Perovskite/Zr-MOF Heterojunction Including Bilayer and Hybrid Structures, Adv. Sci. 6(5) (2019) 1801715, https://doi.org/10.1002/advs.201801715.

[77] R. Vakili, R. Gholami, C.E. Stere, S. Chansai, H. Chen, S.M. Holmes, Y. Jiao, C. Hardacre, X. Fan, Plasma-assisted catalytic

dry reforming of methane (DRM) over metal-organic frameworks (MOFs)-based catalysts, Appl. Catal. B-Environ. 260 (2020) 118195, https://doi.org/10.1016/j.apcatb.2019.118195.

[78] W. Liu, Y. Pan, Y. Zhong, B. Li, Q. Ding, H. Xu, Y. Qiu, F. Ren, B. Li, M. Muddassir, J. Liu, A multifunctional aminated UiO-67 metal-organic framework for enhancing antitumor cytotoxicity through bimodal drug delivery, Chem. Eng. J. 412 (2021) 127899, https://doi.org/10.1016/j.cej.2020.127899.

[79] K. Jayaramulu, M. Horn, A. Schneemann, H. Saini, A. Bakandritsos, V. Ranc, M. Petr, V. Stavila, C. Narayana, B. Scheibe, S. Kment, M. Otyepka, N. Motta, D. Dubal, R. Zboril, R.A. Fischer, Covalent Graphene-MOF Hybrids for High-Performance Asymmetric Supercapacitors, Adv. Mater. 33(4) (2021) e2004560, https://doi.org/10.1002/adma.202004560.

[80] L. Xiao, H. Qi, K. Qu, C. Shi, Y. Cheng, Z. Sun, B. Yuan, Z. Huang, D. Pan, Z. Guo, Layer-by-layer assembled free-standing and flexible nanocellulose/porous Co_3O_4 polyhedron hybrid film as supercapacitor electrodes, Adv. Compos. Hybrid Mater. 4(2) (2021) 306-316, https://doi.org/10.1007/s42114-021-00223-2.

[81] Y. Zhao, F. Liu, K. Zhu, S. Maganti, Z. Zhao, P. Bai, Three-dimensional printing of the copper sulfate hybrid composites for supercapacitor electrodes with ultra-high areal and volumetric capacitances, Adv. Compos. Hybrid Mater. 5(2) (2022) 1537-1547, https://doi.org/10.1007/s42114-022-00430-5.

[82] D. Wang, Y. Xin, X. Li, F. Wang, Y. Wang, W. Zhang, Y. Zheng, D. Yao, Z. Yang, X. Lei, A universal approach to turn UiO-66 into type 1 porous liquids via post-synthetic modification with corona-canopy species for CO_2 capture, Chem. Eng. J. 416 (2021) 127625, https://doi.org/10.1016/j.cej.2020.127625.

[83] M.-J. Chen, A.-C. Yang, N.-H. Wang, H.-C. Chiu, Y.-L. Li, D.-Y. Kang, S.-L. Lo, Influence of crystal topology and interior surface functionality of metal-organic frameworks on PFOA sorption performance, Microporous Mesoporous Mater. 236 (2016) 202-210, https://doi.org/10.1016/j.micromeso.2016.08.046.

[84] P. Arabkhani, H. Javadian, A. Asfaram, M. Ateia, Decorating graphene oxide with zeolitic imidazolate framework (ZIF-8) and pseudo-boehmite offers ultra-high adsorption capacity of diclofenac in hospital effluents, Chemosphere 271 (2021) 129610, https://doi.org/10.1016/j.chemosphere.2021.129610.

[85] Q.T.N. Le, K. Cho, Caesium adsorption on a zeolitic imidazolate framework (ZIF-8) functionalized by ferrocyanide, J. Colloid Interf. Sci. 581(Pt B) (2021) 741-750, https://doi.org/10.1016/j.jcis.2020.08.017.

[86] G. Cui, G. Li, D. Luo, Y. Zhang, Y. Zhao, D. Wang, J. Wang, Z. Zhang, X. Wang, Z. Chen, Three-dimensionally ordered macro-microporous metal organic frameworks with strong sulfur immobilization and catalyzation for high-performance lithium-sulfur

batteries, Nano Energy 72 (2020) 104685, https://doi.org/10.1016/j.nanoen.2020.104685.

[87] Z. Wu, L. Wang, S. Chen, X. Zhu, Q. Deng, J. Wang, Z. Zeng, S. Deng, Facile and low-temperature strategy to prepare hollow ZIF-8/CNT polyhedrons as high-performance lithium-sulfur cathodes, Chem. Eng. J. 404 (2021) 126579, https://doi.org/10.1016/j.cej.2020.126579.

[88] Z. Yan, J. Li, Q. Chen, S. Chen, L. Luo, Y. Chen, Synthesis of $CoSe_2$/Mxene composites using as high-performance anode materials for lithium-ion batteries, Adv. Compos. Hybrid Mater. 5 (2022) 2977–2987, https://doi.org/10.1007/s42114-022-00524-0.

[89] K.M. Gupta, K. Zhang, J. Jiang, Water Desalination through Zeolitic Imidazolate Framework Membranes: Significant Role of Functional Groups, Langmuir 31(48) (2015) 13230-13237, https://doi.org/10.1021/acs.langmuir.5b03593.

[90] Z. Zhao, X. Zhou, K. Kou, H. Wu, PVP-assisted transformation of ZIF-67 into cobalt layered double hydroxide/carbon fiber as electromagnetic wave absorber, Carbon 173 (2021) 80-90, https://doi.org/10.1016/j.carbon.2020.11.009.

[91] K. Yu, D.-I. Won, W.I. Lee, W.-S. Ahn, Porphyrinic zirconium metal-organic frameworks: Synthesis and applications for adsorption/catalysis, Korean J. Chem. Eng. 38(4) (2021) 653-673, https://doi.org/10.1007/s11814-020-0730-z.

[92] D. Feng, Z.-Y. Gu, J.-R. Li, H.-L. Jiang, Z. Wei, H.-C. Zhou, Zirconium-Metalloporphyrin PCN-222: Mesoporous Metal-Organic Frameworks with Ultrahigh Stability as Biomimetic Catalysts, Angew. Chem. Int. Ed. 51(41) (2012) 10307-10310, https://doi.org/10.1002/anie.201204475.

[93] P.J. Meza-Morales, A. Santana-Vargas, M.C. Curet-Arana, DFT analysis of coordination polymer ligands: unraveling the electrostatic properties and their effect on CO_2 interaction, Adsorption 21(6-7) (2015) 533-546, https://doi.org/10.1007/s10450-015-9692-6.

[94] S.D. Marks, K. Riascos-Rodriguez, R.R. Arrieta-Pérez, A.A. Yakovenko, J. Exley, P.G. Evans, A.J. Hernández-Maldonado, Lattice expansion and ligand twist during CO_2 adsorption in flexible Cu bipyridine metal-organic frameworks, J. Mater. Chem. A 8(36) (2020) 18903-18915, https://doi.org/10.1039/d0ta03298k.

[95] F. Zheng, L. Guo, B. Gao, L. Li, Z. Zhang, Q. Yang, Y. Yang, B. Su, Q. Ren, Z. Bao, Engineering the Pore Size of Pillared-Layer Coordination Polymers Enables Highly Efficient Adsorption Separation of Acetylene from Ethylene, ACS Appl. Mater. Inter. 11(31) (2019) 28197-28204, https://doi.org/10.1021/acsami.9b09231.

[96] O.A. Kholdeeva, I.Y. Skobelev, I.D. Ivanchikova, K.A. Kovalenko, V.P. Fedin, A.B. Sorokin, Hydrocarbon oxidation over Fe- and Cr-containing metal-organic frameworks MIL-100 and MIL-101-a comparative study, Catal. Today 238 (2014) 54-61,

https://doi.org/10.1016/j.cattod.2014.01.010.

[97] Q. Wu, M.S. Siddique, W. Yu, Iron-nickel bimetallic metal-organic frameworks as bifunctional Fenton-like catalysts for enhanced adsorption and degradation of organic contaminants under visible light: Kinetics and mechanistic studies, J. Hazard. Mater. 401 (2021) 123261, https://doi.org/10.1016/j.jhazmat.2020.123261.

[98] F. Zhao, Y. Liu, S.B. Hammouda, B. Doshi, N. Guijarro, X. Min, C.-J. Tang, M. Sillanpää, K. Sivula, S. Wang, MIL-101(Fe)/g-C_3N_4 for enhanced visible-light-driven photocatalysis toward simultaneous reduction of Cr(VI) and oxidation of bisphenol A in aqueous media, Appl. Catal. B-Environ. 272 (2020) 119033, https://doi.org/10.1016/j.apcatb.2020.119033.

[99] S. Sarwar, M.-C. Lin, M.R. Ahasan, Y. Wang, R. Wang, X. Zhang, Direct growth of cobalt-doped molybdenum disulfide on graphene nanohybrids through microwave irradiation with enhanced electrocatalytic properties for hydrogen evolution reaction, Adv. Compos. Hybrid Mater. 5(3) (2022) 2339-2352, https://doi.org/10.1007/s42114-022-00424-3.

[100] L.M. Yang, P. Ravindran, P. Vajeeston, M. Tilset, Properties of IRMOF-14 and its analogues M-IRMOF-14 (M = Cd, alkaline earth metals): electronic structure, structural stability, chemical bonding, and optical properties, Phys. Chem. Chem. Phys. 14(14) (2012) 4713-23, https://doi.org/10.1039/c2cp24091b.

[101] S.J. Yang, S. Nam, T. Kim, J.H. Im, H. Jung, J.H. Kang, S. Wi, B. Park, C.R. Park, Preparation and exceptional lithium anodic performance of porous carbon-coated ZnO quantum dots derived from a metal-organic framework, J. Am. Chem. Soc. 135(20) (2013) 7394-7, https://doi.org/10.1021/ja311550t.

[102] J. Yang, L. Tong, A.S. Alsubaie, K.H. Mahmoud, Y. Guo, L. Liu, L. Guo, Z. Sun, C. Wang, Hybrid proton exchange membrane used in fuel cell with amino-functionalized metal-organic framework in sulfonated polyimide to construct efficient ion transport channel, Adv. Compos. Hybrid Mater. 5 (2022) 834-842, https://doi.org/10.1007/s42114-022-00469-4.

[103] Z. Zhang, H.T. Nguyen, S.A. Miller, A.M. Ploskonka, J.B. DeCoste, S.M. Cohen, Polymer-Metal-Organic Frameworks (polyMOFs) as Water Tolerant Materials for Selective Carbon Dioxide Separations, J. Am. Chem. Soc. 138(3) (2016) 920-5, https://doi.org/10.1021/jacs.5b11034.

[104] A. Mavrandonakis, E. Klontzas, E. Tylianakis, G.E.J.J.o.t.A.C.S. Froudakis, Enhancement of hydrogen adsorption in metal-organic frameworks by the incorporation of the sulfonate group and Li cations. A multiscale computational study, JACS 131(37) (2009) 13410-13414, https://doi.org/10.1021/ja9043888.

[105] H. Xu, J. Gao, X. Qian, J. Wang, H. He, Y. Cui, Y. Yang, Z. Wang, G. Qian, Metal-organic framework nanosheets for fast-response and highly sensitive luminescent sensing of Fe^{3+}, J. Mater. Chem. A 4(28) (2016) 10900-10905,

https://doi.org/10.1039/c6ta03065c.

[106] S. Krause, V. Bon, I. Senkovska, U. Stoeck, D. Wallacher, D.M. Tobbens, S. Zander, R.S. Pillai, G. Maurin, F.X. Coudert, S. Kaskel, A pressure-amplifying framework material with negative gas adsorption transitions, Nature 532(7599) (2016) 348-52, https://doi.org/10.1038/nature17430.

[107] F.L. Li, P. Wang, X. Huang, D.J. Young, H.F. Wang, P. Braunstein, J.P. Lang, Large-Scale, Bottom-Up Synthesis of Binary Metal-Organic Framework Nanosheets for Efficient Water Oxidation, Angew. Chem. Int. Ed. 58(21) (2019) 7051-7056, https://doi.org/10.1002/anie.201902588.

[108] H. Wang, X. Yuan, Y. Wu, G. Zeng, X. Chen, L. Leng, Z. Wu, L. Jiang, H. Li, Facile synthesis of amino-functionalized titanium metal-organic frameworks and their superior visible-light photocatalytic activity for Cr(VI) reduction, J. Hazard. Mater. 286 (2015) 187-94, https://doi.org/10.1016/j.jhazmat.2014.11.039.

[109] Y. Pan, S. Yan, Y. Liu, Z. Tian, D. Li, Y. Chen, L. Guo, Y. Wang, Significantly enhanced electrochemical performance of 2D Ni-MOF by carbon quantum dot for high-performance supercapacitors, Electrochim. Acta 422 (2022) 140560, https://doi.org/10.1016/j.electacta.2022.140560.

[110] Q. Li, Y. Liu, S. Niu, C. Li, C. Chen, Q. Liu, J. Huo, Microwave-assisted rapid synthesis and activation of ultrathin trimetal-organic framework nanosheets for efficient electrocatalytic oxygen evolution, J. Colloid Interf. Sci. 603 (2021) 148-156, https://doi.org/10.1016/j.jcis.2021.06.102.

[111] Y. Chen, D. Ni, X. Yang, C. Liu, J. Yin, K. Cai, Microwave-assisted synthesis of honeycomblike hierarchical spherical Zn-doped Ni-MOF as a high-performance battery-type supercapacitor electrode material, Electrochim. Acta 278 (2018) 114-123, https://doi.org/10.1016/j.electacta.2018.05.024.

[112] Y. Choi, T. Chen, D. Kim, S.G. Ji, H. Hong, L. Lyu, M. Jang, Y. Piao, Transformation of microwave synthesized highly uniform FeMo-MIL-88B nanorod to oxynitride derivate for overall water splitting reaction, Appl. Mater. Today 24 (2021) 101093, https://doi.org/10.1016/j.apmt.2021.101093.

[113] A. Asghar, N. Iqbal, T. Noor, B.M. Kariuki, L. Kidwell, T.L. Easun, Efficient electrochemical synthesis of a manganese-based metal–organic framework for H_2 and CO_2 uptake, Green Chem. 23(3) (2021) 1220-1227, https://doi.org/10.1039/d0gc03292a.

[114] Y. Liu, Y. Wei, M. Liu, Y. Bai, X. Wang, S. Shang, J. Chen, Y. Liu, Electrochemical Synthesis of Large Area Two-Dimensional Metal-Organic Framework Films on Copper Anodes, Angew. Chem. Int. Ed. 60(6) (2021) 2887-2891, https://doi.org/10.1002/anie.202012971.

[115] S. Qin, S. Zhang, M. Chen, L. Wu, Electrochemical fabrication of long-range ordered macro-microporous metal–organic framework films, J. Mater. Chem. A 10(17) (2022) 9497-9505, https://doi.org/10.1039/d2ta00226d.

[116] M. Karimi, H. Mohebali, S. Sadeghi, V. Safarifard, A. Mahjoub, A. Heydari, Additive-free aerobic C-H oxidation through a defect-engineered Ce-MOF catalytic system, Microporous Mesoporous Mater. 322 (2021) 111054, https://doi.org/10.1016/j.micromeso.2021.111054.

[117] F. Li, J. Li, L. Zhou, S. Dai, Enhanced OER performance of composite Co–Fe-based MOF catalysts via a one-pot ultrasonic-assisted synthetic approach, Sustain. Energ. Fuels 5(4) (2021) 1095-1102, https://doi.org/10.1039/d0se01750g.

[118] M. Shen, J. Zhou, M. Elhadidy, Y. Xianyu, J. Feng, D. Liu, T. Ding, Cyclodextrin metal-organic framework by ultrasound-assisted rapid synthesis for caffeic acid loading and antibacterial application, Ultrason. Sonochem. 86 (2022) 106003, https://doi.org/10.1016/j.ultsonch.2022.106003.

[119] Y. Wang, Y. Lu, Z. Li, X.W. Sun, W.Y. Zhang, S. Zhang, J. Wang, T.Y. Dang, Z. Zhang, S.X. Liu, One-pot mechanochemical synthesis to encapsulate functional guests into a metal-organic framework for proton conduction, Chem. Commun. 57(71) (2021) 8933-8936, https://doi.org/10.1039/d1cc03482k.

[120] B. Yi, H. Zhao, L. Cao, X. Si, Y. Jiang, P. Cheng, Y. Zuo, Y. Zhang, L. Su, Y. Wang, C.K. Tsung, L.Y. Chou, J. Xie, A direct mechanochemical conversion of Pt-doped metal-organic framework-74 from doped metal oxides for CO oxidation, Mater. Today Nano 17 (2022) 100158, https://doi.org/10.1016/j.mtnano.2021.100158.

[121] P. Liu, T. Zhao, K. Cai, P. Chen, F. Liu, D.-J. Tao, Rapid mechanochemical construction of HKUST-1 with enhancing water stability by hybrid ligands assembly strategy for efficient adsorption of SF_6, Chem. Eng. J. 437 (2022) 135364, https://doi.org/10.1016/j.cej.2022.135364.

[122] N. Wu, B. Zhao, X. Chen, C. Hou, M. Huang, A. Alhadhrami, G.A. Mersal, M.M. Ibrahim, J. Tian, Dielectric properties and electromagnetic simulation of molybdenum disulfide and ferric oxide-modified $Ti_3C_2T_X$ MXene hetero-structure for potential microwave absorption, Adv. Compos. Hybrid Mater. 5(2) (2022) 1548-1556, https://doi.org/10.1007/s42114-022-00490-7.

[123] J. Xiao, X. Qi, X. Gong, Q. Peng, Y. Chen, R. Xie, W. Zhong, Defect and interface engineering in core@shell structure hollow carbon@MoS_2 nanocomposites for boosted microwave absorption performance, Nano Res. 15(9) (2022) 7778-7787, https://doi.org/10.1007/s12274-022-4625-7.

[124] C. Li, X. Qi, X. Gong, Q. Peng, Y. Chen, R. Xie, W. Zhong, Magnetic-dielectric synergy and interfacial engineering to design yolk-shell structured CoNi@void@C and CoNi@void@C@MoS_2 nanocomposites with tunable and strong wideband microwave

absorption, Nano Res. 15 (2022) 6761-6771, https://doi.org/10.1007/s12274-022-4468-2.

[125] R. Wang, E. Yang, X. Qi, R. Xie, S. Qin, C. Deng, W. Zhong, Constructing and optimizing core@ shell structure CNTs@ MoS_2 nanocomposites as outstanding microwave absorbers, Appl. Surf. Sci. 516 (2020) 146159, https://doi.org/10.1016/j.apsusc.2020.146159.

[126] Y. Bi, M. Ma, Z. Jiao, Y. Ma, D. Hou, G. Geng, W. Feng, A. Ma, M. Qiao, Y. Liu, Enhancing electromagnetic wave absorption performance of one-dimensional C@Co/N-doped C@PPy composite fibers, Carbon 197 (2022) 152-162, https://doi.org/10.1016/j.carbon.2022.05.061.

[127] A. Dong, Z. Mu, X. Meng, S. Li, J. Li, L. Dai, J. Lv, P. Li, B. Wang, Fine-tuning the electromagnetic parameters of 2D conjugated metal-organic framework semiconductors for anti-electromagnetic interference in the Ku band, Chem. Eng. J. 444 (2022) 136574, https://doi.org/10.1016/j.cej.2022.136574.

[128] X. Zhang, Y. Zhang, J. He, H. Li, Y. Bai, S. Gao, $ZnFe_2O_4$ nanospheres decorated residual carbon from coal gasification fine slag as an ultra-thin microwave absorber, Fuel 331 (2023) 125811, https://doi.org/10.1016/j.fuel.2022.125811.

[129] Y. Liu, X. Zhou, Z. Jia, H. Wu, G. Wu, Oxygen Vacancy-Induced Dielectric Polarization Prevails in the Electromagnetic Wave-Absorbing Mechanism for Mn-Based MOFs-Derived Composites, Adv. Funct. Mater. 32(34) (2022) 2204499, https://doi.org/10.1002/adfm.202204499.

[130] X. Chen, M. Yang, X. Zhao, D. Hu, W. Liu, W. Ma, Tailoring superhydrophobic PDMS/$CeFe_2O_4$/MWCNTs nanocomposites with conductive network for highly efficient microwave absorption, Chem. Eng. J. 432 (2022) 134226, https://doi.org/10.1016/j.cej.2021.134226.

[131] J. Zhang, Z. Li, X. Qi, X. Gong, R. Xie, C. Deng, W. Zhong, Y. Du, Constructing flower-like core@ shell $MoSe_2$-based nanocomposites as a novel and high-efficient microwave absorber, Compos. Part B-Eng. 222 (2021) 109067, https://doi.org/10.1016/j.compositesb.2021.109067.

[132] J. Zhang, X. Qi, X. Gong, Q. Peng, Y. Chen, R. Xie, W. Zhong, Microstructure optimization of core@ shell structured MSe_2/$FeSe_2$@ $MoSe_2$ (M= Co, Ni) flower-like multicomponent nanocomposites towards high-efficiency microwave absorption, J. Mater. Sci. Technol. 128 (2022) 59-70, https://doi.org/10.1016/j.jmst.2022.04.017.

[133] J. He, M. Han, K. Wen, C. Liu, W. Zhang, Y. Liu, X. Su, C. Zhang, C. Liang, Absorption-dominated electromagnetic interference shielding assembled composites based on modular design with infrared camouflage and response switching, Compos. Sci. Technol. 231 (2023) 109799, https://doi.org/10.1016/j.compscitech.2022.109799.

[134] L. Li, S. Lian, J. Tang, S. Chen, R. Guo, S. Pan, C. Peng, Superhydrophobic nanocomposites of erbium oxide and reduced graphene oxide for high-performance microwave absorption, J. Colloid Interf. Sci. 615 (2022) 69-78, https://doi.org/10.1016/j.jcis.2022.01.169.

[135] J. Liu, Z. Jia, Y. Dong, J. Li, X. Cao, G. Wu, Structural engineering and compositional manipulation for high-efficiency electromagnetic microwave absorption, Mater. Today Phys. 27 (2022) 100801, https://doi.org/10.1016/j.mtphys.2022.100801.

[136] H. Luo, S. Lv, G. Liu, Y. Cheng, X. Ge, X. Wang, R. Gong, F. Chen, Multi-interfacial magnetic carbon nanotubes encapsulated hydrangea-like NiMo/MoC/N-doped carbon composites for efficient microwave absorption, Carbon 196 (2022) 828-839, https://doi.org/10.1016/j.carbon.2022.05.046.

[137] Z. Ma, C.-T. Cao, Q.-F. Liu, J.-B. Wang, A New Method to Calculate the Degree of Electromagnetic Impedance Matching in One-Layer Microwave Absorbers, Chin. Phys. Lett. 29(3) (2012) 038401, https://doi.org/10.1088/0256-307x/29/3/038401.

[138] Z.X. Lei, S.Z. Li, A.Q. Zhang, Y.H. Song, N. He, M.Z. Li, D.Y. Geng, W. Liu, S. Ma, Z.D. Zhang, Electromagnetic wave absorption superalloy/graphite magnetic nanocapsules applied in wide temperature range, Compos. Part B-Eng. 234 (2022) 109692, https://doi.org/10.1016/j.compositesb.2022.109692.

[139] H. Peng, M. He, Y. Zhou, Z. Song, Y. Wang, S. Feng, X. Chen, X. Zhang, H. Chen, Low-temperature carbonized biomimetic cellulose nanofiber/MXene composite membrane with excellent microwave absorption performance and tunable absorption bands, Chem. Eng. J. 433 (2022) 133269, https://doi.org/10.1016/j.cej.2021.133269.

[140] M. Wu, A.K. Darboe, X. Qi, R. Xie, S. Qin, C. Deng, G. Wu, W. Zhong, Optimization, selective and efficient production of CNTs/$Co_xFe_{3-x}O_4$ core/shell nanocomposites as outstanding microwave absorbers, J. Mater. Chem. C 8(34) (2020) 11936-11949, https://doi.org/10.1039/d0tc01970d.

[141] B. Dai, F. Dong, J. Yu, S. Feng, H. Wang, T. Li, M. Ma, J. Ding, Y. Ma, Construction of Ni@polypyrrole nanochains/$Ti_3C_2T_x$ ternary composites with excellent microwave absorption properties, Mater. Chem. Front. 6 (2022) 3179-3192, https://doi.org/10.1039/d2qm00672c.

[142] L. Wang, M. Huang, X. Yu, W. You, B. Zhao, C. Liang, X. Liu, X. Zhang, R. Che, Engineering polarization surface of hierarchical ZnO microspheres via spray-annealing strategy for wide-frequency electromagnetic wave absorption, J. Mater. Sci. Technol. 131 (2022) 231-239, https://doi.org/10.1016/j.jmst.2022.05.015.

[143] Y. Liu, Z. Jia, J. Zhou, G. Wu, Multi-hierarchy heterostructure assembling on MnO_2 nanowires for optimized electromagnetic response, Mater. Today Phys. 28 (2022) 100845, https://doi.org/10.1016/j.mtphys.2022.100845.

[144] L. Long, E. Yang, X. Qi, R. Xie, Z.-c. Bai, S. Qin, C. Deng, W. Zhong, Positive and Reverse Core/Shell Structure $Co_xFe_{3-x}O_4/MoS_2$ and $MoS_2/Co_xFe_{3-x}O_4$ Nanocomposites: Selective Production and Outstanding Electromagnetic Absorption Comprehensive Performance, ACS Sustainable Chem. Eng. 8(1) (2020) 613-623, https://doi.org/10.1021/acssuschemeng.9b06205.

[145] B. Dai, Y. Ma, S. Feng, H. Wang, M. Ma, J. Ding, X. Yin, T. Li, Fabrication of one-dimensional M (Co, Ni)@polyaniline nanochains with adjustable thickness for excellent microwave absorption properties, J. Colloid Interf. Sci. 627 (2022) 113-125, https://doi.org/10.1016/j.jcis.2022.06.137.

[146] J. He, S. Gao, Y. Zhang, X. Zhang, H. Li, N-doped residual carbon from coal gasification fine slag decorated with Fe_3O_4 nanoparticles for electromagnetic wave absorption, J. Mater. Sci. Technol. 104 (2022) 98-108, https://doi.org/10.1016/j.jmst.2021.06.052.

[147] Z. Zou, M. Ning, Z. Lei, X. Zhuang, G. Tan, J. Hou, H. Xu, Q. Man, J. Li, R.-W. Li, 0D/1D/2D architectural Co@C/MXene composite for boosting microwave attenuation performance in 2-18 GHz, Carbon 193 (2022) 182-194, https://doi.org/10.1016/j.carbon.2022.03.017.

[148] J. Zhou, Z. Jia, Y. Zhang, G. Wu, Construction of 3D conductive network by flower-like V_2O_3 synergy with magnetic NiCo for superior electromagnetic wave absorption performance, Mater. Today Phys. 29 (2022) 100902, https://doi.org/10.1016/j.mtphys.2022.100902.

[149] W. Liu, J. Liu, Z. Yang, G. Ji, Extended Working Frequency of Ferrites by Synergistic Attenuation through a Controllable Carbothermal Route Based on Prussian Blue Shell, ACS Appl. Mater. Inter. 10(34) (2018) 28887-28897, https://doi.org/10.1021/acsami.8b09682.

[150] H. Zhao, Y. Cheng, W. Liu, Z. Yang, B. Zhang, G. Ji, Y. Du, The flaky porous Fe_3O_4 with tunable dimensions for enhanced microwave absorption performance in X and C bands, Nanotechnology 29(29) (2018) 295603, https://doi.org/10.1088/1361-6528/aac0de.

[151] Y. Zhao, L. Liu, J. Han, W. Wu, G. Tong, Effective modulation of electromagnetic characteristics by composition and size in expanded graphite/Fe_3O_4 nanoring composites with high Snoek's limit, J. Alloys Compd. 728 (2017) 100-111, https://doi.org/10.1016/j.jallcom.2017.08.238.

[152] O. Acher, S. Dubourg, Generalization of Snoek's law to ferromagnetic films and composites, Phys. Rev. B 77(10) (2008) 104440, https://doi.org/10.1103/PhysRevB.77.104440.

[153] X. Jian, B. Wu, Y. Wei, S.X. Dou, X. Wang, W. He, N. Mahmood, Facile Synthesis of Fe_3O_4/GCs Composites and Their

Enhanced Microwave Absorption Properties, ACS Appl. Mater. Inter. 8(9) (2016) 6101-9, https://doi.org/10.1021/acsami.6b00388.

[154] M. Qiao, X. Lei, Y. Ma, L. Tian, X. He, K. Su, Q. Zhang, Application of yolk–shell Fe_3O_4@N-doped carbon nanochains as highly effective microwave-absorption material, Nano Res. 11(3) (2018) 1500-1519, https://doi.org/10.1007/s12274-017-1767-0.

[155] X. Zhang, X. Dong, H. Huang, Y. Liu, W. Wang, X. Zhu, B. Lv, J. Lei, C. Lee, Microwave absorption properties of the carbon-coated nickel nanocapsules, Appl. Phys. Lett. 89(5) (2006) 053115, https://doi.org/10.1063/1.2236965.

[156] B. Dai, Y. Ma, F. Dong, J. Yu, M. Ma, H.K. Thabet, S.M. El-Bahy, M.M. Ibrahim, M. Huang, I. Seok, G. Roymahapatra, N. Naik, B.B. Xu, J. Ding, T. Li, Overview of MXene and conducting polymer matrix composites for electromagnetic wave absorption, Adv. Compos. Hybrid Mater. 5(2) (2022) 704-754, https://doi.org/10.1007/s42114-022-00510-6.

[157] X. Huang, X. Liu, Z. Jia, B. Wang, X. Wu, G. Wu, Synthesis of 3D cerium oxide/porous carbon for enhanced electromagnetic wave absorption performance, Adv. Compos. Hybrid Mater. 4(4) (2021) 1398-1412, https://doi.org/10.1007/s42114-021-00304-2.

[158] J. Xiao, X. Qi, X. Gong, Q. Peng, Y. Chen, R. Xie, W. Zhong, Tunable and improved microwave absorption of flower-like core@shell MFe_2O_4@MoS_2 (M = Mn, Ni and Zn) nanocomposites by defect and interface engineering, J. Mater. Sci. Technol. 139 (2023) 137-146, https://doi.org/10.1016/j.jmst.2022.08.022.

[159] C. Zhou, Z. Yao, B. Wei, W. Li, Z. Li, X. Tao, J. Zhou, Facile synthesis of ZIF-67 derived dodecahedral C/$NiCO_2S_4$ with broadband microwave absorption performance, Nanoscale 14(29) (2022) 10375-10388, https://doi.org/10.1039/d2nr02490j.

[160] Z. Xiang, Y. Song, J. Xiong, Z. Pan, X. Wang, L. Liu, R. Liu, H. Yang, W. Lu, Enhanced electromagnetic wave absorption of nanoporous Fe_3O_4@carbon composites derived from metal-organic frameworks, Carbon 142 (2019) 20-31, https://doi.org/10.1016/j.carbon.2018.10.014.

[161] Y. Yang, D. Xu, L. Lyu, F. Wang, Z. Wang, L. Wu, W. Liu, J. Liu, Synthesis of MOF-derived Fe_7S_8/C rod-like composites by controlled proportion of carbon for highly efficient electromagnetic wave absorption, Compos. Part A-Appl. S. 142 (2021) 106246, https://doi.org/10.1016/j.compositesa.2020.106246.

[162] M. Huang, L. Wang, K. Pei, W. You, X. Yu, Z. Wu, R. Che, Multidimension-Controllable Synthesis of MOF-Derived Co@N-Doped Carbon Composite with Magnetic-Dielectric Synergy toward Strong Microwave Absorption, Small 16(14) (2020) e2000158, https://doi.org/10.1002/smll.202000158.

[163] Q. Wu, B. Wang, Y. Fu, Z. Zhang, P. Yan, T. Liu, MOF-derived Co/CoO particles prepared by low temperature reduction for microwave absorption, Chem. Eng. J. 410 (2021) 128378, https://doi.org/10.1016/j.cej.2020.128378.

[164] L. Jin, P. Yi, L. Wan, J. Hou, P. Chen, J. Zu, B. Wei, Z. Yao, J. Zhou, Thickness-controllable synthesis of MOF-derived Ni@N-

doped carbon hexagonal nanoflakes with dielectric-magnetic synergy toward wideband electromagnetic wave absorption, Chem. Eng. J. 427 (2022) 130940, https://doi.org/10.1016/j.cej.2021.130940.

[165] Y. Qiu, Y. Lin, H. Yang, L. Wang, M. Wang, B. Wen, Hollow Ni/C microspheres derived from Ni-metal organic framework for electromagnetic wave absorption, Chem. Eng. J. 383 (2020) 123207, https://doi.org/10.1016/j.cej.2019.123207.

[166] Y. Wei, M. Zheng, W. Luo, B. Dai, J. Ren, M. Ma, T. Li, Y. Ma, All pseudocapacitive MXene-MnO_2 flexible asymmetric supercapacitor, J. Energy Storage 45 (2022) 103715, https://doi.org/10.1016/j.est.2021.103715.

[167] M. Zheng, J. Ren, C. Wang, Y. Ma, J. Ding, T. Li, A.Y. Elnaggar, I.H.E. Azab, M.H.H. Mahmoud, S.M. El-Bahy, I. Seok, N. Naik, G. Roymahapatra, V. Murugadoss, M. Huang, B.B. Xu, Z. Guo, Magnetite@poly(p-phenylenediamine) core-shell composite modified with salicylaldehyde for adsorption and separation of Mn (VII) from polluted water, J. Nanostruct. Chem. 12(6) (2022) 1155-1168, https://doi.org/10.1007/s40097-022-00510-4.

[168] W. Li, J. Chen, P. Gao, MOFs-derived hollow Copper-based sulfides for optimized electromagnetic behaviors, J. Colloid Interf. Sci. 606 (2022) 719-727, https://doi.org/10.1016/j.jcis.2021.08.019.

[169] J. Ma, X. Zhang, W. Liu, G. Ji, Direct synthesis of MOF-derived nanoporous CuO/carbon composites for high impedance matching and advanced microwave absorption, J. Mater. Chem. C 4(48) (2016) 11419-11426, https://doi.org/10.1039/c6tc04048a.

[170] H. Yang, Z. Shen, H. Peng, Z. Xiong, C. Liu, Y. Xie, 1D-3D mixed-dimensional MnO_2@nanoporous carbon composites derived from Mn-metal organic framework with full-band ultra-strong microwave absorption response, Chem. Eng. J. 417 (2021) 128087, https://doi.org/10.1016/j.cej.2020.128087.

[171] X. Zhang, J. Qiao, C. Liu, F. Wang, Y. Jiang, P. Cui, Q. Wang, Z. Wang, L. Wu, J. Liu, A MOF-derived ZrO_2/C nanocomposite for efficient electromagnetic wave absorption, Inorg. Chem. Front. 7(2) (2020) 385-393, https://doi.org/10.1039/c9qi01259a.

[172] Y. Qiu, H. Yang, Y. Cheng, X. Bai, B. Wen, Y. Lin, Constructing a nitrogen-doped carbon and nickel composite derived from a mixed ligand nickel-based a metal-organic framework toward adjustable microwave absorption, Nanoscale 13(20) (2021) 9204-9216, https://doi.org/10.1039/d1nr01607e.

[173] H. Wang, L. Xiang, W. Wei, J. An, J. He, C. Gong, Y. Hou, Efficient and Lightweight Electromagnetic Wave Absorber Derived from Metal Organic Framework-Encapsulated Cobalt Nanoparticles, ACS Appl. Mater. Inter. 9(48) (2017) 42102-42110, https://doi.org/10.1021/acsami.7b13796.

[174] K. Wang, Y. Chen, R. Tian, H. Li, Y. Zhou, H. Duan, H. Liu, Porous Co-C Core-Shell Nanocomposites Derived from Co-MOF-74 with Enhanced Electromagnetic Wave Absorption Performance, ACS Appl. Mater. Inter. 10(13) (2018) 11333-11342,

https://doi.org/10.1021/acsami.8b00965.

[175] H. Wei, Y. Tian, Q. Chen, D. Estevez, P. Xu, H.-X. Peng, F. Qin, Microwave absorption performance of 2D Iron-Quinoid MOF, Chem. Eng. J. 405 (2021) 126637, https://doi.org/10.1016/j.cej.2020.126637.

[176] J. Yan, Y. Huang, Y. Yan, L. Ding, P. Liu, High-Performance Electromagnetic Wave Absorbers Based on Two Kinds of Nickel-Based MOF-Derived Ni@C Microspheres, ACS Appl. Mater. Inter. 11(43) (2019) 40781-40792, https://doi.org/10.1021/acsami.9b12850.

[177] Y. Lu, Y. Wang, H. Li, Y. Lin, Z. Jiang, Z. Xie, Q. Kuang, L. Zheng, MOF-Derived Porous Co/C Nanocomposites with Excellent Electromagnetic Wave Absorption Properties, ACS Appl. Mater. Inter. 7(24) (2015) 13604-11, https://doi.org/10.1021/acsami.5b03177.

[178] G. Liu, C. Wu, L. Hu, X. Hu, X. Zhang, J. Tang, H. Du, X. Wang, M.J.C. Yan, Anisotropy engineering of metal organic framework derivatives for effective electromagnetic wave absorption, Carbon 181 (2021) 48-57, https://doi.org/10.1016/j.carbon.2021.05.015.

[179] N. Wu, B. Zhao, J. Liu, Y. Li, Y. Chen, L. Chen, M. Wang, Z. Guo, MOF-derived porous hollow Ni/C composites with optimized impedance matching as lightweight microwave absorption materials, Adv. Compos. Hybrid Mater. 4(3) (2021) 707-715, https://doi.org/10.1007/s42114-021-00307-z.

[180] Z. Yang, Y. Zhang, M. Li, L. Yang, J. Liu, Y. Hou, Y. Yang, Surface Architecture of Ni-Based Metal Organic Framework Hollow Spheres for Adjustable Microwave Absorption, ACS Appl. Nano Mater. 2(12) (2019) 7888-7897, https://doi.org/10.1021/acsanm.9b01881.

[181] Q. Zeng, L. Wang, X. Li, W. You, J. Zhang, X. Liu, M. Wang, R. Che, Double ligand MOF-derived pomegranate-like Ni@C microspheres as high-performance microwave absorber, Appl. Surf. Sci. 538 (2021) 148051, https://doi.org/10.1016/j.apsusc.2020.148051.

[182] Y. Qiu, H. Yang, Y. Cheng, Y. Lin, MOFs derived flower-like nickel and carbon composites with controllable structure toward efficient microwave absorption, Compos. Part A-Appl. S. 154 (2022) 106772, https://doi.org/10.1016/j.compositesa.2021.106772.

[183] X. Xiao, W. zhu, Z. Tan, W. Tian, Y. Guo, H. Wang, J. Fu, X. Jian, Ultra-small Co/CNTs nanohybrid from metal organic framework with highly efficient microwave absorption, Compos. Part B-Eng. 152 (2018) 316-323, https://doi.org/10.1016/j.compositesb.2018.08.109.

[184] Y. Liu, Z. Yao, J. Zhou, L. Jin, B. Wei, X. He, Facile synthesis of MOF-derived concave cube nanocomposite by self-templated

toward lightweight and wideband microwave absorption, Carbon 186 (2022) 574-588, https://doi.org/10.1016/j.carbon.2021.10.044.

[185] Y. Zhang, S. Gao, Y. Wang, Metal-organic framework derived magnetic carbon Ni@ C octahedron composite as an excellent microwave absorber, Compos. Commun. 31 (2022) 101135, https://doi.org/10.1016/j.coco.2022.101135.

[186] Z. Li, X. Han, Y. Ma, D. Liu, Y. Wang, P. Xu, C. Li, Y. Du, MOFs-Derived Hollow Co/C Microspheres with Enhanced Microwave Absorption Performance, ACS Sustainable Chem. Eng. 6(7) (2018) 8904-8913, https://doi.org/10.1021/acssuschemeng.8b01270.

[187] X. Liang, C. Wang, M. Yu, Z. Yao, Y. Zhang, Fe-MOFs derived porous Fe_4N@carbon composites with excellent broadband electromagnetic wave absorption properties, J. Alloys Compd. 910 (2022) 164844, https://doi.org/10.1016/j.jallcom.2022.164844.

[188] Z. Zhao, K. Kou, L. Zhang, H. Wu, Optimal particle distribution induced interfacial polarization in bouquet-like hierarchical composites for electromagnetic wave absorption, Carbon 186 (2022) 323-332, https://doi.org/10.1016/j.carbon.2021.10.052.

[189] P. Miao, J. Chen, Y. Tang, K.-J. Chen, J. Kong, Highly efficient and broad electromagnetic wave absorbers tuned via topology-controllable metal-organic frameworks, Sci. China Mater. 63(10) (2020) 2050-2061, https://doi.org/10.1007/s40843-020-1333-9.

[190] J. Pan, H. Yang, Q. Hong, H.-M. Wen, J.Q. Xiao, J. Hu, Bimetal–organic frameworks derived tuneable Co nanoparticles embedded in porous nitrogen-doped carbon nanorods as high-performance electromagnetic wave absorption materials, J. Mater. Chem. C 9(23) (2021) 7302-7309, https://doi.org/10.1039/d1tc00841b.

[191] J. Qiao, X. Zhang, C. Liu, L. Lyu, Y. Yang, Z. Wang, L. Wu, W. Liu, F. Wang, J. Liu, Non-Magnetic Bimetallic MOF-Derived Porous Carbon-Wrapped TiO_2/$ZrTiO_4$ Composites for Efficient Electromagnetic Wave Absorption, Nano-Micro Lett. 13(1) (2021) 75, https://doi.org/10.1007/s40820-021-00606-6.

[192] L. Wang, B. Wen, H. Yang, Y. Qiu, N. He, Hierarchical nest-like structure of Co/Fe MOF derived CoFe@C composite as wide-bandwidth microwave absorber, Compos. Part A-Appl. S. 135 (2020) 105958, https://doi.org/10.1016/j.compositesa.2020.105958.

[193] K. Yang, Y. Cui, L. Wan, Q. Zhang, B. Zhang, MOF-derived magnetic-dielectric balanced Co@ZnO@N-doped carbon composite materials for strong microwave absorption, Carbon 190 (2022) 366-375, https://doi.org/10.1016/j.carbon.2022.01.032.

[194] B. Wen, H. Yang, Y. Lin, Y. Qiu, Y. Cheng, L. Jin, Novel bimetallic MOF derived hierarchical Co@C composites modified with carbon nanotubes and its excellent electromagnetic wave absorption properties, J. Colloid Interf. Sci. 605 (2022) 657-666, https://doi.org/10.1016/j.jcis.2021.07.118.

[195] Y. Cui, Z. Liu, X. Li, J. Ren, Y. Wang, Q. Zhang, B. Zhang, MOF-derived yolk-shell Co@ZnO/Ni@NC nanocage: Structure control and electromagnetic wave absorption performance, J. Colloid Interf. Sci. 600 (2021) 99-110, https://doi.org/10.1016/j.jcis.2021.05.015.

[196] J. Ouyang, Z. He, Y. Zhang, H. Yang, Q. Zhao, Trimetallic FeCoNi@C Nanocomposite Hollow Spheres Derived from Metal-Organic Frameworks with Superior Electromagnetic Wave Absorption Ability, ACS Appl. Mater. Inter. 11(42) (2019) 39304-39314, https://doi.org/10.1021/acsami.9b11430.

[197] M. Kong, X. Liu, Z. Jia, B. Wang, X. Wu, G. Wu, Porous magnetic carbon CoFe alloys@ZnO@C composites based on Zn/Co-based bimetallic MOF with efficient electromagnetic wave absorption, J. Colloid Interf. Sci. 604 (2021) 39-51, https://doi.org/10.1016/j.jcis.2021.07.003.

[198] J. Yan, Y. Huang, Y. Yan, X. Zhao, P. Liu, The composition design of MOF-derived Co-Fe bimetallic autocatalysis carbon nanotubes with controllable electromagnetic properties, Compos. Part A-Appl. S. 139 (2020) 106107, https://doi.org/10.1016/j.compositesa.2020.106107.

[199] F. Wu, Q. Li, Z. Liu, T. Shah, M. Ahmad, Q. Zhang, B. Zhang, Fabrication of binary MOF-derived hybrid nanoflowers via selective assembly and their microwave absorbing properties, Carbon 182 (2021) 484-496, https://doi.org/10.1016/j.carbon.2021.06.044.

[200] R. Cheng, Y. Wang, X. Di, Z. Lu, P. Wang, M. Ma, J. Ye, Construction of MOF-derived plum-like NiCo@C composite with enhanced multi-polarization for high-efficiency microwave absorption, J. Colloid Interf. Sci. 609 (2021) 224-234, https://doi.org/10.1016/j.jcis.2021.11.197.

[201] Z. Gao, Y. Song, S. Zhang, D. Lan, Z. Zhao, Z. Wang, D. Zang, G. Wu, H. Wu, Electromagnetic absorbers with Schottky contacts derived from interfacial ligand exchanging metal-organic frameworks, J. Colloid Interf. Sci. 600 (2021) 288-298, https://doi.org/10.1016/j.jcis.2021.05.009.

[202] L. Huang, C. Chen, X. Huang, S. Ruan, Y.-J. Zeng, Enhanced electromagnetic absorbing performance of MOF-derived Ni/NiO/Cu@C composites, Compos. Part B-Eng. 164 (2019) 583-589, https://doi.org/10.1016/j.compositesb.2019.01.081.

[203] Y. Jiao, S. Cheng, F. Wu, X. Pan, A. Xie, X. Zhu, W. Dong, MOF-Guest complex derived Cu/C nanocomposites with multiple heterogeneous interfaces for excellent electromagnetic waves absorption, Compos. Part B-Eng. 211 (2021) 108643, https://doi.org/10.1016/j.compositesb.2021.108643.

[204] Q. Liao, M. He, Y. Zhou, S. Nie, Y. Wang, S. Hu, H. Yang, H. Li, Y. Tong, Highly Cuboid-Shaped Heterobimetallic Metal-

Organic Frameworks Derived from Porous Co/ZnO/C Microrods with Improved Electromagnetic Wave Absorption Capabilities, ACS Appl. Mater. Inter. 10(34) (2018) 29136-29144, https://doi.org/10.1021/acsami.8b09093.

[205] G. Liu, J. Tu, C. Wu, Y. Fu, C. Chu, Z. Zhu, X. Wang, M. Yan, High-Yield Two-Dimensional Metal-Organic Framework Derivatives for Wideband Electromagnetic Wave Absorption, ACS Appl. Mater. Inter. 13(17) (2021) 20459-20466, https://doi.org/10.1021/acsami.1c00281.

[206] W. Liu, L. Liu, G. Ji, D. Li, Y. Zhang, J. Ma, Y. Du, Composition Design and Structural Characterization of MOF-Derived Composites with Controllable Electromagnetic Properties, ACS Sustainable Chem. Eng. 5(9) (2017) 7961-7971, https://doi.org/10.1021/acssuschemeng.7b01514.

[207] W. Liu, L. Liu, Z. Yang, J. Xu, Y. Hou, G. Ji, A Versatile Route toward the Electromagnetic Functionalization of Metal-Organic Framework-Derived Three-Dimensional Nanoporous Carbon Composites, ACS Appl. Mater. Inter. 10(10) (2018) 8965-8975, https://doi.org/10.1021/acsami.8b00320.

[208] Y. Qiu, B. Wen, H. Yang, Y. Lin, Y. Cheng, L. Jin, MOFs derived Co@C@MnO nanorods with enhanced interfacial polarization for boosting the electromagnetic wave absorption, J. Colloid Interf. Sci. 602 (2021) 242-250, https://doi.org/10.1016/j.jcis.2021.06.006.

[209] Z. Shen, H. Yang, C. Liu, E. Guo, S. Huang, Z. Xiong, Polymetallic MOF-derived corn-like composites for magnetic-dielectric balance to facilitate broadband electromagnetic wave absorption, Carbon 185 (2021) 464-476, https://doi.org/10.1016/j.carbon.2021.09.041.

[210] G. Song, K. Yang, L. Gai, Y. Li, Q. An, Z. Xiao, S. Zhai, ZIF-67/CMC-derived 3D N-doped hierarchical porous carbon with in-situ encapsulated bimetallic sulfide and Ni NPs for synergistic microwave absorption, Compos. Part A-Appl. S. 149 (2021) 106584, https://doi.org/10.1016/j.compositesa.2021.106584.

[211] L. Wang, M. Huang, X. Qian, L. Liu, W. You, J. Zhang, M. Wang, R. Che, Confined Magnetic-Dielectric Balance Boosted Electromagnetic Wave Absorption, Small 17(30) (2021) e2100970, https://doi.org/10.1002/smll.202100970.

[212] L. Wang, M. Huang, X. Yu, W. You, J. Zhang, X. Liu, M. Wang, R. Che, MOF-Derived $Ni_{1-x}Co_x$@Carbon with Tunable Nano-Microstructure as Lightweight and Highly Efficient Electromagnetic Wave Absorber, Nano-Micro Lett. 12(1) (2020) 150, https://doi.org/10.1007/s40820-020-00488-0.

[213] L. Wang, X. Yu, X. Li, J. Zhang, M. Wang, R. Che, MOF-derived yolk-shell Ni@C@ZnO Schottky contact structure for enhanced microwave absorption, Chem. Eng. J. 383 (2020) 123099, https://doi.org/10.1016/j.cej.2019.123099.

[214] Y. Wang, W. Zhong, S. Zhang, X. Zhang, C. Zhu, X. Zhang, X. Zhang, Y. Chen, Pearl necklace-like CoMn-based nanostructures derived from metal-organic frames for enhanced electromagnetic wave absorption, Carbon 188 (2022) 254-264, https://doi.org/10.1016/j.carbon.2021.12.030.

[215] Y.-L. Wang, S.-H. Yang, H.-Y. Wang, G.-S. Wang, X.-B. Sun, P.-G. Yin, Hollow porous CoNi/C composite nanomaterials derived from MOFs for efficient and lightweight electromagnetic wave absorber, Carbon 167 (2020) 485-494, https://doi.org/10.1016/j.carbon.2020.06.014.

[216] S. Wei, T. Chen, Q. Wang, Z. Shi, W. Li, S. Chen, Metal-organic framework derived hollow CoFe@C composites by the tunable chemical composition for efficient microwave absorption, J. Colloid Interf. Sci. 593 (2021) 370-379, https://doi.org/10.1016/j.jcis.2021.02.120.

[217] X. Xu, F. Ran, Z. Fan, H. Lai, Z. Cheng, T. Lv, L. Shao, Y. Liu, Cactus-Inspired Bimetallic Metal-Organic Framework-Derived 1D-2D Hierarchical Co/N-Decorated Carbon Architecture toward Enhanced Electromagnetic Wave Absorbing Performance, ACS Appl. Mater. Inter. 11(14) (2019) 13564-13573, https://doi.org/10.1021/acsami.9b00356.

[218] X. Zhang, J. Qiao, J. Zhao, D. Xu, F. Wang, C. Liu, Y. Jiang, L. Wu, P. Cui, L. Lv, Q. Wang, W. Liu, Z. Wang, J. Liu, High-Efficiency Electromagnetic Wave Absorption of Cobalt-Decorated NH_2-UIO-66-Derived Porous ZrO_2/C, ACS Appl. Mater. Inter. 11(39) (2019) 35959-35968, https://doi.org/10.1021/acsami.9b10168.

[219] H. Zhu, Q. Jiao, R. Fu, P. Su, C. Yang, C. Feng, H. Li, D. Shi, Y. Zhao, Cu/NC@Co/NC composites derived from core-shell Cu-MOF@Co-MOF and their electromagnetic wave absorption properties, J. Colloid Interf. Sci. 613 (2022) 182-193, https://doi.org/10.1016/j.jcis.2021.11.166.

[220] X. Ren, Y. Song, Z. Gao, Y. Wu, Z. Jia, G. Wu, Rational manipulation of composition and construction toward Zn/Co bimetal hybrids for electromagnetic wave absorption, J. Mater. Sci. Technol. 134 (2023) 254-261, https://doi.org/10.1016/j.jmst.2022.07.004.

[221] C. Liang, J. He, Y. Zhang, W. Zhang, C. Liu, X. Ma, Y. Liu, J. Gu, MOF-derived CoNi@C-silver nanowires/cellulose nanofiber composite papers with excellent thermal management capability for outstanding electromagnetic interference shielding, Compos. Sci. Technol. 224 (2022) 109445, https://doi.org/10.1016/j.compscitech.2022.109445.

[222] W. Wang, D. Liu, H. Cheng, T. Cao, Y. Li, Y. Deng, W. Xie, Structural design and broadband radar absorbing performance of multi-layer patch using carbon black, Adv. Compos. Hybrid Mater. 5 (2022) 3137-3145, https://doi.org/10.1007/s42114-021-00399-7.

[223] Z. Li, W. Xie, F. Yao, A. Du, Q. Wang, Z. Guo, H. Gu, Comprehensive electrocatalytic degradation of tetracycline in wastewater by electrospun perovskite manganite nanoparticles supported on carbon nanofibers, Adv. Compos. Hybrid Mater. 5(3) (2022) 2092-2105, https://doi.org/10.1007/s42114-022-00550-y.

[224] N. Wu, J. Qiao, J. Liu, W. Du, D. Xu, W. Liu, Strengthened electromagnetic absorption performance derived from synergistic effect of carbon nanotube hybrid with Co@ C beads, Adv. Compos. Hybrid Mater. 1(1) (2018) 149-159, https://doi.org/10.1007/s42114-017-0008-z.

[225] M. Liu, H. Wu, Y. Wu, P. Xie, R.A. Pashameah, H.M. Abo-Dief, S.M. El-Bahy, Y. Wei, G. Li, W. Li, The weakly negative permittivity with low-frequency-dispersion behavior in percolative carbon nanotubes/epoxy nanocomposites at radio-frequency range, Adv. Compos. Hybrid Mater. 5(3) (2022) 2021-2030, https://doi.org/10.1007/s42114-022-00541-z.

[226] J. Zhao, J. Zhang, L. Wang, S. Lyu, W. Ye, B.B. Xu, H. Qiu, L. Chen, J. Gu, Fabrication and investigation on ternary heterogeneous MWCNT@TiO_2-C fillers and their silicone rubber wave-absorbing composites, Compos. Part A-Appl. S. 129 (2020) 105714, https://doi.org/10.1016/j.compositesa.2019.105714.

[227] K. Ruan, J. Gu, Ordered Alignment of Liquid Crystalline Graphene Fluoride for Significantly Enhancing Thermal Conductivities of Liquid Crystalline Polyimide Composite Films, Macromolecules 55(10) (2022) 4134-4145, https://doi.org/10.1021/acs.macromol.2c00491.

[228] P. Song, C. Liang, L. Wang, H. Qiu, H. Gu, J. Kong, J. Gu, Obviously improved electromagnetic interference shielding performances for epoxy composites via constructing honeycomb structural reduced graphene oxide, Compos. Sci. Technol. 181 (2019) 107698, https://doi.org/10.1016/j.compscitech.2019.107698.

[229] L. Wang, X. Shi, J. Zhang, Y. Zhang, J. Gu, Lightweight and robust rGO/sugarcane derived hybrid carbon foams with outstanding EMI shielding performance, J. Mater. Sci. Technol. 52 (2020) 119-126, https://doi.org/10.1016/j.jmst.2020.03.029.

[230] P. Wang, L. Yang, J. Ling, J. Song, T. Song, X. Chen, S. Gao, S. Feng, Y. Ding, V. Murugadoss, Frontal ring-opening metathesis polymerized polydicyclopentadiene carbon nanotube/graphene aerogel composites with enhanced electromagnetic interference shielding, Adv. Compos. Hybrid Mater. 5(3) (2022) 2066-2077, https://doi.org/10.1007/s42114-022-00543-x.

[231] J.W. Fang, Y. Ma, Z.Y. Zhang, B.Z. Yang, Y.S. Li, Y.Y. Hu, Y.H. Yin, X.B. Liu, Z.P. Wu, Metal-Organic Framework-Derived Carbon/Carbon Nanotubes Mediate Impedance Matching for Strong Microwave Absorption at Fairly Low Temperatures, ACS Appl. Mater. Inter. 13(28) (2021) 33496-33504, https://doi.org/10.1021/acsami.1c07792.

[232] Q. Hu, R. Yang, S. Yang, W. Huang, Z. Zeng, X. Gui, Metal-Organic Framework-Derived Core-Shell Nanospheres Anchored

on Fe-Filled Carbon Nanotube Sponge for Strong Wideband Microwave Absorption, ACS Appl. Mater. Inter. 14(8) (2022) 10577-10587, https://doi.org/10.1021/acsami.1c25019.

[233] X. Li, L. Wang, X. Li, J. Zhang, M. Wang, R. Che, Multi-dimensional ZnO@MWCNTs assembly derived from MOF-5 heterojunction as highly efficient microwave absorber, Carbon 172 (2021) 15-25, https://doi.org/10.1016/j.carbon.2020.09.068.

[234] J. Chen, J. Zheng, F. Wang, Q. Huang, G. Ji, Carbon fibers embedded with FeIII-MOF-5-derived composites for enhanced microwave absorption, Carbon 174 (2021) 509-517, https://doi.org/10.1016/j.carbon.2020.12.077.

[235] Y. Guo, D. Wang, J. Wang, Y. Tian, H. Liu, C. Liu, C. Shen, Hierarchical HCF@NC/Co Derived from Hollow Loofah Fiber Anchored with Metal–Organic Frameworks for Highly Efficient Microwave Absorption, ACS Appl. Mater. Inter. 14(1) (2021) 2038-2050, https://doi.org/10.1021/acsami.1c21396.

[236] J. Tao, Z. Jiao, L. Xu, P. Yi, Z. Yao, F. Yang, C. Zhou, P. Chen, J. Zhou, Z. Li, Construction of MOF-Derived Co/C shell on carbon fiber surface to enhance multi-polarization effect towards efficient broadband electromagnetic wave absorption, Carbon 184 (2021) 571-582, https://doi.org/10.1016/j.carbon.2021.08.064.

[237] Q. Li, Y. Zhao, X. Li, L. Wang, X. Li, J. Zhang, R. Che, MOF Induces 2D GO to Assemble into 3D Accordion-Like Composites for Tunable and Optimized Microwave Absorption Performance, Small 16(42) (2020) e2003905, https://doi.org/10.1002/smll.202003905.

[238] L. Wang, X. Bai, B. Wen, Z. Du, Y. Lin, Honeycomb-like Co/C composites derived from hierarchically nanoporous ZIF-67 as a lightweight and highly efficient microwave absorber, Compos. Part B-Eng. 166 (2019) 464-471, https://doi.org/10.1016/j.compositesb.2019.02.054.

[239] S. Wang, Y. Xu, R. Fu, H. Zhu, Q. Jiao, T. Feng, C. Feng, D. Shi, H. Li, Y. Zhao, Rational Construction of Hierarchically Porous Fe-Co/N-Doped Carbon/rGO Composites for Broadband Microwave Absorption, Nano-Micro Lett. 11(1) (2019) 76, https://doi.org/10.1007/s40820-019-0307-8.

[240] Y. Zhao, W. Wang, J. Wang, J. Zhai, X. Lei, W. Zhao, J. Li, H. Yang, J. Tian, J. Yan, Constructing multiple heterogeneous interfaces in the composite of bimetallic MOF-derivatives and rGO for excellent microwave absorption performance, Carbon 173 (2021) 1059-1072, https://doi.org/10.1016/j.carbon.2020.11.090.

[241] P. Liu, C. Zhu, S. Gao, C. Guan, Y. Huang, W. He, N-doped porous carbon nanoplates embedded with CoS_2 vertically anchored on carbon cloths for flexible and ultrahigh microwave absorption, Carbon 163 (2020) 348-359, https://doi.org/10.1016/j.carbon.2020.03.041.

[242] Y. Xiong, L. Xu, C. Yang, Q. Sun, X. Xu, Implanting FeCo/C nanocages with tunable electromagnetic parameters in anisotropic wood carbon aerogels for efficient microwave absorption, J. Mater. Chem. A 8(36) (2020) 18863-18871, https://doi.org/10.1039/d0ta05540a.

[243] F. Zhang, Z. Jia, Z. Wang, C. Zhang, B. Wang, B. Xu, X. Liu, G. Wu, Tailoring nanoparticles composites derived from metal-organic framework as electromagnetic wave absorber, Mater. Today Phys. 20 (2021) 100475, https://doi.org/10.1016/j.mtphys.2021.100475.

[244] W. Luo, Y. Ma, T. Li, H.K. Thabet, C. Hou, M.M. Ibrahim, S.M. El-Bahy, B.B. Xu, Z. Guo, Overview of MXene/conducting polymer composites for supercapacitors, J. Energy Storage 52 (2022) 105008, https://doi.org/10.1016/j.est.2022.105008.

[245] J. Wang, P. Li, P. Yu, T. Leydecker, I.S. Bayer, D. Losic, A. Neogi, Z. Wang, Efficient photothermal deicing employing superhydrophobic plasmonic MXene composites, Adv. Compos. Hybrid Mater. 5 (2022) 3035-3044, https://doi.org/10.1007/s42114-022-00549-5.

[246] X. Li, Z. Lin, Y. Wei, W. Luo, J. Ding, T. Li, Y. Ma, MXene-MnO_2-CoNi layered double hydroxides//activated carbon flexible asymmetric supercapacitor, J. Energy Storage 55 (2022) 105668, https://doi.org/10.1016/j.est.2022.105668.

[247] A. Chen, C. Wang, O.A. Abu Ali, S.F. Mahmoud, Y. Shi, Y. Ji, H. Algadi, S.M. El-Bahy, M. Huang, Z. Guo, D. Cui, H. Wei, MXene@nitrogen-doped carbon films for supercapacitor and piezoresistive sensing applications, Compos. Part A-Appl. S. 163 (2022) 107174, https://doi.org/10.1016/j.compositesa.2022.107174.

[248] Y. Wei, W. Luo, X. Li, Z. Lin, C. Hou, M. Ma, J. Ding, T. Li, Y. Ma, PANI-MnO_2 and $Ti_3C_2T_x$ (MXene) as electrodes for high-performance flexible asymmetric supercapacitors, Electrochim. Acta 406 (2022) 139874, https://doi.org/10.1016/j.electacta.2022.139874.

[249] Y. Wei, W. Luo, Z. Zhuang, B. Dai, J. Ding, T. Li, M. Ma, X. Yin, Y. Ma, Fabrication of ternary MXene/MnO_2/polyaniline nanostructure with good electrochemical performances, Adv. Compos. Hybrid Mater. 4(4) (2021) 1082-1091, https://doi.org/10.1007/s42114-021-00323-z.

[250] Y. Zhang, Y. Yan, H. Qiu, Z. Ma, K. Ruan, J. Gu, A mini-review of MXene porous films: Preparation, mechanism and application, J. Mater. Sci. Technol. 103 (2022) 42-49, https://doi.org/10.1016/j.jmst.2021.08.001.

[251] J. Zhou, F. Guo, J. Luo, G. Hao, G. Liu, Y. Hu, G. Zhang, H. Guo, H. Zhou, W. Jiang, Designed 3D heterostructure with 0D/1D/2D hierarchy for low-frequency microwave absorption in the S-band, J. Mater. Chem. C 10(4) (2022) 1470-1478, https://doi.org/10.1039/d1tc04881c.

[252] F. Chen, S. Zhang, B. Ma, Y. Xiong, H. Luo, Y. Cheng, X. Li, X. Wang, R. Gong, Bimetallic CoFe-MOF@$Ti_3C_2T_x$ MXene derived composites for broadband microwave absorption, Chem. Eng. J. 431 (2022) 134007, https://doi.org/10.1016/j.cej.2021.134007.

[253] H.-Y. Wang, X.-b. Sun, G.-S. Wang, A MXene-modulated 3D crosslinking network of hierarchical flower-like MOF derivatives towards ultra-efficient microwave absorption properties, J. Mater. Chem. A 9(43) (2021) 24571-24581, https://doi.org/10.1039/d1ta06505j.

[254] B. Deng, Z. Xiang, J. Xiong, Z. Liu, L. Yu, W. Lu, Sandwich-Like Fe&TiO_2@C Nanocomposites Derived from MXene/Fe-MOFs Hybrids for Electromagnetic Absorption, Nano-Micro Lett. 12(1) (2020) 55, https://doi.org/10.1007/s40820-020-0398-2.

[255] F. Wu, Z. Liu, J. Wang, T. Shah, P. Liu, Q. Zhang, B. Zhang, Template-free self-assembly of MXene and CoNi-bimetal MOF into intertwined one-dimensional heterostructure and its microwave absorbing properties, Chem. Eng. J. 422 (2021) 130591, https://doi.org/10.1016/j.cej.2021.130591.

[256] M. Zheng, Y. Wei, J. Ren, B. Dai, W. luo, M. Ma, T. Li, Y. Ma, 2-aminopyridine functionalized magnetic core–shell Fe_3O_4@polypyrrole composite for removal of Mn (VII) from aqueous solution by double-layer adsorption, Sep. Purif. Technol. 277 (2021) 119455, https://doi.org/10.1016/j.seppur.2021.119455.

[257] J. Guo, Z. Chen, Z.M. El-Bahy, H. Liu, H.M. Abo-Dief, W. Abdul, K.M. Abualnaja, A.K. Alanazi, P. Zhang, M. Huang, Tunable negative dielectric properties of magnetic $CoFe_2O_4$/graphite-polypyrrole metacomposites, Adv. Compos. Hybrid Mater. 5 (2022) 899-906, https://doi.org/10.1007/s42114-022-00485-4.

[258] C. Liang, Z. Gu, Y. Zhang, Z. Ma, H. Qiu, J. Gu, Structural Design Strategies of Polymer Matrix Composites for Electromagnetic Interference Shielding: A Review, Nano-Micro Lett. 13(1) (2021) 181, https://doi.org/10.1007/s40820-021-00707-2.

[259] Y. Zhang, J. Gu, A Perspective for Developing Polymer-Based Electromagnetic Interference Shielding Composites, Nano-Micro Lett. 14(1) (2022) 89, https://doi.org/10.1007/s40820-022-00843-3.

[260] W. Luo, Y. Wei, Z. Zhuang, Z. Lin, X. Li, C. Hou, T. Li, Y. Ma, Fabrication of $Ti_3C_2T_x$ MXene/polyaniline composite films with adjustable thickness for high-performance flexible all-solid-state symmetric supercapacitors, Electrochim. Acta 406 (2022) 139871, https://doi.org/10.1016/j.electacta.2022.139871.

[261] G. Li, L. Wang, X. Lei, Z. Peng, T. Wan, S. Maganti, M. Huang, V. Murugadoss, I. Seok, Q. Jiang, Flexible, yet robust polyaniline coated foamed polylactic acid composite electrodes for high-performance supercapacitors, Adv. Compos. Hybrid Mater.

5(2) (2022) 853-863, https://doi.org/10.1007/s42114-022-00501-7.

[262] H. Li, W. Huang, B. Qiu, H.K. Thabet, D. Alhashmialameer, M. Huang, Z. Guo, Effective removal of proteins and polysaccharides from biotreated wastewater by polyaniline composites, Adv. Compos. Hybrid Mater. 5 (2022) 1888-1898, https://doi.org/10.1007/s42114-022-00508-0.

[263] L. Ouyang, W. Huang, M. Huang, B.J.A.C. Qiu, H. Materials, Polyaniline improves granulation and stability of aerobic granular sludge, Adv. Compos. Hybrid Mater. 5 (2022) 1126-1136, https://doi.org/10.1007/s42114-022-00450-1.

[264] W. Wang, J. Ren, C. Wang, M. Zheng, Y. Ma, X. Yin, J. Ding, C. Hou, T. Li, Magnetic Fe_3O_4/polypyrrole-salicylaldehyde composite for efficient removal of Mn (VII) from aqueous solution by double-layer adsorption, J. Appl. Polym. Sci. 139(28) (2022) e52515, https://doi.org/10.1002/app.52515.

[265] W. Wang, M. Zheng, J. Ren, M. Ma, X. Yin, T. Li, Y. Ma, Fabrication of magnetic Fe_3O_4 /MnO_2/TiO_2/polypyrrole heterostructure for efficient adsorption of Mn^{7+} from aqueous solution, J. Appl. Polym. Sci. 139(21) (2022) 52199, https://doi.org/10.1002/app.52199.

[266] Y. Bi, M. Ma, Y. Liu, Z. Tong, R. Wang, K.L. Chung, A. Ma, G. Wu, Y. Ma, C. He, P. Liu, L. Hu, Microwave absorption enhancement of 2-dimensional CoZn/C@MoS_2@PPy composites derived from metal-organic framework, J. Colloid Interf. Sci. 600 (2021) 209-218, https://doi.org/10.1016/j.jcis.2021.04.137.

[267] X. Sun, X. Lv, M. Sui, X. Weng, X. Li, J. Wang, Decorating MOF-Derived Nanoporous Co/C in Chain-Like Polypyrrole (PPy) Aerogel: A Lightweight Material with Excellent Electromagnetic Absorption, Materials 11(5) (2018) 781, https://doi.org/10.3390/ma11050781.

[268] Y. Wang, W. Zhang, X. Wu, C. Luo, Q. Wang, J. Li, L. Hu, Conducting polymer coated metal-organic framework nanoparticles: Facile synthesis and enhanced electromagnetic absorption properties, Synth. Met. 228 (2017) 18-24, https://doi.org/10.1016/j.synthmet.2017.04.009.

[269] X. Han, Y. Huang, L. Ding, Y. Song, T. Li, P. Liu, $Ti_3C_2T_x$ MXene Nanosheet/Metal-Organic Framework Composites for Microwave Absorption, ACS Appl. Nano Mater. 4(1) (2020) 691-701, https://doi.org/10.1021/acsanm.0c02983.

[270] Y. Jiao, J. Li, A. Xie, F. Wu, K. Zhang, W. Dong, X. Zhu, Confined polymerization strategy to construct polypyrrole/zeolitic imidazolate frameworks (PPy/ZIFs) nanocomposites for tunable electrical conductivity and excellent electromagnetic absorption, Compos. Sci. Technol. 174 (2019) 232-240, https://doi.org/10.1016/j.compscitech.2019.03.003.

[271] G. Liu, L. Wang, H. Zhang, Z. Du, X. Zhou, K. Wang, Y. Sun, S. Gao, Cage-structured $CoFe_2O_4$@CNTs from Fe-Co-MOF

confined growth in CNTs for high electromagnetic wave absorption performances, Compos. Commun. 27 (2021) 100910, https://doi.org/10.1016/j.coco.2021.100910.

[272] L. Lyu, S. Zheng, F. Wang, Y. Liu, J. Liu, High-performance microwave absorption of MOF-derived Co_3O_4@N-doped carbon anchored on carbon foam, J. Colloid Interf. Sci. 602 (2021) 197-206, https://doi.org/10.1016/j.jcis.2021.05.184.

[273] Y. Qiu, H. Yang, L. Ma, Y. Lin, H. Zong, B. Wen, X. Bai, M. Wang, In situ-derived carbon nanotube-decorated nitrogen-doped carbon-coated nickel hybrids from MOF/melamine for efficient electromagnetic wave absorption, J. Colloid Interf. Sci. 581(Pt B) (2021) 783-793, https://doi.org/10.1016/j.jcis.2020.07.151.

[274] W. Wang, H. Zhang, Y. Zhao, J. Wang, H. Zhao, P. Li, J. Yun, Z. Deng, Z. Zhang, J. Tian, J. Yan, W. Zhao, F. Zhang, A novel MOF-drived self-decomposition strategy for CoO@N/C-Co/Ni-$NiCo_2O_4$ multi-heterostructure composite as high-performance electromagnetic wave absorbing materials, Chem. Eng. J. 426 (2021) 131667, https://doi.org/10.1016/j.cej.2021.131667.

[275] Y. Wang, H. Wang, J. Ye, L. Shi, X. Feng, Magnetic CoFe alloy@C nanocomposites derived from ZnCo-MOF for electromagnetic wave absorption, Chem. Eng. J. 383 (2020) 123096, https://doi.org/10.1016/j.cej.2019.123096.

[276] B. Wen, H. Yang, Y. Lin, L. Ma, Y. Qiu, F. Hu, Y. Zheng, Synthesis of core-shell Co@S-doped carbon@ mesoporous N-doped carbon nanosheets with a hierarchically porous structure for strong electromagnetic wave absorption, J. Mater. Chem. A 9(6) (2021) 3567-3575, https://doi.org/10.1039/d0ta09393a.

[277] Z. Xiang, X. Wang, X. Zhang, Y. Shi, L. Cai, X. Zhu, Y. Dong, W. Lu, Self-assembly of nano/microstructured 2D Ti_3CNT_x MXene-based composites for electromagnetic pollution elimination and Joule energy conversion application, Carbon 189 (2022) 305-318, https://doi.org/10.1016/j.carbon.2021.12.075.

[278] X. Xu, F. Ran, Z. Fan, Z. Cheng, T. Lv, L. Shao, Y. Liu, Bimetallic Metal-Organic Framework-Derived Pomegranate-like Nanoclusters Coupled with CoNi-Doped Graphene for Strong Wideband Microwave Absorption, ACS Appl. Mater. Inter. 12(15) (2020) 17870-17880, https://doi.org/10.1021/acsami.0c01572.

[279] X. Xu, F. Ran, H. Lai, Z. Cheng, T. Lv, L. Shao, Y. Liu, In Situ Confined Bimetallic Metal-Organic Framework Derived Nanostructure within 3D Interconnected Bamboo-like Carbon Nanotube Networks for Boosting Electromagnetic Wave Absorbing Performances, ACS Appl. Mater. Inter. 11(39) (2019) 35999-36009, https://doi.org/10.1021/acsami.9b14754.

[280] W. Xue, G. Yang, S. Bi, J. Zhang, Z.-L. Hou, Construction of caterpillar-like hierarchically structured Co/MnO/CNTs derived from MnO_2/ZIF-8@ZIF-67 for electromagnetic wave absorption, Carbon 173 (2021) 521-527, https://doi.org/10.1016/j.carbon.2020.11.016.

[281] J. Yan, Y. Huang, X. Han, X. Gao, P. Liu, Metal organic framework (ZIF-67)-derived hollow CoS_2/N-doped carbon nanotube composites for extraordinary electromagnetic wave absorption, Compos. Part B-Eng. 163 (2019) 67-76, https://doi.org/10.1016/j.compositesb.2018.11.008.

[282] M. Yang, Y. Yuan, Y. Li, X. Sun, S. Wang, L. Liang, Y. Ning, J. Li, W. Yin, R. Che, Y. Li, Dramatically enhanced electromagnetic wave absorption of hierarchical CNT/Co/C fiber derived from cotton and metal-organic-framework, Carbon 161 (2020) 517-527, https://doi.org/10.1016/j.carbon.2020.01.073.

[283] R. Yang, J. Yuan, C. Yu, K. Yan, Y. Fu, H. Xie, J. Chen, P.K. Chu, X. Wu, Efficient electromagnetic wave absorption by SiC/Ni/NiO/C nanocomposites, J. Alloys Compd. 816 (2020) 152519, https://doi.org/10.1016/j.jallcom.2019.152519.

[284] Z. Yang, H. Lv, R. Wu, Rational construction of graphene oxide with MOF-derived porous NiFe@C nanocubes for high-performance microwave attenuation, Nano Res. 9(12) (2016) 3671-3682, https://doi.org/10.1007/s12274-016-1238-z.

[285] P. Yi, Z. Yao, J. Zhou, B. Wei, L. Lei, R. Tan, H. Fan, Facile synthesis of 3D Ni@C nanocomposites derived from two kinds of petal-like Ni-based MOFs towards lightweight and efficient microwave absorbers, Nanoscale 13(5) (2021) 3119-3135, https://doi.org/10.1039/d0nr07991j.

[286] Y. Yin, X. Liu, X. Wei, Y. Li, X. Nie, R. Yu, J. Shui, Magnetically Aligned Co-C/MWCNTs Composite Derived from MWCNT-Interconnected Zeolitic Imidazolate Frameworks for a Lightweight and Highly Efficient Electromagnetic Wave Absorber, ACS Appl. Mater. Inter. 9(36) (2017) 30850-30861, https://doi.org/10.1021/acsami.7b10067.

[287] X. Zhang, Z. Jia, F. Zhang, Z. Xia, J. Zou, Z. Gu, G. Wu, MOF-derived $NiFe_2S_4$/Porous carbon composites as electromagnetic wave absorber, J. Colloid Interf. Sci. 610 (2022) 610-620, https://doi.org/10.1016/j.jcis.2021.11.110.

[288] X. Zhang, Z. Wang, L. Xu, K. Zuraiqi, T. Daeneke, Z. Yao, D.C. Qi, A. Zavabeti, Liquid metal derived MOF functionalized nanoarrays with ultra-wideband electromagnetic absorption, J. Colloid Interf. Sci. 606(Pt 2) (2022) 1852-1865, https://doi.org/10.1016/j.jcis.2021.08.143.

[289] Y. Zhao, W. Wang, Q. Wang, H. Zhao, P. Li, J. Yan, G. Wang, W. Zhao, J. Yun, Z. Deng, Z. Zhang, Construction of excellent electromagnetic wave absorber from multi-heterostructure materials derived from $ZnCo_2O_4$ and ZIF-67 composite, Carbon 185 (2021) 514-525, https://doi.org/10.1016/j.carbon.2021.09.049.

[290] Y. Zhou, W. Zhou, C. Ni, S. Yan, L. Yu, X. Li, "Tree blossom" Ni/NC/C composites as high-efficiency microwave absorbents, Chem. Eng. J. 430 (2022) 132621, https://doi.org/10.1016/j.cej.2021.132621.

[291] X. Zhu, H. Qiu, P. Chen, G. Chen, W. Min, Anemone-shaped ZIF-67@CNTs as effective electromagnetic absorbent covered

the whole X-band, Carbon 173 (2021) 1-10, https://doi.org/10.1016/j.carbon.2020.10.055.

[292] X. Ling, K. Wang, W. Zhang, Y. Wu, Q. Jin, D. Zhang, Bio-inspired, bimetal ZIF-derived hollow carbon/MXene microstructure aim for superior microwave absorption, J. Colloid Interf. Sci. 625 (2022) 317-327, https://doi.org/10.1016/j.jcis.2022.06.011.

[293] S. Ur Rehman, M. Sun, M. Xu, J. Liu, R. Ahmed, M.A. Aslam, R.A. Ahmad, H. Bi, Carbonized zeolitic imidazolate framework-67/polypyrrole: A magnetic-dielectric interface for enhanced microwave absorption properties, J. Colloid Interf. Sci. 574 (2020) 87-96, https://doi.org/10.1016/j.jcis.2020.04.053.